ROLES OF UREG AND UREF IN UREASE ACTIVATION

Ву

Jodi Lynn Boer

A DISSERTATION

Submitted to
Michigan State University
In partial fulfillment of the requirements
For the degree of

DOCTOR OF PHILOSOPHY

Biochemistry and Molecular Biology

2012

ABSTRACT

ROLES OF UREG AND UREF IN UREASE ACTIVATION

By

Jodi Lynn Boer

Urease hydrolyzes urea to ammonia and carbamic acid, which then spontaneously decomposes into another ammonia molecule and carbonic acid. The active site contains two nickel atoms bridged by a carbamylated lysine residue. In order to assemble the active site, four accessory proteins, UreD, UreE, UreF, and UreG, are necessary. This dissertation focuses on the roles UreG and UreF play in the activation process by investigating the individual characteristics of these proteins as purified, as well as determining how they interact with the other urease accessory proteins in the *Klebsiella aerogenes* system.

UreG is a GTPase required for the assembly of the urease active site; however, it has no GTPase activity when purified alone. A *Strep*-tagged version, $UreG_{Str}$, as well as several site-directed variants were constructed and their effects on urease activation, metal-binding properties, and protein: protein interactions with other urease-related proteins were assessed. The *Strep*-tag had no effect on the ability of UreG to participate in urease activation, but the K20A, D49A, C72A, H74A, D80A, and S111A variants essentially abolished enzyme activity. $UreG_{Str}$ binds one nickel or zinc ion per monomer ($K_d \sim 5 \mu M$ for each metal ion). The binding site includes residue Cys72 as shown by the 12-fold increase in the K_d for nickel ions in this variant, as well as a lack of a thiolate-to-nickel charge-transfer band in the UV-visible spectrum. Based on homology to HypB, a hydrogenase maturation protein, His74 is also a likely metal

ligand. Pull-down assays in cell-free extracts demonstrated that Asp80 is essential for stabilizing the $UreG_{Str}$ interaction with UreABC-UreD-UreF. In vitro pull-down assays demonstrated that the interaction between $UreG_{Str}$ and UreE is metal-dependent. This result suggests that UreE transfers its bound Ni to UreG in the UreABC-UreD-UreF-UreG complex, where it can then be passed to the nascent active site, possibly via UreD.

UreF was proposed previously to be a GTPase activating protein (GAP) for the GTPase UreG. Based on the UreF crystal structure from Helicobacter pylori, sixteen residues in K. aerogenes UreF were chosen for mutagenesis to alanine. When produced in the context of the urease gene cluster, cell-free extracts of nine site-directed mutants had less than 10% of the wild-type activity. Using the UreE-F construct and its variants in the same context, UreE-F was demonstrated to co-purify with urease apoprotein, UreD, and in some cases UreG from cellfree extracts. The variants that did not bind UreG correlated with low urease activity mutant cells, and mapped to a distinct surface on the UreF structure, defining the UreG binding site. In contrast to the GAP hypothesis for UreF, the UreABC—UreD—UreF(K165A)—UreG_{Str} complex had higher GTPase activity than the wild-type complex according to urease activation assays on purified protein. Further studies showed that the urease activity and GTPase activity were uncoupled in the K165A UreF-containing complex. Additional experiments with these complexes demonstrated that UreF gates the GTPase activity of UreG in order to enhance the fidelity of urease activation and guard against incorrect metal insertion in the presence of Zn.

To my parents, who always believed in me and taught me to do my best To Tom, for encouraging me and loving me

ACKNOWLEDGEMENTS

Many people have been essential to my success in graduate school. I would not have been able to do any of this work without the guidance of Dr. Robert Hausinger, who has been a wonderful person to work for. I have appreciated how he is always available to talk to. My fellow graduate students in the Hausinger lab – Soledad, Jana, Eric, Nicholas, and Mark all contributed to thought-provoking conversations. The post-docs who have worked here – "Big" Scott, Tina, Piotr, Hajime, Lee, and William have all helped me out as well. I especially thank Brittnie DeVries, who worked as "my" undergrad for two years and did much of the cloning, protein purification, and pull-down assays described here. I thank Tejas and Chris who both worked with me for a while, as well as the other undergrads who worked in the lab. I thank my classmates who got me through the first year of classes. My committee members also have my gratitude for their input.

I would not have gotten this far without the support of my family. My parents have always believed in and pushed me to do my best. I thank Tom for all of his encouragement. Though I didn't know him when I started, he has been my rock through this push to the finish. I thank my extended family for all their prayers and reminding me that there is life outside the lab. I thank my friends, especially my Bible studies through the years for their prayer support. Most of all, I am grateful to the Lord for all the blessings in my life.

TABLE OF CONTENTS

LIST OF TABLES	ix
LIST OF FIGURES	x
LIST OF ABBREVIATIONS	xii
CHAPTER 1	
INTRODUCTION	1
Introduction to Ni-binding sites	2
Common features of Ni-binding sites	2
Ni-binding sites in enzymes	3
Ni-binding sites in non-catalytic proteins	8
Ni-substituted proteins	12
Ni-binding to His-tagged proteins	14
Introduction to urease	15
Urease structure	16
Urease activation	18
Eukaryotic urease activation	24
Remaining questions	27
References	29
CHAPTER 2 MUTAGENESIS OF KLEBSIELLA AEROGENES UREG TO PROBE NICKEL BINDING AND INTERACTIONS WITH OTHER UREASE-RELATED PROTEINS	
Abstract	
Experimental Procedures	
Vector construction, cell growth, and purification of <i>Strep</i> -tagged UreG	
UreE purification	
Site-directed mutagenesis	
Circular dichroism	
Analytical gel filtration chromatography	
<i>In vivo</i> expression of UreG _{Str} variants in the context of the urease operon	
Urease activity assays	
Metal quantification	
Metal binding analysis	
UV/Visible spectroscopy	
Pull-down assays	
Western blot	56

Results	57
Characterization of Strep-tagged UreG	57
Targeting residues for mutagenesis	60
Effect of UreG _{Str} variants on urease activity in cell extracts	61
Metal binding to UreG, UreG _{Str} , and UreG _{Str} variants	63
Pull-down assays	73
Discussion	78
References	85
CHAPTER 3	
KLEBSIELLA AEROGENES UREF: IDENTIFICATION OF THE UREG BINDING SITE AND ROLE	IN
ENHANCING THE FIDELITY OF UREASE ACTIVATION	90
Abstract	91
Introduction	92
Experimental Procedures	97
Plasmids, oligonucleotides, and site-directed mutagenesis	97
Protein purification	99
Sodium dodecyl sulfate (SDS)-polyacrylamide gel electrophoresis (PAGE)	101
Pull-down assays using cell-free extracts	101
In vitro pull-down assays	101
Urease activity and protein assays	102
Urease activation assays	103
GTPase activity assays	103
Results	105
Targets for site directed mutagenesis	105
Mutants in ureF have variable effects on in vivo urease activity	
UreF variants primarily affect binding of UreG in cell-free extracts	109
UreF variants affect in vitro binding to (UreABC—UreD) ₃ and UreG _{Str}	112
Examination of UreF as a GTPase activating protein	116
UreF functions to increase the fidelity of urease activation	120
Discussion	124
References	130
CHAPTER 4	
ADDITIONAL STUDIES, CONCLUSIONS, AND REMAINING QUESTIONS	134
Additional Studies	
Metal analysis of (UreABC*) ₃ and Ure(AC) ₃	135
Crystallization Attempts	
XAS studies on UreG	
In vitro pull-down assays with UreE-F and MBP-UreD	
Characterization of MBP-UreD—UreF—UreG	
Characterization of LIreABC—LIreD—LIreF—LIreGov.	1/19

Conclusions and Remaining Questions	
References	
APPENDIX A	158
RFFFRENCES	161

LIST OF TABLES

Table 2.1 Plasmids and <i>E. coli</i> strains used in this study	19
Table 2.2 Oligonucleotides used to generate UreG mutations	52
Table 2.3 Effects of UreG mutations on the urease activity in soluble cell-free extracts 6	53
Table 2.4 Thermodynamics of nickel ion binding to UreG, UreG _{Str} , and its variants 6	59
Table 3.1 Plasmid properties9	98
Table 3.2 Oligonucleotides used in this study9	9
Table 3.3 Effect of UreF variants on urease activity in cell-free extracts)9
Table 3.4 Binding of UreABC—UreD by control and variant UreE-F samples 11	L 4
Table 3.5 Binding of control and variant UreE-F by UreG _{Str}	L5
Table 4.1 Metal content of urease apoprotein samples subjected to activation conditions 13	38
Table 4.2 Samples sent for XAS analysis	10
Table 4.3 Binding of control and mutant UreE-F to MBP-UreD14	12
Table 4.4 GTPase activities of MBP-UreD—UreF—UreG samples	15
Table 4.5 GTPase activities of MBP-UreD—UreF—UreG(T21A) samples	16
Table 4.6 GTPase activity of His-MBP-UreD—UreF—UreG and variants	18
Table A.1 Plasmids used in this work	59

LIST OF FIGURES

Figure 1.1 Active sites of Ni-containing enzymes
Figure 1.2 Ni-binding sites in Ni-sensor or Ni-delivery proteins
Figure 1.3 Ni-substituted protein metallocenters
Figure 1.4 His-tag used for affinity purification14
Figure 1.5 Genetic structures of the urease gene clusters from <i>K. aerogenes</i> and <i>H. pylori</i> 17
Figure 1.6 Urease structures can form different supramolecular structures 17
Figure 1.7 Interactions among urease-related proteins19
Figure 1.8 Crystal structure (3FS5) of (UreH—UreF) ₂ from <i>H. pylori</i>
Figure 1.9 Crystal structure (1GMW) of truncated UreE from <i>K. aerogenes</i> 24
Figure 2.1 Simplified scheme of the urease activation process
Figure 2.2 Multiple sequence alignment of the <i>K. aerogenes</i> UreG, <i>B. pasteurii</i> UreG, and <i>M. jannaschii</i> HypB
Figure 2.3 Purification of Ure G_{Str} and size exclusion chromatography native size analysis 59
Figure 2.4 Equilibrium dialysis analysis of metal binding to wild type and Strep-tagged UreG 6
Figure 2.5 Equilibrium dialysis analyses to assess the competition of nickel and zinc ions 6
Figure 2.6 UV-visible spectral titrations of UreG $_{Str}$ and its C28A variant with NiCl $_2$ 73
Figure 2.7 Difference in UV-visible absorbance spectra according to Ni concentration
Figure 2.8 Interactions of $UreG_{Str}$ with urease proteins using cell-free extracts and in vitro interactions between $UreG_{Str}$ and $UreE$
Figure 2.9 Chromatography of the UreG _{Str} :UreE complex
Figure 2.10 Model of UreG:UreE interaction in the urease activation process
Figure 3.1 Simplified scheme of the urease activation process

Figure 3.2 Alignment of UreF sequences from selected microorganisms	. 106
Figure 3.3 Mutagenesis of <i>K. aerogenes</i> UreF	. 107
Figure 3.4 Effect of UreF variants on urease activity in cell-free extracts	. 108
Figure 3.5 UreE-F pull-down analyses of cell-free extracts	. 111
Figure 3.6 UreF mutations affecting UreG binding	. 112
Figure 3.7 In vitro pull-down assay examples	. 116
Figure 3.8 Effect of K165A UreF on GTP-dependent activation and phosphate release UreABC—UreD—UreF—UreG _{Str}	
Figure 3.9 Comparison of activation time course for UreABC—UreD—UreF—UreG $_{Str}$ comand UreABC—UreD—UreF(K165A)—UreG $_{Str}$	-
Figure 3.10 Zn inhibition of UreABC—UreD—UreF—UreG _{Str} activation for complexes conta wild type and K165A UreF	_
Figure 4.1 UreB of <i>K. aerogenes</i> urease blocks access to the active site	. 136
Figure 4.2 Fractions of MBP-UreD—UreF—UreG tested for GTPase activity	. 145
Figure 4.3 Fractions of MBP-UreD—UreF—UreG(T21A) tested for GTPase activity	. 146
Figure 4.4 Fractions of His-MBP-UreD—UreF—UreG, His-MBP-UreD—UreF—UreG(T21A), His-MBP-UreD—UreF(K165A)—UreG that were tested for GTPase activity	
Figure 4.5 Effect of adding GTP to MBP-UreD—UreF—UreG	. 149
Figure 4.6 Gel filtration profile of UreABC—UreD—UreF—UreG _{Str}	. 150
Figure 4.7 Native gel of UreABC—UreD—UreF—UreG _{Str} and UreABC—UreD—UreF—UreG.	. 151
Figure 4.8 Thermal stability of UreABC—UreD—UreF—UreGstr	. 153

ABBREVIATIONS

CD circular dichroism

DTT dithiothreitol

EDTA Ethylenediaminetetraacetic acid

GAP GTPase activating protein

HEPES 4-(2-hydroxyethyl)-1-piperazineethanesulfonic acid

ICP-AES inductively coupled plasma-atomic emission spectroscopy

IPTG isopropyl β-D-1-thiogalactopyranoside

MBP maltose binding protein

MWCO molecular weight cut-off

NTA nitrilotriacetic acid

NMR nuclear magnetic resonance

PAGE polyacrylamide gel electrophoresis

PCR polymerase chain reaction

PAR 4-(2-pyridylazo)-resorcinol

SAXS small-angle x-ray scattering

SDS-PAGE sodium dodecyl sulfate-polyacrylamide gel electrophoresis

TCEP tris(2-carboxyethyl)phosphine

Tris 2-amino-2-(hydroxymethyl)-1,3-propanediol

(UreABC)₃ urease apoprotein

(UreABC*)₃ complex formed by incubating purified (UreAC)₃ with UreB

UreE-F translational fusion of UreE and UreF

UreG_{Str} UreG tagged with Strep II

XAS X-ray absorption spectroscopy

Chapter 1

Introduction

Portions of this chapter were adapted from
Boer, J. L., and Hausinger, R. P. (2012) Ni-binding sites in proteins, in *Encyclopedia of Metalloproteins* (Vladimir Uversky, R. H. K., Eugene A. Permyakov, Ed.) (in press)

and

Carter, E. L., Flugga, N., Boer, J. L., Mulrooney, S. M., and Hausinger, R. P. (2009) Interplay of metal ions and urease, *Metallomics* 1, 207-221

This thesis describes the characterization of two proteins, UreF and UreG, required for activation of urease, a Ni-containing enzyme. To place my work in context, this introductory chapter (i) describes well-defined structures of Ni-binding sites in proteins, (ii) provides an overview of what is known about urease and its maturation, and (iii) highlights remaining questions related to urease and describes where my work has filled in some gaps.

INTRODUCTION TO NI-BINDING SITES

Ni is essential to many life forms, but excess levels are toxic and carcinogenic; thus, cells have devised mechanisms to sense Ni concentrations and maintain homeostatic control of this metal ion (1, 2). Ni-binding sites occur in Ni-dependent enzymes and a wide variety of proteins that transport or deliver Ni, regulate transcription of genes involved in Ni metabolism, or adventitiously bind the metal ion. Understanding the features of Ni-binding sites in proteins with well-defined structures gives a wide view of how Ni is used in nature, and also allows for a better understanding of how Ni-binding proteins that do not have defined structures may chelate the metal. Understanding of Ni-binding sites is applicable to the urease maturation system, where we only have partial knowledge of some of the Ni-binding sites, and do not know the specifics of how the Ni is transferred into the active site.

Common features of Ni-binding sites

The most common oxidation state for Ni in biology is Ni²⁺, although redox active sites are present in some Ni enzymes leading to Ni⁺¹ or Ni⁺³ states. The metal ion is most often found in six-coordinate octahedral configuration; however, planar or tetrahedral four-coordinate geometries and various five-coordinate ligand environments are known. The

imidazole group of His side chains is the most common amino acid ligand of Ni, with other amino acids coordinating the metal via the sulfur atoms of Cys or Met and the carboxylate groups of Glu and Asp residues (2). Backbone amides and amino-terminal amine groups bind the metal ion in some proteins, and Ni can be part of a larger metallocluster or incorporated into a tetrapyrrole bound to some proteins.

Ni-binding sites in enzymes

Enzymes utilize Ni to perform a wide variety of reactions, from hydrolysis to redox chemistry. A key aspect of Ni binding at enzyme active sites is that the metal ion must retain at least one open coordination site in order to bind the substrate. This open site may be occupied by water in the resting enzyme. Ni ligands in these enzymes vary widely, typically involving amino acid side chains but also sometimes utilizing backbone atoms and non-protein cofactors (1-5). Figure 1.1 illustrates the active sites with known structures of Ni-containing enzymes. All are crystal structures except for that of acireductone dioxygenase, which is derived from NMR studies.

Glyoxalase I binds the hemithioacetal derived from addition of glutathione and methylglyoxal, then uses Ni to catalyze its conversion to *S*-D-lactoylglutathione (*6*). The substrate likely displaces one or both water ligand(s) when coordinating to the Ni, and the oxidation state remains Ni²⁺ throughout the reaction. This protein illustrates how multiple peptide chains, in this case two, can cooperate to form a single Ni-binding site.

Acireductone dioxygenase uses the Ni at its active site to catalyze the cleavage of 1,2-dihydroxy-3-keto-5-methylthiopentane (acireductone) by reaction with oxygen, producing methylthiopropionate, formic acid, and carbon monoxide (7). Ni likely remains in the 2+

oxidation state during the reaction, acting as a Lewis acid. This enzyme alternatively binds Fe²⁺, resulting in the distinct products formic acid plus the α -keto acid precursor of Met, which is used as part of a salvage pathway (8).

Ni-superoxide dismutase catalyzes the disproportionation of two molecules of superoxide to form oxygen and hydrogen peroxide, identical in chemistry to the Cu/Zn-, Mn-, and Fe-superoxide dismutases, which are unrelated in sequence (9, 10). In this case, Ni cycles between Ni²⁺ in a square planar configuration and Ni³⁺ in a square pyramidal coordination. Unique to the Ni superoxide dismutase, the protein backbone forms part of the coordination sphere of the metal, using both the N-terminal amine and amide nitrogen ligands. His, a fifth ligand in the oxidized form of the enzyme, swings away from the metal ion in the reduced form.

Methyl coenzyme M reductase catalyzes the final step in methane formation in methanogenic archaea. reacts methyl-coenzyme (methyl-S-The enzyme thioethanesulfonate) with coenzyme B (N-7-mercaptoheptanoylthreonine phosphate), producing methane and disulfide-linked CoM-CoB. The active site contains an F430 cofactor, which is a Ni-containing tetrapyrrole related to, but extensively modified from, sirohemes and corrinoids (11). A Gln side chain coordinates at an axial ligand position, and substrates react at the other axial site. A very similar Ni-tetrapyrrole is found in an enzyme related in sequence to methyl coenzyme M reductase, but in that case it participates in anaerobic methane oxidation (12). The Ni cofactors in these enzymes undergo redox chemistry that includes Ni⁺¹ along with Ni⁺² and/or Ni⁺³ states.

Urease (discussed in detail below) catalyzes the hydrolysis of urea to ammonia and

carbamate, which then dissociates into another molecule of ammonia and bicarbonate. The urease active site contains a dinuclear Ni center, with the two metals bridged by a Lys carbamate (13, 14). The metallocluster is thought to both bind the urea and activate a water molecule for nucleophilic attack.

[NiFe] hydrogenases catalyze the reversible reduction of protons to H₂. The active site contains both Ni and Fe, with the Ni coordinated by four Cys residues (or in some cases three Cys and one Se-Cys) while Fe is coordinated by two of the same Cys residues and several diatomic molecules identified as cyanide or carbon monoxide (*15, 16*). There is a bridging ligand as well, with its identity depending on the state of the enzyme. Several other iron-sulfur clusters typically are present to serve as a conduit for electrons to electron carrier proteins. The mechanism is still being investigated, although spectroscopic evidence shows the Ni cycles between +2 and +3 oxidation states.

Carbon monoxide dehydrogenase (CODH) catalyzes the reversible oxidation of CO to CO₂. The protein contains a catalytic C-cluster with variations on a [Ni-4Fe-5S] cluster, depending on the source organism (*17, 18*). Ni is the likely site of CO binding, and one of the Fe atoms activates a hydroxide to attack the CO to form the product. The two electrons generated by this oxidative reaction are transferred through other iron sulfur clusters in the protein to reduce partner electron carrier proteins.

Acetyl-coenzyme A (CoA) synthase (ACS) often is found in a large complex that includes CODH. In this protein complex, CO₂ is reduced by the metallocenter of CODH to form CO and at a separate active site this toxic intermediate becomes linked to a methyl group, provided by a

corrinoid/iron-sulfur protein, and to CoA, thus forming acetyl-CoA (*18, 19*). The CO-producing and CO-consuming sites are linked by an ~70 Å long molecular tunnel through the protein complex. In addition to the Ni cluster in the CODH, the acetyl-CoA synthase active site contains two Ni atoms as well as a [4Fe-4S] cluster. One relatively stable Ni is bound via two backbone amides and two Cys residues. The second Ni, easily replaced by Cu or Zn, is coordinated by the same two Cys along with a third Cys that also serves as a ligand to the iron sulfur cluster. An analogous protein complex found in acetate-degrading methanogens carries out nearly the reverse reaction (*20*). It splits acetyl-CoA into a CO, CoA, and methyl group bound to CoM; in this case, oxidation of CO to CO₂ is used to provide electrons for conversion of methyl-CoM into methane. Several mechanisms have been proposed for the C-C and C-S bond formation/cleavage events, with variations in the order of substrate binding and the oxidation states of the Ni sites.

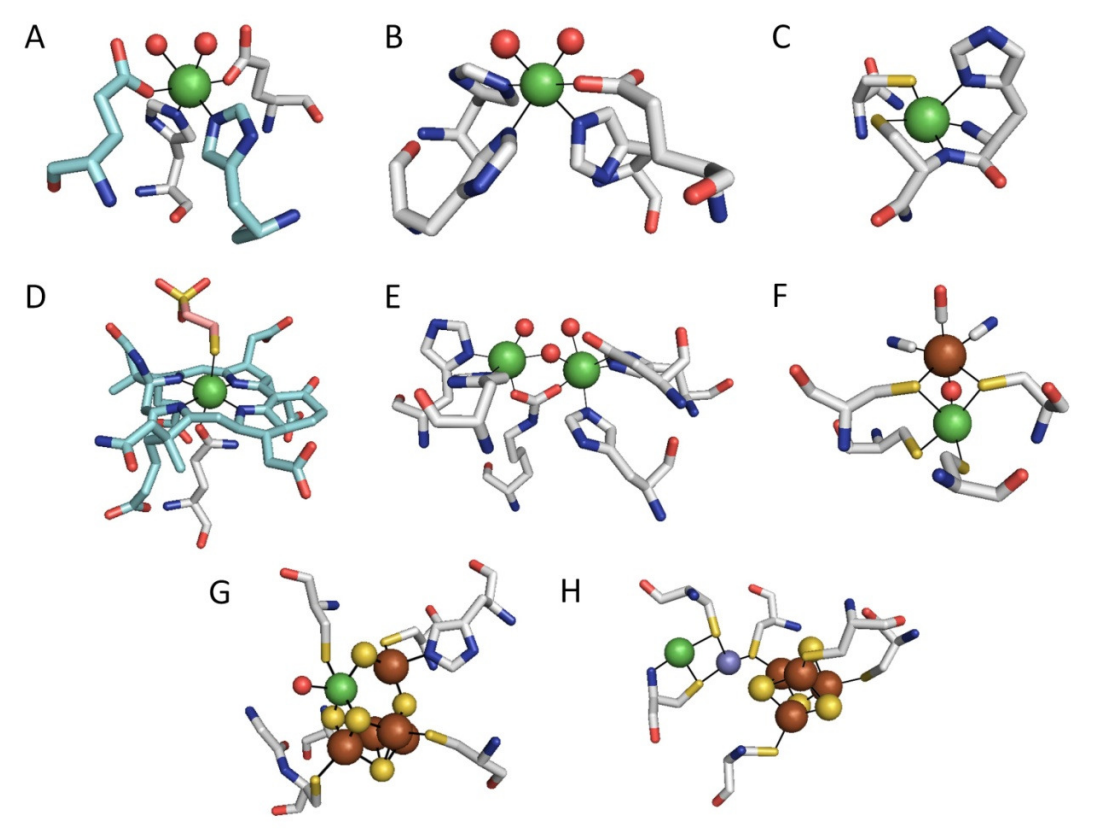


Figure 1.1: Active sites of Ni-containing enzymes. (A) Ni-Glyoxalase I (1F9Z, Escherichia coli). The Ni (green sphere) bridges two subunits (carbons colored by subunit) and is bound by two His and two Glu, with two coordinated waters (red spheres). (B) Acireductone dioxygenase (1ZRR, NMR structure, Klebsiella oxytoca). Ni is coordinated by three His and one Glu, leaving two open coordination sites filled by water. (C) Ni-superoxide dismutase (1T6U, Streptomyces coelicolor). In the oxidized form (shown), the Ni is coordinated by two Cys, the amino-terminal amine, a backbone amide, and an axial His. In the reduced form, the His swings away, leaving a square-planar geometry (not shown). (D) Methyl coenzyme M reductase (1MRO, Methanothermobacter margburgensis). The structure contains a Ni-tetrapyrrole, termed coenzyme F430, with axial coordination by Gln and coenzyme M. (E) Urease (1FWJ, Klebsiella aerogenes). Each Ni is coordinated by two His, terminal waters, and, in one case, by Asp, and the metals are bridged by a lysine carbamate and a hydroxyl group. (F) [NiFe]-Hydrogenase (1YRQ, Desulfovibrio fructosovorans). The Ni is coordinated by four Cys residues, two of which also coordinate Fe (that has a carbon monoxide and two cyanide ligands), plus a bridging ligand whose identity and presence depend on the state of the enzyme. (G) Carbon monoxide dehydrogenase (CODH, 1SU7, Carboxydothermus hydrogenoformans). The Ni is part of a [Ni-4Fe-5S] metallocluster, where the composition varies for proteins from different sources. (H) Acetyl-CoA synthase (ACS, 2Z8Y, Morella thermocetica). One Ni is bound in square-planar geometry to two backbone amides and two Cys while a second Ni (shown here replaced by Cu in blue) is bound to the same two Cys as well as another that is linked to a [4Fe-4S] cluster. A third Ni (not shown) at a distant site in this protein is in a cluster that functions like and closely resembles that in CODH. For interpretation the references to color in this and all other figures, the reader is referred to the electronic version of this dissertation.

Ni-binding sites in non-catalytic proteins

Non-catalytic Ni-binding proteins contain metallocenters (Figure 1.2) that function in Ni sensing, regulation, transport, and delivery (3, 21). These proteins use the same amino acids as already noted for the Ni-enzymes, but an open coordination site is not required. As with some enzymes, non-protein ligands may be used.

Ni sensors and regulators

Ni sensors and regulators play important roles in Ni homeostasis by allowing organisms to maintain constant cellular Ni concentrations through modulation of the transcription of genes encoding Ni uptake or efflux pumps. From a structural perspective, the best studied example of such a protein is NikR. This protein is a repressor of the *nikABCDE* gene cluster encoding a Ni uptake system in *Escherichia coli* and other bacteria (*22, 23*). NikR is a tetramer consisting of two DNA-binding domains and four metal-binding domains. The NikR tetramer binds four Ni ions, each coordinated to a Cys and 3 His (one from a different chain) in a square-planar geometry. NikR from *Helicobacter pylori* has additional five or six-coordinate Ni binding sites, and is a global regulator rather than the more specific *E. coli* homolog (*24*).

Nur is a Ni-dependent regulator that controls expression of Ni- and Fe- superoxide dismutases. It uses three His residues to bind one face of Ni while the remaining octahedral coordination sites can bind other ligands; in the crystal structure those sites are occupied by malonate and ethylene glycol from the crystallization buffer (25).

The Ni sensor RcnR regulates the Ni efflux transporter RcnA. Although no crystal structure is available, site-directed mutagenesis and X-ray absorption spectroscopic results indicate that Ni is coordinated by using 2 His, 1Cys, the amino terminus, a backbone nitrogen,

and another unknown ligand (26). Members of the ArsR/SmtB family also regulate Ni related genes, although the structural details of the metal binding sites are not known (27).

Ni uptake and efflux systems

Much less is known about the structure of Ni binding sites in proteins that import or export this metal ion. The NikABCDE transport system belongs to the ATP-binding cassette transporters (28). NikA is a periplasmic protein that binds Ni using a single His residue and an unidentified organic complex, modeled in the crystal structure as butane-1,2,4-tricarboxylate (29). NikB and NikC are transmembrane proteins, and NikD and NikE are nucleotide-binding proteins. The amino acid ligands used to transiently coordinate Ni as it is taken into the cell remain undefined. In contrast, some potential Ni binding ligands are proposed for the NiCoT family proteins (transporting Ni, Co, or both, depending on the protein) on the basis of mutagenesis studies (30). Nevertheless, the mechanism for discriminating between these metals and the structural details of the metal binding sites are largely unknown (3, 4).

In addition to importing Ni, cells must export this metal ion when in excess. Very little is known about how the Ni efflux proteins bind the metal. For example, *E. coli* uses RcnA as a nickel exporter, however no details about its metal binding site are known.

Metal delivery

Some Ni-containing enzymes require intracellular chaperones to deliver the Ni to the active site (4, 31). For example, ureases generally require four accessory proteins for enzyme activation with UreE serving as a metallochaperone that delivers the Ni (32). This protein binds Ni using His residues which are sometimes localized in His-rich C-termini of the dimeric protein (33-35). Mutagenesis studies have shown that the His-coordinated Ni binding site at the

interface of the UreE dimer (or in the UreE tetramer formed at elevated protein concentrations) is needed for Ni transfer to the urease apoprotein (36). The UreG and UreD urease accessory proteins also have been shown to bind Ni with the metal ligands still undefined, and urease activation may involve a series of Ni transfers (as discussed later).

[NiFe] hydrogenases also require accessory proteins for their assembly. HypA binds one molecule of Zn, which is likely structural, as well as one Ni atom at a second site, the ligands for which are unknown (37, 38). HypB also binds Ni and Zn, and has different numbers of metal binding sites depending on the organism (39-41). Some HypB sequences also have a His-rich tail that can bind multiple Ni atoms (42). A His-rich metal binding domain of *E. coli* SlyD is known to play a role in maturation of its cognate hydrogenase (43, 44) and the Ni-bound structure is available for SlyD from a thermophilic microorganism (45), however not every SlyD homolog possesses this domain.

CODH also has accessory proteins necessary for enzyme activation. A CooC-like protein from *Carboxydothermus hydrogenoformans* has been shown to bind Ni (46, 47), but the homolog in *Rhodospirillum rubrum* did not exhibit detectable Ni binding (48). CooJ contains a multi-His metal-binding motif at its C-terminus and binds four Ni per monomer, but the structural details of those binding sites are unknown (49).

Ni-binding sites also are important in proteins that function in extracellular metal delivery within multi-cellular organisms. Although a structure is not available, extensive studies have shown how serum albumin binds Ni at its amino terminus, including the use of the amino terminal amine, two backbone amides, an Asp, and a His (50).

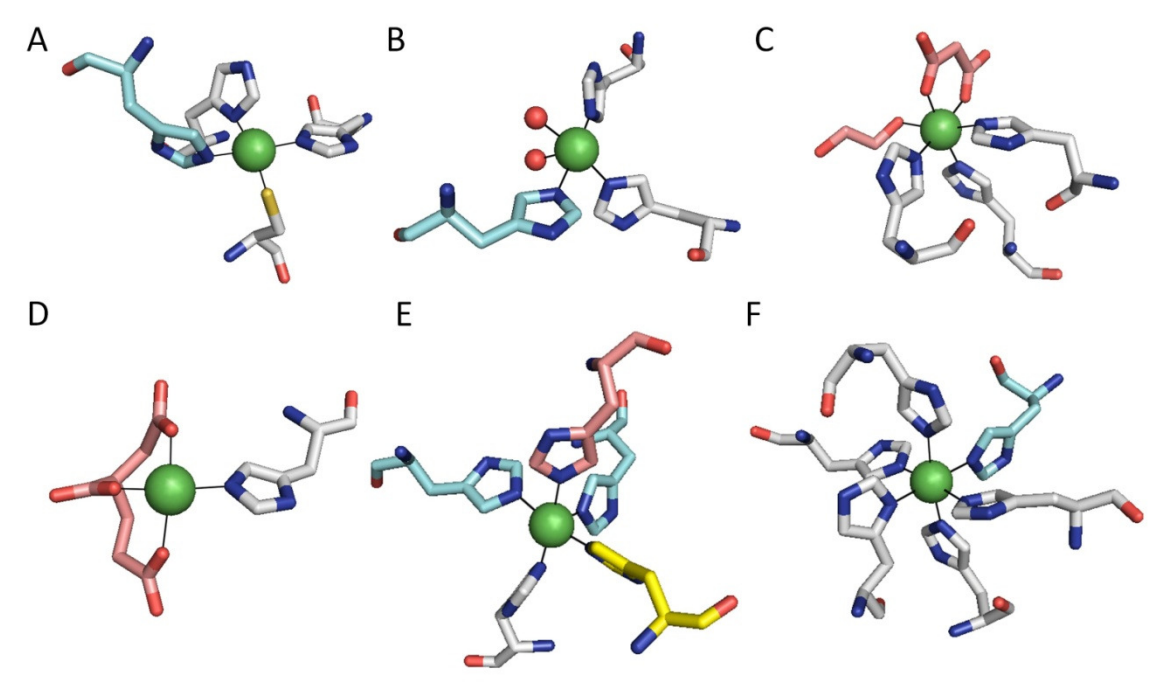


Figure 1.2: Ni-binding sites in Ni-sensor or Ni-delivery proteins. (A) *E. coli* NikR (2HZV) is a tetrameric Ni-responsive repressor with four high affinity binding sites, each coordinated in square-planar geometry by three His and one Cys between subunit pairs. (B) NikR from *Helicobacter pylori* (3LGH) binds Ni in the same manner as the *E. coli* protein in some subunits and forms a distinct five- or six- coordinate site bound to three His in other subunits. (C) Nur (3EYY, *Streptomyces coelicolor*) is a Ni-responsive repressor that is structurally distinct from NikR. The Ni is coordinated by three His, with malonate and ethylene glycol occupying additional sites in the crystal structure shown. (D) NikA (3DP8, *E. coli*) is a periplasmic protein that binds Ni to a single His, additionally using an organic metallophore that was modeled as butane-1,2,4-tricarboxylate. (E) UreE (3NYO, *Helicobacter pylori*) is a metallochaperone involved in urease maturation. The structure shown depicts Ni bound non-symmetrically to five His derived from four different subunits. (F) SlyD (3CGM, *Thermus thermophilus*) is a peptidyl-prolyl isomerase with six His coordinating the metal. The *E. coli* protein has been implicated in Ni metabolism during hydrogenase maturation.

Ni-substituted proteins

Many proteins bind Ni in place of the native metal (Figure 1.3). The first row transition elements Fe, Ni, Cu, and Zn all have similar atomic radii and proteins use the same amino acids to coordinate them. How proteins discriminate between different metals is an open question in the biochemistry of metals. In peptide deformylase, Ni²⁺ substitutes for the physiological, but oxygen-labile, Fe²⁺ and still allows the enzyme to turn over, albeit with reduced kinetics (51). In other cases, Ni substitution for Fe results in a nonfunctional enzyme, as in the lysyl hydroxylase JMJD6 and other α -ketoglutarate dependent dioxygenases (52, 53). substitution of this metal into other members of this enzyme family leads to the hypoxia mimicking effects of Ni²⁺ (54). DtxR, an Fe²⁺-sensitive regulator, also binds Ni²⁺ which promotes its binding to the appropriate sites on DNA in vitro (55). Due to its relatively stable Ni²⁺ redox state, substitution of this metal into Fe or Cu proteins such as rubredoxin (56) or azurin (57) eliminates their electron transfer activities. Finally, there are examples of adventitious Ni-binding sites that are unrelated to protein function, such as the site in ornithine transcarbamylase that connects three subunits (58). Non-catalytic metal binding sites can participate in protein stabilization.

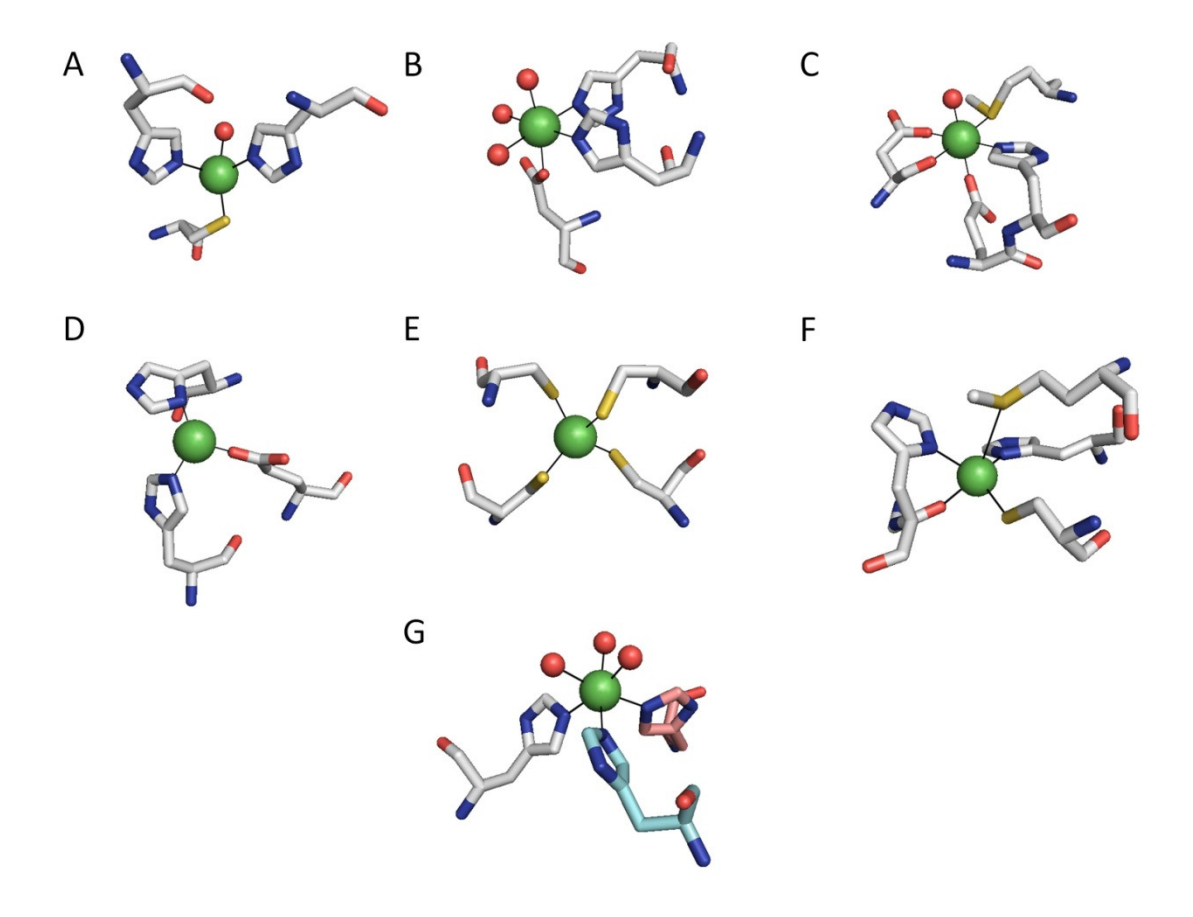


Figure 1.3: Ni-substituted protein metallocenters. (A) Peptide deformylase (1BS7, *E. coli*) is an Fe²⁺ enzyme, but can also bind Ni²⁺ using two His and a Cys to form a site capable of catalyzing the removal of the formyl group from the N-terminus of polypeptide chains. (B) Lysyl hydroxylase JMJD6 (3K2O, *Homo sapiens*), an α-ketoglutarate-dependent dioxygenase, is inhibited by Ni replacing Fe²⁺ at its active site consisting of a two-His-one-carboxylate motif. (C and D) DtxR (2TDX, *Corynebacterium diphtheriae*) regulates genes that encode proteins important to iron uptake and storage. *In vivo* it is specific for iron, but nickel and cobalt bind at two sites (one involving one His, one Met, one Glu, and the side chain and amide of an Asp; the second comprised of two His and one Glu) *in vitro* and promote DNA binding. (E) Rubredoxin (1ROJ, *Clostridium pasteurianum*) contains Fe coordinated by four Cys natively, but the Ni²⁺-substituted protein has been crystallized. (F) Azurin (1NZR, *Pseudomonas aeruginosa*) is a Cucontaining electron carrier that was crystallized with Ni bound to two His (including one His amide), one Cys, and one Met. (G) Ornithine transcarbamylase (2W37, *Lactobacillus hilgardii*) binds metals, including Ni, using three His side chains at its three-fold symmetry axis that is distant from the active site.

Ni-binding to His-tagged proteins

A common purification strategy is to create a fusion between the protein of interest and a poly-His tag (59). The His-rich region serves as an affinity tag for binding to immobilized-metal ion chromatography beads containing attached Ni (60). This tag, though useful for purification, can cause protein aggregation due to the His residues from multiple proteins coalescing to chelate nickel. Figure 1.4 shows the poly-His tail from three subunits of a tagged protein coming together to bind Ni (61).

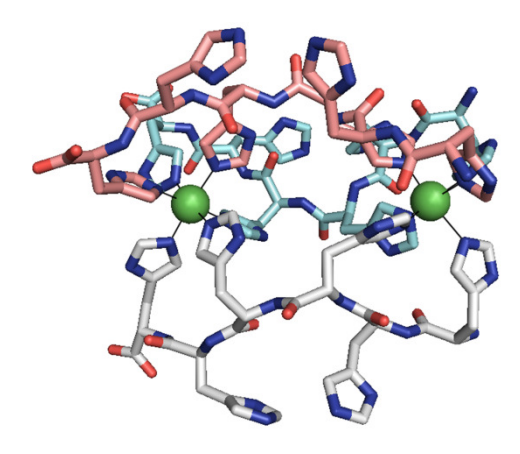


Figure 1.4: His-tag used for affinity purification. A commonly used protein purification procedure is to construct an expression system where the gene of interest is fused to a sequence encoding a poly-His tag, allowing for isolation by immobilized-metal ion chromatography. The structure shown (1Q3I, a sodium, potassium-ATPase) illustrates the mode by which the His region of three tags can aggregate when binding Ni, with each metal ion coordinated by six His.

INTRODUCTION TO UREASE

Urease is typically a Ni-containing enzyme (although there is an Fe-containing example (62)) found in plants, fungi, and bacteria. It was the first enzyme to be crystallized (63), as well as the first shown to contain Ni (64). It catalyzes the hydrolysis of urea into ammonia and carbamic acid, which spontaneously decomposes into carbonic acid and ammonia as shown below.

$$H_2N-C(O)-NH_2 + H_2O \rightarrow NH_3 + H_2N-COOH$$

$$H_2N$$
-COOH + $H_2O \rightarrow NH_3 + H_2CO_3$

Urease plays a significant role in several biological processes. Perhaps of greatest importance, it is a virulence factor in many pathogenic organisms. For example, *Helicobacter pylori* utilizes a high concentration of urease (up to 10% of the cellular protein (65)) to produce ammonia which buffers the acidic environment of the stomach. *H. pylori* infection, occurring in approximately half of the world's population, can result in gastric ulcers in a small percentage of cases which may develop into carcinomas if left untreated (66). Other organisms (e.g. *Proteus mirabilis*) cause infection stones and pyelonephritis due to urease-derived increase in pH, with consequent precipitation of struvite or apatite crystals, and elevated ammonia concentrations (67). Urease also is involved in the plant nitrogen cycle, where a variety of enzymes in plant tissues degrade fixed forms of nitrogen (proteins and nucleotides) to urea, and then cytoplasmic urease releases ammonia which is used by the plant (68). Finally, urea is a common fertilizer that is decomposed by plant ureases, but it comes with the inherent

problem of potentially uncontrolled hydrolysis by microorganisms in the soil, which can lead to pH imbalance and ammonia toxicity (68).

Urease structure

Ureases from bacteria and plants have a similar tertiary structure and active site (Figure 1.1E), despite being derived from differing numbers of gene products (Figure 1.5). *K. aerogenes* urease has been well-studied and has a structure typical of many bacterial ureases (13, 14) The gene products from *ureA*, *ureB*, and *ureC* produce the subunits that form the urease enzyme (69); *ureD*, *ureE*, *ureF*, and *ureG* encode accessory proteins needed for maturation. UreA and UreB are small (11.1 and 11.7 kDa, respectively), whereas UreC, which contains the active site residues, is much larger (60 kDa). These subunits come together to form a (UreABC)₃ structure (Figure 1.6A) (13). In *Helicobacter* species, UreA is a fusion of the two small subunits in *K. aerogenes*, and UreB is equivalent to *K. aerogenes* UreC. *Helicobacter* proteins UreA and UreB form a homodimer, three of these dimers trimerize, and four of these trimers create the supramolecular structure of ((UreAB)₃)₄ (Figure 1.6B) (70). Ureases from eukaryotes only contain one polypeptide, which is a fusion of all three subunits from *K. aerogenes*. These come together to form a trimer, which then dimerizes (Figure 1.6C) (71, 72).

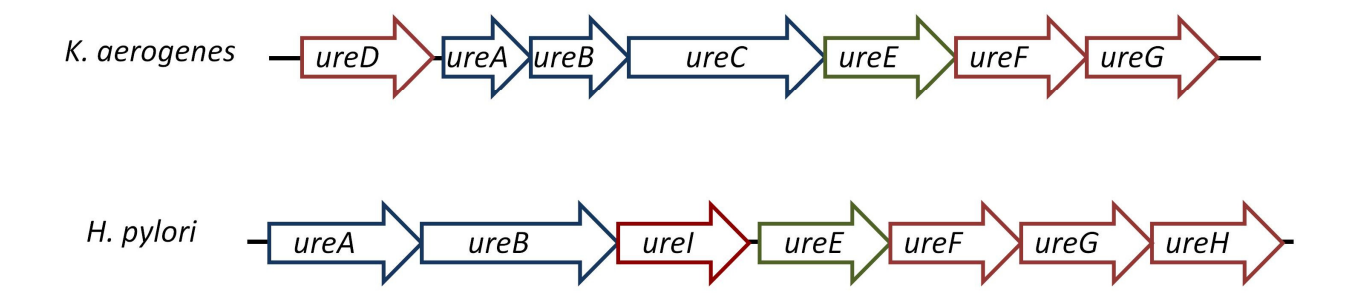


Figure 1.5: Genetic structures of the urease gene clusters from *K. aerogenes* and *H. pylori*. Three genes encoding the *K. aerogenes* enzyme subunits are show in blue, whereas accessory genes are shown in magenta or, for the gene encoding a metallochaperone, in green. In *H. pylori*, sequences corresponding to the above small urease subunit genes are fused into a single gene labeled *ureA*, the large subunit is named *ureB*, *ureD* is renamed *ureH* and shifted in position, and a proton-gated urea channel gene (*ureI*) is inserted.

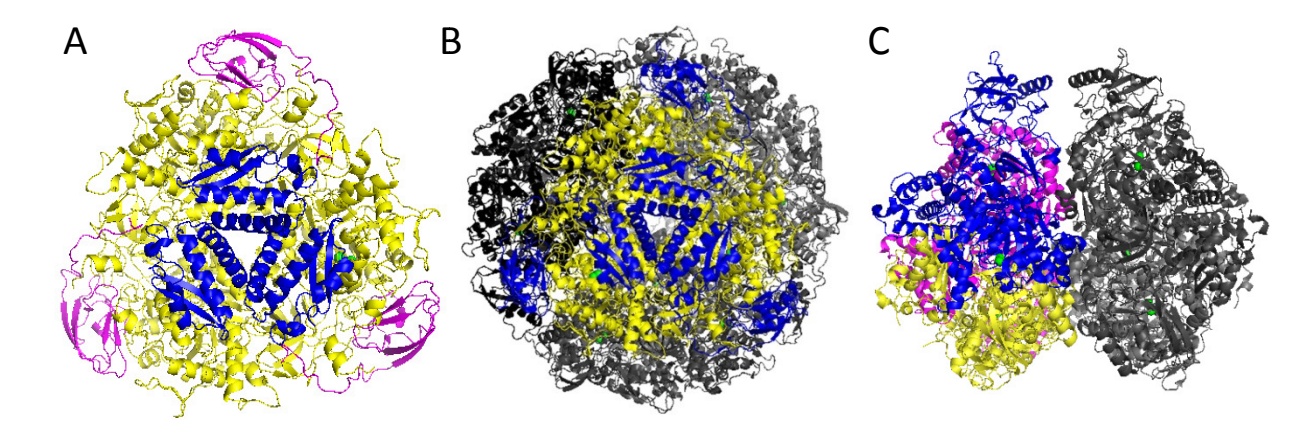


Figure 1.6: Urease structures can form different supramolecular structures. A. Cartoon representation of urease from *Klebsiella aerogenes* (1FWJ) with UreA in blue, UreB in magenta, UreC in yellow, and Ni atoms represented as green spheres. UreABC forms a trimer. B. Urease from *H. pylori* (1E9Z) is presented with UreA in blue and UreB in yellow for one trimer of dimers. This trimer comes together with three more trimers (shades of gray) to form a ((UreAB)₃)₄ structure. C. Jack bean urease (3LA4) is a single polypeptide (shown in blue, yellow, or maroon). Three of these polypeptides come together to form a trimer similar to the *K. aerogenes* structure, which then dimerizes (dimer partner in gray, figure is rotated 90° compared to the other two).

Urease from *K. aerogenes* can be purified in a Ni-free (apoprotein) form, which also lacks the carbamylated Lys residue (73, 74). Under conditions with high levels of nickel and

bicarbonate (100 μ M and 100 mM, respectively, with the latter needed as a CO₂ donor for the carbamylated lysine at the active site), purified apoprotein can be activated to about 15% of the fully active enzyme (purified from *E. coli* expressing the urease operon and supplemented with Ni) (75). After apoprotein activation there are nearly two Ni atoms per UreC, indicating that most of the active sites are not properly formed even though they have the correct number of metal ions (76).

Urease activation

Maturation of urease requires four other genes that typically are found surrounding the urease structural genes in bacteria: *ureD* (*ureH* in *Helicobacter* species), *ureE*, *ureF*, and *ureG* (Figure 1.5). Deletions in *K. aerogenes ureD*, *ureF*, or *ureG* expressed in *E. coli* resulted in inactive urease; deletions in *ureE* allowed for partially active urease (69). These genes encode accessory proteins necessary for delivering the Ni and assembling the active site. The best-studied activation system is that from *K. aerogenes*, where the accessory proteins have been purified and characterized individually, as well as in complexes. Figure 1.7 summarizes what is known about the activation process.

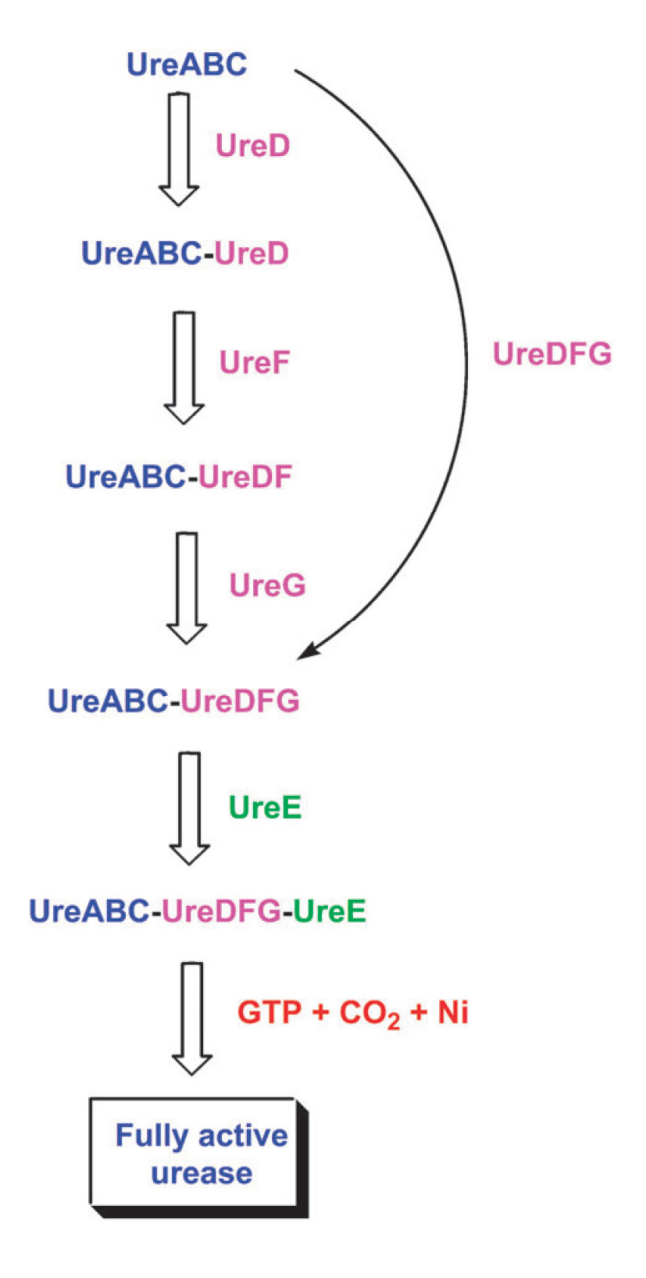


Figure 1.7: Interactions among urease-related proteins. The urease apoprotein either sequentially binds UreD, UreF, and UreG or a preformed UreD—UreF—UreG (abbreviated UreDFG) complex. In the resulting pre-activation complex, the UreDFG heterotrimer acts as a GTP-dependent molecular chaperone. UreE serves as a metallochaperone, delivering the Ni atoms necessary for active site formation to the UreABC—UreDFG complex. CO₂ is required to form the carbamylated lysine metal ligand, and GTP hydrolysis (occurring in UreG) drives the metallocenter assembly process to form active urease. Finally, the accessory proteins are released.

UreD is insoluble when expressed alone, but a translational fusion with maltose binding protein (MBP) allowed for the creation of the soluble MBP-UreD (77). MBP-UreD partially complements a ureD knockout strain, indicating that it can functionally replace UreD. MBP-UreD binds ~2.5 Ni (K_d 50 μ M) or ~4 Zn (K_d 5 μ M) per protomer. This fusion protein forms a complex with (UreABC)₃ when the genes are co-expressed, but surprisingly does not when the purified proteins are incubated together. Experiments using cell-free extracts of cells coexpressing MBP-UreD with the other accessory proteins demonstrated interactions between UreD and UreF, UreD and UreG, and UreD, UreF, and UreG. In vitro experiments confirmed the interaction between MBP-UreD and UreF (as UreE-F) (77). A complex of (UreABC—UreD)₃ also can be purified, and it has greater in vitro activation competence (30% of available active sites) than the urease apoprotein alone (15%) when incubated with high levels of Ni and bicarbonate (78). This complex represents the urease apoprotein with UreD binding at the vertices of the triangular structure according to small angle X-ray scattering (SAXS) (79) and chemical crosslinking (80) experiments. A crystal structure of the UreD homolog from H. pylori (UreH) has been solved in complex with UreF as a (UreH-UreF)₂ heterodimer (Figure 1.8). UreH has a novel protein fold containing 17 β -sheets and 2 α -helices (81).

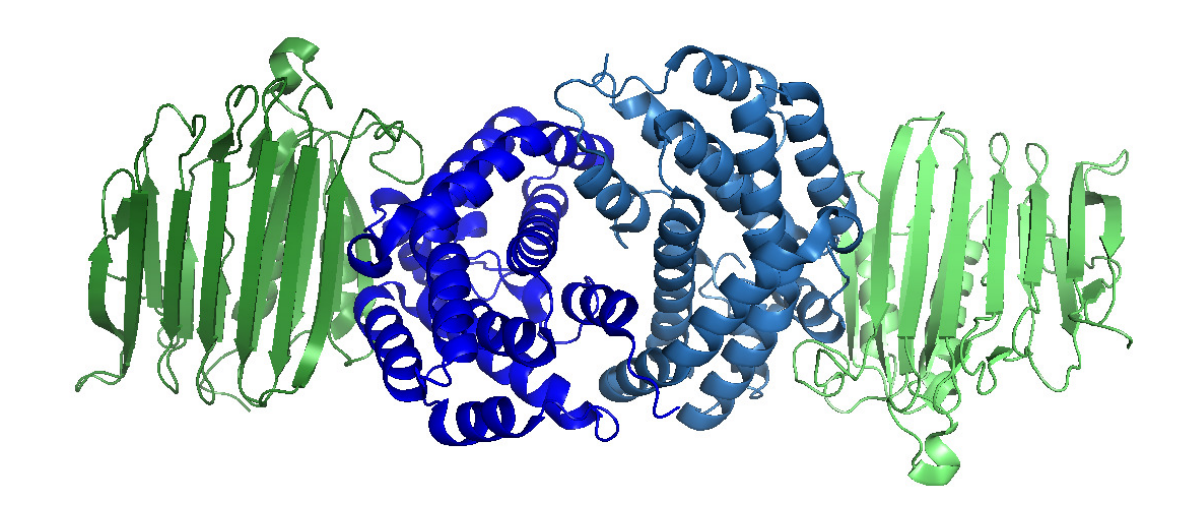


Figure 1.8: Crystal structure (3FS5) of (UreH—UreF)₂ from *H. pylori*. The UreF dimer is shown in shades of blue, and UreH is in shades of green.

UreF from *H. pylori* has been crystallized, both as a C-terminal truncation (*82*) and as a (UreH—UreF)₂ complex (Figure 1.8) (*81*). This protein crystallizes as a dimer, and its N-terminal 24 residues are disordered (these residues are not present in *K. aerogenes* UreF). It has a novel all alpha-helical fold with highly conserved residues mapping to one face of the crystal dimer (*82*). A modeling study of UreF from *Bacillus pasteruii* suggested that it may play a role as a GTPase activating protein (GAP), stimulating the GTPase activity of UreG (*83*). *K. aerogenes* UreF is insoluble when expressed alone; whereas a MalE fusion is soluble, but has not been characterized (*84*). A translational fusion of *ureE* and *ureF* (termed UreE-F) is also soluble and complements a UreF knockout strain, indicating that it is a functional UreF (*85*). Deletion mutants demonstrated that the N- and C-termini are essential for urease activation, and the highly conserved C-terminal 15 residues are essential for binding the activation complex. UreE-F is able to bind (UreABC—UreD)₃ *in vivo* and *in vitro* (*85*). A complex of (UreABC—UreD—UreF)₃ can be purified from cells expressing all five genes; however, no complex is formed

when UreD is absent (86). This complex represents the UreD—UreF heterodimer binding to the vertices of the (UreABC)₃ apoprotein according to SAXS analysis (79). *In vitro* activation of this species results in the same percentage of active urease as the complex containing only apoprotein and UreD; however, the complex can be activated under lower concentrations of bicarbonate due to less nickel-dependent inhibition (86). Cross-linking studies of the (UreABC—UreD—UreF)₃ complex demonstrated a link between residues in UreB and UreC, known in the crystal structure to be very distant from each other, leading to the hypothesis that this complex allows for UreB to undergo a conformational change to allow access to the active site during the activation process (79, 80).

UreG is soluble when expressed alone, and has been characterized in *K. aerogenes*, *H. pylori*, *B. pasteurii*, and *Mycobacterium tuberculosis* (87-91). It belongs to the G3E class of SIMBI small GTPases, characterized by a signature motif (ESGG at positions 104-107 in *K. aerogenes* UreG), as well as a P-loop motif and a guanine specificity loop (92, 93). Other members of this family include HypB, a structurally-characterized [Ni-Fe] hydrogenase maturation protein (39), and MeaB, which is involved in delivering vitamin B₁₂ to methylmalonyl-CoA mutase (94). Despite having a sequence characteristic of a GTPase, UreG from *K. aerogenes* and *H. pylori* do not have any GTPase activity as purified (87, 91); UreG from *B. pasteurii* and *M. tuberculosis* have very low but detectable levels (88, 90). UreG from *K. aerogenes* is monomeric (87), whereas the *B. pasteruii* and *M. tuberculosis* proteins are dimeric (89, 90), and *H. pylori* UreG undergoes zinc-dependent dimerization (91). All UreG proteins are known to bind metal ions, although the number and binding affinities vary depending on the

source organism (88, 90, 91). The UreABC—UreD—UreF—UreG complex from *K. aerogenes* has been purified (95). This complex demonstrates GTP-dependent urease activation, and 60% of the protein can be activated under optimal conditions of GTP, Ni, and bicarbonate concentrations. Mutations in the P-loop of UreG eliminate the GTP-dependence and have very low activity *in vivo*, highlighting the importance of GTP binding for urease activation. GMP-PNP, a non-hydrolysable GTP analog, does not have the same enhancement effect, indicating that hydrolysis of GTP is essential for urease activation (95). No crystal structure is available for UreG, possibly because of its intrinsically disordered nature according to nuclear magnetic resonance (NMR), circular dichroism, and fluorescence spectroscopic analysis (89, 96). A crystal structure for a related protein, HypB from *Methanocaldococcus jannaschii*, is known (39). This crystal structure shows a dimeric protein when GTP is bound containing two types of zinc binding sites: a mononuclear site in each subunit uses residues not conserved in UreG, and a nonsymmetrical dinuclear binding site at the subunit interface, the ligands for which are conserved in UreG.

In addition to the individually purified proteins and their complexes with apourease, several complexes containing UreD—UreF—UreG have been isolated. When the *ureD*, *ureF*, and *ureG* genes are expressed together, a predominantly insoluble UreD—UreF—UreG complex is formed. This complex can be partially solubilized by low concentrations of detergent and purified using ATP-linked agarose (87). The MBP-UreD—UreF—UreG complex is soluble, has been purified, and forms a complex with (UreABC)₃ *in vitro* (77, 97). These complexes demonstrate that UreD, UreF, and UreG may not bind sequentially to urease, but instead may assemble into a pre-formed complex before binding to apourease.

UreE is the metallochaperone that delivers the Ni ions to the activation complex. The structures of a C-terminal truncation form of the protein from *K. aerogenes* (*35*), and the full-length proteins from *B. pasteruii* (*33*) and *H. pylori* (*34*) have been solved with bound Cu, Zn, and Ni respectively (Figure 1.2E, 1.9). In *K. aerogenes*, UreE binds approximately six Ni atoms per homodimer, mostly utilizing a His-rich tail that is not essential for urease activation (*98*). Using a truncation mutant lacking the His-rich C-terminus (UreE H144*), it was shown that two other His residues, 110 and 112, participate in binding Ni, but these sites are not necessary for urease activation (*36*). By contrast, His 96 plays a critical role in transferring the metal to the active site (*99*). Importantly, when UreE is incubated with the UreABC—UreD—UreF—UreG complex under biologically relevant concentrations of Ni, bicarbonate, and GTP, urease activity reaches wild-type levels (*100*).

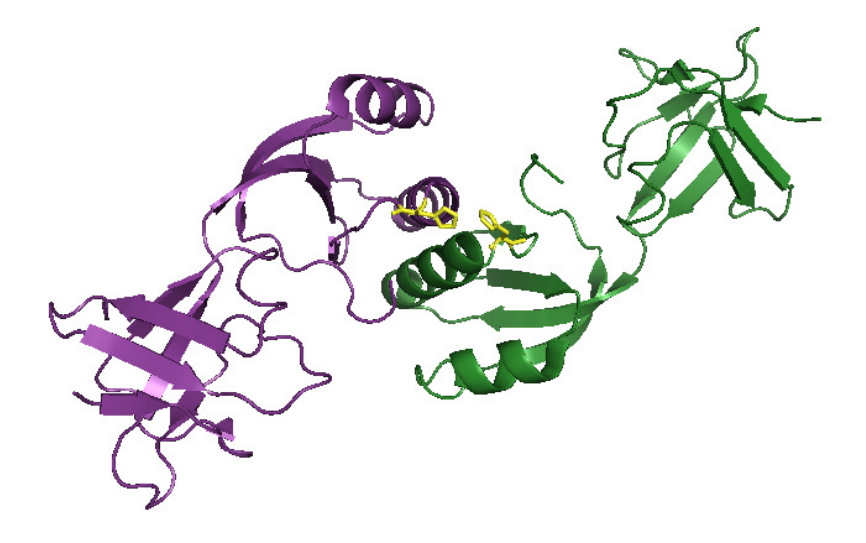


Figure 1.9: Crystal structure (1GMW) of truncated UreE from *K. aerogenes*. Protomers are shown in purple and green. Key Ni-binding residue His96 in each subunit is shown in yellow.

Eukaryotic urease activation

The mechanism of urease activation has been extensively investigated in the case of bacterial ureases; however, many fungi and plants also possess this enzyme which must

undergo analogous activation processes. Genetic and biochemical studies related to urease activation in eukaryotes are summarized below.

Fungal ureases contain a single type of subunit, but genetic studies reveal that multiple genes are needed for urease expression. For example, early studies with *Neurospora crassa* (101-103), *Aspergillus nidulans* (104, 105), and *Schizosaccharomyces pombe* (106) show that four distinct loci are required for obtaining active enzyme. The best studied fungal urease system is that in the fission yeast *S. pombe* where the enzyme was purified (107), the structural gene (*ure2*) identified (108), and candidate genes encoding UreD (*ure4*), UreF (*ure3*), and UreG (*ure1*) were identified (109). Of interest, the fungal UreG has 61% sequence identity to soybean UreG (see below) including the presence of a His-rich N-terminus that is not found in bacterial UreG sequences. The fungal UreF protein of *S. pombe* shares only 20% sequence identity with the soybean protein, but the plant gene rescues the corresponding yeast mutant, whereas this situation is not observed for UreD where the proteins share 30% sequence identity (109).

Plants can possess multiple urease isozymes as well as genes encoding several maturation proteins. The historically interesting jack bean (*Canavalia ensiformis*) system includes two structural urease genes (*110*, *111*), but no accessory genes have yet been reported. The better-studied soybean (*Glycine max*) system also has two urease isozymes: an embryo-specific form encoded at the *Eu1* locus (*112*, *113*) and a ubiquitously-expressed species encoded at the *Eu4* locus (*114*, *115*). In addition, this plant contains several demonstrated urease accessory genes. For example, soybean genes encoding UreD and UreF are orthologues of the bacterial and fungal genes; in the latter case, the plant gene complements a mutant involving the corresponding gene in *S. pombe* (*109*). The *Eu3* locus was long known to exhibit

pleiotropic effects on both ureases (113), and more recently was shown to encode a protein related to bacterial UreG proteins with a conserved P-loop motif and an added His-rich N-terminus that resembles the C-terminus of some bacterial UreE proteins and is probably involved in nickel binding (116). This UreG was purified from seeds and as a recombinant protein. It binds Zn very tightly, and Ni with less affinity. Zn also stabilizes a dimeric form of the protein. As with bacterial UreGs, this UreG is intrinsically disordered according to NMR (117). Eu2 encodes another protein necessary for activation of both ureases (113). This gene, analogous to bacterial *ureF*, was duplicated and found on chromosome 2 and chromosome 14, with the Ch2 copy being the dominant one (118). Homologues encoding UreD-, UreF-, and UreG-like proteins are now known to exist in many other plant species, including tomato (Lycopersicon esculentum), potato (Solanum tuberosum), and Arabidopsis thaliana (109, 119, 120). Of interest, the gene encoding potato UreG complements a K. aerogenes ureG mutation (119) and insertions into each of the three accessory genes of A. thaliana abolished urease activity (120).

REMAINING QUESTIONS

Even though the accessory proteins involved in urease activation are known, the details of how they work together to assemble the active site are still elusive. There is no clear picture of how UreD, UreF, UreG and UreE interact, or how the accessory proteins bind to (UreABC)3. UreD and UreG bind Ni, but the ligands they use and how Ni is transferred from UreE into the active site of urease remains elusive. One hypothesis is that UreE transfers the Ni to UreG, which shifts it to UreD, and then into the active site (121). There are several possible roles for GTPase activity in the activation process that need to be tested. It could be utilized to activate bicarbonate for lysine carbamylation (as stated in several publications (117, 122), but without any evidence), it might be needed for a series of metal transfers, it may play a role in "gating" the active site from incorrect metal incorporation, or it could be needed for dissociation of the accessory proteins after the activation is complete.

This dissertation seeks to answer some of the remaining questions about the functions of UreG and UreF. In chapter 2, I present my work on UreG that describes the Ni- and Zn-binding properties of wild-type and *Strep*-tagged versions of the protein, along with mutants involving potential metal-binding residues. I also examine these UreG variants for their abilities to disrupt the binding to the other urease proteins in cell-free extracts. Additionally I investigate the Ni-dependent interaction between UreG and UreE. In chapter 3 I move to UreF, first elucidating the roles played by conserved residues in protein:protein interactions, then looking into UreF's proposed role as a GTPase activating protein (GAP) for UreG by focusing on the conserved residue Lys165. Finally, in chapter 4 I describe some additional studies I have done, including my role in a collaborative effort trying to understand the role of UreB and

REFERENCES

REFERENCES

- 1. Hausinger, R. P. (1993) *Biochemistry of Nickel*, Plenum Press, New York.
- 2. Sigel, A., Sigel, H., and Sigel, R. K. O., (Eds.) (2007) *Nickel and Its Surprising Impact in Nature*, Vol. 2, John Wiley & Sons, Ltd, Chichester, UK.
- 3. Li, Y., and Zamble, D. B. (2009) Nickel homeostasis and nickel regulation: an overview, *Chem. Rev.* 109, 4617-4643.
- 4. Mulrooney, S. B., and Hausinger, R. P. (2003) Nickel uptake and utilization by microorganisms, *FEMS Microbiol. Rev.* 27, 239-261.
- 5. Ragsdale, S. W. (2009) Nickel-based enzyme systems, J. Biol. Chem. 284, 18571-18575.
- 6. He, M. M., Clugston, S. L., Honek, J. F., and Matthews, B. W. (2000) Determination of the structure of *Escherichia coli* glyoxalase I suggests a structural basis for differential metal activation, *Biochemistry 39*, 8719-8727.
- 7. Pochapsky, T. C., Pochapsky, S. S., Ju, T. T., Hoefler, C., and Liang, J. (2006) A refined model for the structure of acireductone dioxygenase from *Klebsiella* ATCC 8724 incorporating residual dipolar couplings, *J. Biomol. NMR 34*, 117-127.
- 8. Chai, S. C., Ju, T. T., Dang, M., Goldsmith, R. B., Maroney, M. J., and Pochapsky, T. C. (2008) Characterization of metal binding in the active sites of acireductone dioxygenase isoforms from *Klebsiella* ATCC 8724, *Biochemistry 47*, 2428-2438.
- 9. Barondeau, D. P., Kassmann, C. J., Bruns, C. K., Tainer, J. A., and Getzoff, E. D. (2004) Nickel superoxide dismutase structure and mechanism, *Biochemistry 43*, 8038-8047.
- 10. Wuerges, J., Lee, J. W., Yim, Y. I., Yim, H. S., Kang, S. O., and Carugo, K. D. (2004) Crystal structure of nickel-containing superoxide dismutase reveals another type of active site, *Proc. Natl. Acad. Sci. U.S.A. 101*, 8569-8574.
- 11. Ermler, U., Grabarse, W., Shima, S., Goubeaud, M., and Thauer, R. K. (1997) Crystal structure of methyl coenzyme M reductase: The key enzyme of biological methane formation, *Science 278*, 1457-1462.
- 12. Shima, S., Krueger, M., Weinert, T., Demmer, U., Kahnt, J., Thauer, R. K., and Ermler, U. (2012) Structure of a methyl-coenzyme M reductase from Black Sea mats that oxidize methane anaerobically, *Nature 481*, 98-101.
- 13. Jabri, E., Carr, M. B., Hausinger, R. P., and Karplus, P. A. (1995) The crystal structure of urease from *Klebsiella aerogenes*, *Science 268*, 998-1004.

- 14. Pearson, M. A., Schaller, R. A., Michel, L. O., Karplus, P. A., and Hausinger, R. P. (1998) Chemical rescue of *Klebsiella aerogenes* urease variants lacking the carbamylated-lysine nickel ligand, *Biochemistry 37*, 6214-6220.
- 15. Volbeda, A., Martin, L., Cavazza, C., Matho, M., Faber, B. W., Roseboom, W., Albracht, S. P. J., Garcin, E., Rousset, M., and Fontecilla-Camps, J. C. (2005) Structural differences between the ready and unready oxidized states of [NiFe] hydrogenases, *J. Biol. Inorg. Chem.* 10, 239-249.
- 16. Eidsness, M. K., Scott, R. A., Prickril, B. C., Dervartanian, D. V., Legall, J., Moura, I., Moura, J. J. G., and Peck, H. D. (1989) Evidence for selenocysteine coordination of the active site nickel in the [NiFeSe] hydrogenases from *Desulfovibrio baculatus, Proc. Natl. Acad. Sci. U.S.A. 86*, 147-151.
- 17. Dobbek, H., Svetlitchnyi, V., Liss, J., and Meyer, O. (2004) Carbon monoxide induced decomposition of the active site [Ni-4Fe-5S] cluster of CO dehydrogenase, *J. Am. Chem. Soc. 126*, 5382-5387.
- 18. Bender, G., Pierce, E., Hill, J. A., Darty, J. E., and Ragsdale, S. W. (2011) Metal centers in the anaerobic microbial metabolism of CO and CO₂, *Metallomics 3*, 797-815.
- 19. Doukov, T. I., Blasiak, L. C., Seravalli, J., Ragsdale, S. W., and Drennan, C. L. (2008) Xenon in and at the end of the tunnel of bifunctional carbon monoxide dehydrogenase/acetyl-CoA synthase, *Biochemistry 47*, 3474-3483.
- 20. Gencic, S., and Grahame, D. A. (2003) Nickel in subunit beta of the acetyl-CoA decarbonylase/synthase multienzyme complex in methanogens, *J. Biol. Chem. 278*, 6101-6110.
- 21. Kaluarachchi, H., Chan Chung, K. C., and Zamble, D. B. (2010) Microbial nickel proteins, *Nat. Prod. Rep. 27*, 681-694.
- 22. De Pina, K., Desjardin, V., Mandrand-Berthelot, M. A., Giordano, G., and Wu, L. F. (1999) Isolation and characterization of the *nikR* gene encoding a nickel-responsive regulator in *Escherichia coli*, *J. Bacteriol.* 181, 670-674.
- 23. Schreiter, E. R., Wang, S. C., Zamble, D. B., and Drennan, C. L. (2006) NikR-operator complex structure and the mechanism of repressor activation by metal ions, *Proc. Natl. Acad. Sci. U.S.A.* 103, 13676-13681.
- 24. West, A. L., St John, F., Lopes, P. E. M., MacKerell, A. D., Jr., Pozharski, E., and Michel, S. L. J. (2010) Holo-Ni(II)*Hp*NikR Is an asymmetric tetramer containing two different nickel-binding sites, *J. Am. Chem. Soc.* 132, 14447-14456.

- 25. An, Y. J., Ahn, B.-E., Han, A. R., Kim, H.-M., Chung, K. M., Shin, J.-H., Cho, Y.-B., Roe, J.-H., and Cha, S.-S. (2009) Structural basis for the specialization of Nur, a nickel-specific Fur homolog, in metal sensing and DNA recognition, *Nucleic Acids Research 37*, 3442-3451.
- 26. Iwig, J. S., Leitch, S., Herbst, R. W., Maroney, M. J., and Chivers, P. T. (2008) Ni(II) and Co(II) sensing by *Escherichia coli* RcnR, *J. Am. Chem. Soc. 130*, 7592-7606.
- 27. Ma, Z., Jacobsen, F. E., and Giedroc, D. P. (2009) Coordination chemistry of bacterial metal transport and sensing, *Chem. Rev.* 109, 4644-4681.
- 28. Navarro, C., Wu, L. F., and Mandrandberthelot, M. A. (1993) The Nik operon of *Escherichia coli* encodes a periplasmic binding protein-dependent transport system for nickel, *Mol. Microbiol. 9*, 1181-1191.
- 29. Cherrier, M. V., Cavazza, C., Bochot, C., Lemaire, D., and Fontecilla-Camps, J. C. (2008) Structural characterization of a putative endogenous metal chelator in the periplasmic nickel transporter NikA, *Biochemistry 47*, 9937-9943.
- 30. Eitinger, T., Suhr, J., Moore, L., and Smith, J. A. C. (2005) Secondary transporters for nickel and cobalt ions: Theme and variations, *Biometals* 18, 399-405.
- 31. Quiroz, S., Kim, J. K., Mulrooney, S. M., and Hausinger, R. P. (2007) Chaperones of nickel metabolism, in *Nickel and Its Surprising Impact on Nature* (Sigel, A., H. Sidel, R. K. O. Sigel, Ed.), pp 519-544, John Wiley & Sons, Ltd., Chichester, UK.
- 32. Carter, E. L., Flugga, N., Boer, J. L., Mulrooney, S. M., and Hausinger, R. P. (2009) Interplay of metal ions and urease, *Metallomics* 1, 207-221.
- 33. Remaut, H., Safarov, N., Ciurli, S., and Van Beeumen, J. (2001) Structural basis for Ni²⁺ transport and assembly of the urease active site by the metallochaperone UreE from *Bacillus pasteurii*, *J. Biol. Chem. 276*, 49365-49370.
- 34. Banaszak, K., Martin-Diaconescu, V., Bellucci, M., Zambelli, B., Rypniewski, W., Maroney, M. J., and Ciurli, S. (2012) Crystallographic and X-ray absorption spectroscopic characterization of *Helicobacter pylori* UreE bound to Ni²⁺ and Zn²⁺ reveals a role for the disordered C-terminal arm in metal trafficking, *Biochem. J. 441*, 1017-1026.
- 35. Song, H. K., Mulrooney, S. B., Huber, R., and Hausinger, R. P. (2001) Crystal structure of *Klebsiella aerogenes* UreE, a nickel-binding metallochaperone for urease activation, *J. Biol. Chem.* 276, 49359-49364.
- 36. Colpas, G. J., Brayman, T. G., Ming, L. J., and Hausinger, R. P. (1999) Identification of metal-binding residues in the *Klebsiella aerogenes* urease nickel metallochaperone, UreE, *Biochemistry 38*, 4078-4088.

- 37. Watanabe, S., Arai, T., Matsumi, R., Atomi, H., Imanaka, T., and Miki, K. (2009) Crystal structure of HypA, a nickel-binding metallochaperone for [NiFe] hydrogenase maturation, *J. Mol. Biol.* 394, 448-459.
- 38. Xia, W., Li, H., Sze, K.-H., and Sun, H. (2009) Structure of a nickel chaperone, HypA, from *Helicobacter pylori* reveals two distinct metal binding sites, *J. Am. Chem. Soc. 131*, 10031-10040.
- 39. Gasper, R., Scrima, A., and Wittinghofer, A. (2006) Structural insights into HypB, a GTP-binding protein that regulates metal binding, *J. Biol. Chem.* 281, 27492-27502.
- 40. Leach, M. R., Sandal, S., Sun, H. W., and Zamble, D. B. (2005) Metal binding activity of the *Escherichia coli* hydrogenase maturation factor HypB, *Biochemistry 44*, 12229-12238.
- 41. Sydor, A. M., Liu, J., and Zamble, D. B. (2011) Effects of metal on the biochemical properties of *Helicobacter pylori* HypB, a maturation factor of [NiFe]-hydrogenase and urease, *Journal of Bacteriology* 193, 1359-1368.
- 42. Olson, J. W., Fu, C. L., and Maier, R. J. (1997) The HypB protein from *Bradyrhizobium japonicum* can store nickel and is required for the nickel-dependent transcriptional regulation of hydrogenase, *Mol. Microbiol.* 24, 119-128.
- 43. Kaluarachchi, H., Zhang, J. W., and Zamble, D. B. (2011) *Escherichia coli* SlyD, more than a Ni(II) reservoir, *Biochemistry 50*, 10761-10763.
- 44. Leach, M. R., Zhang, J. W., and Zamble, D. B. (2007) The role of complex formation between the *Escherichia coli* hydrogenase accessory factors HypB and SlyD, *J. Biol. Chem.* 282, 16177-16186.
- 45. Loew, C., Neumann, P., Tidow, H., Weininger, U., Haupt, C., Friedrich-Epler, B., Scholz, C., Stubbs, M. T., and Balbach, J. (2010) Crystal structure determination and functional characterization of the metallochaperone SlyD from *Thermus thermophilus*, *J. Mol. Biol.* 398, 375-390.
- 46. Jeoung, J.-H., Giese, T., Gruenwald, M., and Dobbek, H. (2010) Crystal structure of the ATP-dependent maturation factor of Ni,Fe-containing carbon monoxide dehydrogenases, *J. Mol. Biol.* 396, 1165-1179.
- 47. Jeoung, J.-H., Giese, T., Gruenwald, M., and Dobbek, H. (2009) CooC1 from *Carboxydothermus hydrogenoformans* is a nickel-binding ATPase, *Biochemistry 48*, 11505-11513.
- 48. Jeon, W. B., Cheng, J. J., and Ludden, P. W. (2001) Purification and characterization of membrane-associated CooC protein and its functional role in the insertion of nickel into

- carbon monoxide dehydrogenase from *Rhodospirillum rubrum*, *J. Biol. Chem. 276*, 38602-38609.
- 49. Watt, R. K., and Ludden, P. W. (1998) The identification, purification, and characterization of CooJ A nickel-binding protein that is CO-regulated with the Nicontaining CO dehydrogenase from *Rhodospirillum rubrum*, *J. Biol. Chem. 273*, 10019-10025.
- 50. Sadler, P. J., Tucker, A., and Viles, J. H. (1994) Involvement of a lysine residue in the N-terminal Ni²⁺ and Cu²⁺ binding site of serum albumins comparison with Co²⁺, Cd²⁺ and Al³⁺, Euro. J. Biochem. 220, 193-200.
- 51. Becker, A., Schlichting, I., Kabsch, W., Schultz, S., and Wagner, A. F. V. (1998) Structure of peptide deformylase and identification of the substrate binding site, *J. Biol. Chem.* 273, 11413-11416.
- 52. Mantri, M., Krojer, T., Bagg, E. A., Webby, C. J., Butler, D. S., Kochan, G., Kavanagh, K. L., Oppermann, U., McDonough, M. A., and Schofield, C. J. (2010) Crystal structure of the 2-Oxoglutarate- and Fe(II)-dependent lysyl hydroxylase JMJD6, *J. Mol. Biol. 401*, 211-222.
- 53. Kalliri, E., Grzyska, P. K., and Hausinger, R. P. (2005) Kinetic and spectroscopic investigation of Co-II, Ni-II, and N-oxalylglycine inhibition of the Fe-II/alphaketoglutarate dioxygenase, TauD, *Biochem. Biophys. Res. Commun.* 338, 191-197.
- 54. Chen, H., and Costa, M. (2009) Iron- and 2-oxoglutarate-dependent dioxygenases: An emerging group of molecular targets for nickel toxicity and carcinogenicity, *Biometals* 22, 191-196.
- 55. White, A., Ding, X. C., VanderSpek, J. C., Murphy, J. R., and Ringe, D. (1998) Structure of the metal-ion-activated diphtheria toxin repressor tox operator complex, *Nature 394*, 502-506.
- 56. Maher, M., Cross, M., Wilce, M. C. J., Guss, J. M., and Wedd, A. G. (2004) Metal-substituted derivatives of the rubredoxin from *Clostridium pasteurianum*, *Acta Crystallogr.*, *Sect. D 60*, 298-303.
- 57. Tsai, L. C., Sjolin, L., Langer, V., Bonander, N., Karlsson, B. G., Vanngard, T., Hammann, C., and Nar, H. (1995) Structure of the azurin mutant nickel-Tryp48Met from *Pseudomonas aeruginosa* at 2.2 A resolution, *Acta Crystallogr., Sect. D* 51, 711-717.
- 58. de las Rivas, B., Fox, G. C., Angulo, I., Ripoll, M. M., Rodriguez, H., Munoz, R., and Mancheno, J. M. (2009) Crystal structure of the hexameric catabolic ornithine transcarbamylase from *Lactobacillus hilgardii*: Structural insights into the oligomeric assembly and metal binding, *J. Mol. Biol. 393*, 425-434.

- 59. Ford, C. F., Suominen, I., and Glatz, C. E. (1991) Fusion tails for the recovery and purification of recombinant proteins, *Prot. Express. Purif.* 2, 95-107.
- 60. Hochuli, E., Dobeli, H., and Schacher, A. (1987) New metal chelate adsorbent selective for proteins and peptides containing neighboring histidine residues, *J. Chromat.* 411, 177-184.
- 61. Hakansson, K. O. (2003) The crystallographic structure of Na,K-ATPase N-domain at 2.6 A resolution, *J. Mol. Biol. 332*, 1175-1182.
- 62. Carter, E. L., Tronrud, D. E., Taber, S. R., Karplus, P. A., and Hausinger, R. P. (2011) Iron-containing urease in a pathogenic bacterium, *Proc. Natl. Acad. Sci. U.S.A. 108*, 13095-13099.
- 63. Sumner, J. B. (1926) The isolation and crystallization of the enzyme urease, *J. Biol. Chem.* 69, 435-441.
- 64. Dixon, N. E., Gazzola, C., Blakeley, R. L., and Zerner, B. (1975) Jack Bean urease (EC 3.5.1.5). A metalloenzyme. A simple biological role for nickel?, *J. Am. Chem. Soc. 97*, 4131-4133.
- 65. Bauerfeind, P., Garner, R., Dunn, B. E., and Mobley, H. L. (1997) Synthesis and activity of *Helicobacter pylori* urease and catalase at low pH, *Gut 40*, 25-30.
- 66. Atherton, J. C. (2006) The pathogenesis of *Helicobacter pylori*-induced gastro-duodenal diseases, *Annu. Rev. Pathol.* 1, 63-96.
- 67. Mobley, H. L. T., Island, M. D., and Hausinger, R. P. (1995) Molecular biology of microbial ureases *Microbiol. Rev. 59*, 451-480.
- 68. Mobley, H. L. T., and R. P. Hausinger. (1989) Microbial ureases: Significance, regulation, and molecular characterization., *Microbiol. Rev.* 53, 85-108.
- 69. Lee, M. H., Mulrooney, S. B., Renner, M. J., Markowicz, Y., and Hausinger, R. P. (1992) *Klebsiella aerogenes* urease gene cluster: sequence of *ureD* and demonstration that 4 accessory genes (*ureD*, *ureE*, *ureF*, and *ureG*) are involved in nickel metallocenter biosynthesis, *J. Bacteriol.* 174, 4324-4330.
- 70. Ha, N. C., Oh, S. T., Sung, J. Y., Cha, K. A., Lee, M. H., and Oh, B. H. (2001) Supramolecular assembly and acid resistance of *Helicobacter pylori* urease, *Nat. Struct. Biol. 8*, 505-509.
- 71. Balasubramanian, A., and Ponnuraj, K. (2010) Crystal structure of the first plant urease from jack bean: 83 years of journey from its first crystal to molecular structure, *J. Mol. Biol.* 400, 274-283.

- 72. Sheridan, L., Wilmot, C. M., Cromie, K. D., van der Logt, P., and Phillips, S. E. V. (2002) Crystallization and preliminary X-ray structure determination of jack bean urease with a bound antibody fragment, *Acta Crystallogr. Sect. D* 58, 374-376.
- 73. Jabri, E., and Karplus, P. A. (1996) Structures of the *Klebsiella aerogenes* urease apoenzyme and two active-site mutants, *Biochemistry 35*, 10616-10626.
- 74. Lee, M. H., Mulrooney, S. B., and Hausinger, R. P. (1990) Purification, characterization, and *in vivo* reconstitution of *Klebsiella aerogenes* urease apoenzyme, *J. Bacteriol.* 172, 4427-4431.
- 75. Park, I. S., and Hausinger, R. P. (1995) Requirement of carbon dioxide for *in vitro* assembly of the urease nickel metallocenter, *Science 267*, 1156-1158.
- 76. Park, I. S., and Hausinger, R. P. (1996) Metal ion interactions with urease and UreDurease apoproteins, *Biochemistry 35*, 5345-5352.
- 77. Carter, E. L., and Hausinger, R. P. (2010) Characterization of *Klebsiella aerogenes* urease accessory protein UreD in fusion with the maltose binding protein, *J. Bacteriol.* 192, 2294-2304.
- 78. Park, I. S., Carr, M. B., and Hausinger, R. P. (1994) *In vitro* activation of urease apoprotein and role of UreD as a chaperone required for nickel metallocenter assembly, *Proc. Natl. Acad. Sci. U.S.A.* 91, 3233-3237.
- 79. Quiroz-Valenzuela, S., Sukuru, S. C. K., Hausinger, R. P., Kuhn, L. A., and Heller, W. T. (2008) The structure of urease activation complexes examined by flexibility analysis, mutagenesis, and small-angle X-ray scattering, *Arch. Biochem. Biophys* 480, 51-57.
- 80. Chang, Z. Z., Kuchar, J., and Hausinger, R. P. (2004) Chemical cross-linking and mass spectrometric identification of sites of interaction for UreD, UreF, and urease, *J. Biol. Chem.* 279, 15305-15313.
- 81. Fong, Y. H., Wong, H. C., Chuck, C. P., Chen, Y. W., Sun, H., and Wong, K.-B. (2011) Assembly of preactivation complex for urease maturation in *Helicobacter pylori*, *J. Biol. Chem.* 286, 43241-43249.
- 82. Lam, R., Romanov, V., Johns, K., Battaile, K. P., Wu-Brown, J., Guthrie, J. L., Hausinger, R. P., Pai, E. F., and Chirgadze, N. Y. (2010) Crystal structure of a truncated urease accessory protein UreF from *Helicobacter pylori*, *Proteins 78*, 2839-2848.
- 83. Salomone-Stagni, M., Zambelli, B., Musiani, F, and Ciurli, S. (2007) A model-based proposal for the role of UreF as a GTPase-activating protein in the urease active site biosynthesis, *Proteins 68*, 749-761.

- 84. Kim, K. Y., Yang, C. H., and Lee, M. H. (1999) Expression of the recombinant *Klebsiella* aerogenes UreF protein as a MalE fusion, *Arch. Pharm. Res.* 22, 274-278.
- 85. Kim, J. K., Mulrooney, S. B., and Hausinger, R. P. (2006) The UreEF fusion protein provides a soluble and functional form of the UreF urease accessory protein, *J. Bacteriol.* 188, 8413-8420.
- 86. Moncrief, M. B. C., and Hausinger, R. P. (1996) Purification and activation properties of UreD-UreF-urease apoprotein complexes, *J. Bacteriol.* 178, 5417-5421.
- 87. Moncrief, M. B. C., and Hausinger, R. P. (1997) Characterization of UreG, identification of a UreD-UreF-UreG complex, and evidence suggesting that a nucleotide-binding site in UreG is required for in vivo metallocenter assembly of *Klebsiella aerogenes* urease, *J. Bacteriol.* 179, 4081-4086.
- 88. Zambelli, B., Stola, M., Musiani, F., De Vriendt, K., Samyn, B., Devreese, B., Van Beeumen, J., Turano, P., Dikiy, A., Bryant, D. A., and Ciurli, S. (2005) UreG, a chaperone in the urease assembly process, is an intrinsically unstructured GTPase that specifically binds Zn²⁺, *J. Biol. Chem. 280*, 4684-4695.
- 89. Neyroz, P., Zambelli, B., and Ciurli, S. (2006) Intrinsically disordered structure of *Bacillus pasteurii* UreG as revealed by steady-state and time-resolved fluorescence spectroscopy, *Biochemistry 45*, 8918-8930.
- 90. Zambelli, B., Musiani, F., Savini, M., Tucker, P., and Ciurli, S. (2007) Biochemical studies on *Mycobacterium tuberculosis* UreG and comparative modeling reveal structural and functional conservation among the bacterial UreG family, *Biochemistry 46*, 3171-3182.
- 91. Zambelli, B., Turano, P., Musiani, F., Neyroz, P., and Ciurli, S. (2009) Zn²⁺-linked dimerization of UreG from *Helicobacter pylori*, a chaperone involved in nickel trafficking and urease activation, *Proteins 74*, 222-239.
- 92. Leipe, D. D., Wolf, Y. I., Koonin, E. V., and Aravind, L. (2002) Classification and evolution of P-loop GTPases and related ATPases, *J. Mol. Biol. 317*, 41-72.
- 93. Haas, C. E., Rodionov, D. A., Kropat, J., Malasarn, D., Merchant, S. S., and de Crecy-Lagard, V. (2009) A subset of the diverse COG0523 family of putative metal chaperones is linked to zinc homeostasis in all kingdoms of life, *BMC Genomics 10*.
- 94. Padovani, D., and Banerjee, R. (2009) A G-protein editor gates coenzyme B-12 loading and is corrupted in methylmalonic aciduria, *Proc. Natl. Acad. Sci. U.S.A.* 106, 21567-21572.

- 95. Soriano, A., and Hausinger, R. P. (1999) GTP-dependent activation of urease apoprotein in complex with the UreD, UreF, and UreG accessory proteins, *Proc. Natl. Acad. Sci. U.S.A. 96*, 11140-11144.
- 96. Zambelli, B., Cremades, N., Neyroz, P., Turano, P., Uversky, V. N., and Ciurli, S. (2012) Insights in the (un)structural organization of *Bacillus pasteurii* UreG, an intrinsically disordered GTPase enzyme, *Mol. Biosyst. 8*, 220-228.
- 97. Carter, E. L., Boer, J. L., Farrugia, M. A., Flugga, N., Towns, C. L., and Hausinger, R. P. (2011) The function of UreB in *Klebsiella aerogenes* urease, *Biochemistry 50*, 9296-9308.
- 98. Brayman, T. G., and Hausinger, R. P. (1996) Purification, characterization, and functional analysis of a truncated *Klebsiella aerogenes* UreE urease accessory protein lacking the histidine-rich carboxyl terminus, *J. Bacteriol.* 178, 5410-5416.
- 99. Colpas, G. J., and Hausinger, R. P. (2000) *In vivo* and *in vitro* kinetics of metal transfer by the *Klebsiella aerogenes* urease nickel metallochaperone, UreE, *J. Biol. Chem. 275*, 10731-10737.
- 100. Soriano, A., Colpas, G. J., and Hausinger, R. P. (2000) UreE stimulation of GTP-dependent urease activation in the UreD-UreF-UreG-urease apoprotein complex, *Biochemistry 39*, 12435-12440.
- 101. Kolmark, H. G. (1969) Genetic studies of urease mutants in *Neurospora crassa*, *Mut. Research* 8, 51.
- 102. Haysman, P., and Howe, H. B. (1971) Some genetic and physiological characteristics of urease-defective strains of *Neurospora crassa*, *Can. J. of Gen. and Cyt. 13*, 256-&.
- 103. Benson, E. W., and Howe, H. B. (1978) Reversion and interallelic complementation at four urease loci in *Neurospora crassa*, *Mol. Gen. Genet. 165*, 277-282.
- 104. Mackay, E. M., and Pateman, J. A. (1980) Nickel requirement of a urease-deficient mutant in *Aspergillus nidulans*, *J. Gen. Microbiol.* 116, 249-251.
- 105. Mackay, E. M., and Pateman, J. A. (1982) The regulation of urease activity in *Aspergillus nidulans*, *Biochem. Genet. 20*, 763-776.
- 106. Kinghorn, J. R., and Fluri, R. (1984) Genetic studies of purine breakdown in the fission yeast *Schizosaccharomyces pombe*, *Curr. Genet.* 8, 99-105.
- 107. Lubbers, M. W., Rodriguez, S. B., Honey, N. K., and Thornton, R. J. (1996) Purification and characterization of urease from *Schizosaccharomyces pombe, Can. J. Microbiol.* 42, 132-140.

- 108. Tange, Y., and Niwa, O. (1997) Identification of the ure1(+) gene encoding urease in fission yeast, *Curr. Genet. 32*, 244-246.
- 109. Bacanamwo, M., Witte, C. P., Lubbers, M. W., and Polacco, J. C. (2002) Activation of the urease of *Schizosaccharomyces pombe* by the UreF accessory protein from soybean, *Mol. Genet. Genomics* 268, 525-534.
- 110. Riddles, P. W., Whan, V., Blakeley, R. L., and Zerner, B. (1991) Cloning and sequencing of a jack bean urease-encoding cDNA, *Gene 108*, 265-267.
- 111. Pires-Alves, M., Grossi-de-Sa, M. F., Barcellos, G. B. S., Carlini, C. R., and Moraes, M. G. (2003) Characterization and expression of a novel member (JBURE-II) of the urease gene family from jackbean [*Canavalia ensiformis* (L.) DC], *Plant Cell Physiol.* 44, 139-145.
- 112. Krueger, R. W., Holland, M. A., Chisholm, D., and Polacco, J. C. (1987) Recovery of a soybean urease genomic clone by sequential library screening with two synthetic oligodeoxynucleotides, *Gene 54*, 41-50.
- 113. Meyer-Bothling, L. E., Polacco, J. C., and Cianzio, S. R. (1987) Pleotropic soybean mutants defective in both urease isozymes, *Mol. Gen. Genet.* 209, 432-438.
- 114. Holland, M. A., Griffin, J. D., Meyerbothling, L. E., and Polacco, J. C. (1987) Developmental genetics of the soybean urease isozymes, *Dev. Genet.* 8, 375-387.
- 115. Torisky, R. S., Griffin, J. D., Yenofsky, R. L., and Polacco, J. C. (1994) A single-gene (Eu4) encodes the tissue-ubiquitous urease of soybean, *Mol. Gen. Genet.* 242, 404-414.
- 116. Freyermuth, S. K., Bacanamwo, M., and Polacco, J. C. (2000) The soybean Eu3 gene encodes an Ni-binding protein necessary for urease activity, *Plant J. 21*, 53-60.
- 117. Real-Guerra, R., Staniscuaski, F., Zambelli, B., Musiani, F., Ciurli, S., and Carlini, C. R. (2012) Biochemical and structural studies on native and recombinant *Glycine max* UreG: a detailed characterization of a plant urease accessory protein, *Plant Mol. Biol. in press*.
- 118. Polacco, J. C., Hyten, D. L., Medeiros-Silva, M., Sleper, D. A., and Bilyeu, K. D. (2011) Mutational analysis of the major soybean UreF paralogue involved in urease activation, *J. Exp. Bot. 62*, 3599-3608.
- 119. Witte, C. P., Isidore, E., Tiller, S. A., Davies, H. V., and Taylor, M. A. (2001) Functional characterisation of urease accessory protein G (ureG) from potato, *Plant Mol. Biol. 45*, 169-179.
- 120. Witte, C. P., Rosso, M. G., and Romeis, T. (2005) Identification of three urease accessory proteins that are required for urease activation in Arabidopsis, *Plant Physiol.* 139, 1155-1162.

- 121. Boer, J. L., Quiroz-Valenzuela, S., Anderson, K. L., and Hausinger, R. P. (2010) Mutagenesis of *Klebsiella aerogenes* UreG to probe nickel binding and interactions with other urease-related proteins, *Biochemistry 49*, 5859-5869.
- 122. Zambelli, B., Musiani, F., Benini, S., and Ciurli, S. (2011) Chemistry of Ni²⁺ in Urease: Sensing, Trafficking, and Catalysis, *Acc. Chem. Res. 44*, 520-530.



Mutagenesis of Klebsiella aerogenes UreG to Probe Nickel Binding and Interactions with Other Urease-Related Proteins

This chapter is adapted from Boer, J. L., Quiroz-Valenzuela, S., Anderson, K. L., and Hausinger, R. P. (2010) Mutagenesis of *Klebsiella aerogenes* UreG to probe nickel binding and interactions with other urease-related proteins, *Biochemistry 49*, 5859-5869.

The cloning, initial purification, and partial characterization of UreG_{Str} using circular dichroism spectroscopy, inductively coupled plasma-emission spectroscopy, pull-down studies with cell-free extracts and western blot analysis were performed by Soledad Quiroz-Valenzuela and Kimberly L. Anderson.

ABSTRACT

UreG is a GTPase required for assembly of the nickel-containing active site of urease. Herein, a Strep-tagged Klebsiella aerogenes UreG (UreG_{Str}) and selected site-directed variants of UreG_{Str} were constructed for studying the *in vivo* effects on urease activation in recombinant Escherichia coli cells, characterizing properties of the purified proteins, and analysis of proteinprotein interactions using cell-free extracts and in vitro. Whereas the Strep-tag had no effect on UreG's ability to activate urease, enzyme activity was essentially abolished in the K20A, D49A, C72A, H74A, D80A, and S111A UreG_{Str} variants, with diminished activity also noted with E25A, C28A, and S115A proteins. Lys20 and Asp49 are likely to function in binding/hydrolysis of GTP and binding of Mg, respectively. Ure G_{Str} binds one nickel or zinc ion per monomer ($K_d = ^5$ μM for each metal ion) at a binding site that includes Cys72, as shown by a 12-fold increased Kd for nickel ions using C72A UreG_{Str} and by a thiolate-to-nickel charge-transfer band that is absent in the mutant protein. Based on UreG homology to HypB, a GTPase needed for hydrogenase assembly, along with the mutation results, His74 is likely to be an additional metal ligand. Pull-down assays in cell-free extracts revealed Asp80 as critical for stabilizing UreG_{Str} interaction with the UreABC—UreD—UreF complex. In vitro pull-down assays demonstrated UreG binding to UreE, with the interaction enhanced by nickel or zinc ions. The metallochaperone UreE is suggested to transfer its bound nickel to UreG in the UreABC— UreD—UreF—UreG complex, with the metal ion subsequently transferring to UreD, and then into the nascent active site of urease in a GTP-dependent process.

INTRODUCTION

Urease, a nickel-containing enzyme found in plants and microorganisms, catalyzes the hydrolysis of urea to form ammonia and carbamate, which spontaneously decomposes to carbon dioxide and ammonia (1, 2). Structures of several ureases (3-6) reveal dinuclear nickel metallocenters deeply buried in structural subunits that coalesce with three-fold symmetry. With the possible exception of the Bacillus subtilis enzyme (7), activation of urease has been shown to require a series of accessory proteins to assemble the active site (1, 8). The best understood urease activation system involves the ureDABCEFG genes of the enterobacterium Klebsiella aerogenes expressed in Escherichia coli. This model urease system begins with the structural subunits (UreA, UreB, and UreC) assembling into the urease apoprotein (UreABC)₃ (9, 10), with UreD, UreF, and UreG sequentially associating with the apoprotein to form the (UreABC—UreD)3 (11) (UreABC—UreD—UreF)₃ (12), and (UreABC—UreD—UreF—UreG)₃ (13) activation complexes (Figure 2.1). Finally, in a process that requires GTP hydrolysis, CO₂ incorporation as an active site lysine carbamate, and the nickel-delivering metallochaperone UreE, the active site assembles, and then the accessory proteins release from the active enzyme (14, 15). As described below, the roles of UreD, UreF, and UreG in urease activation are poorly understood.

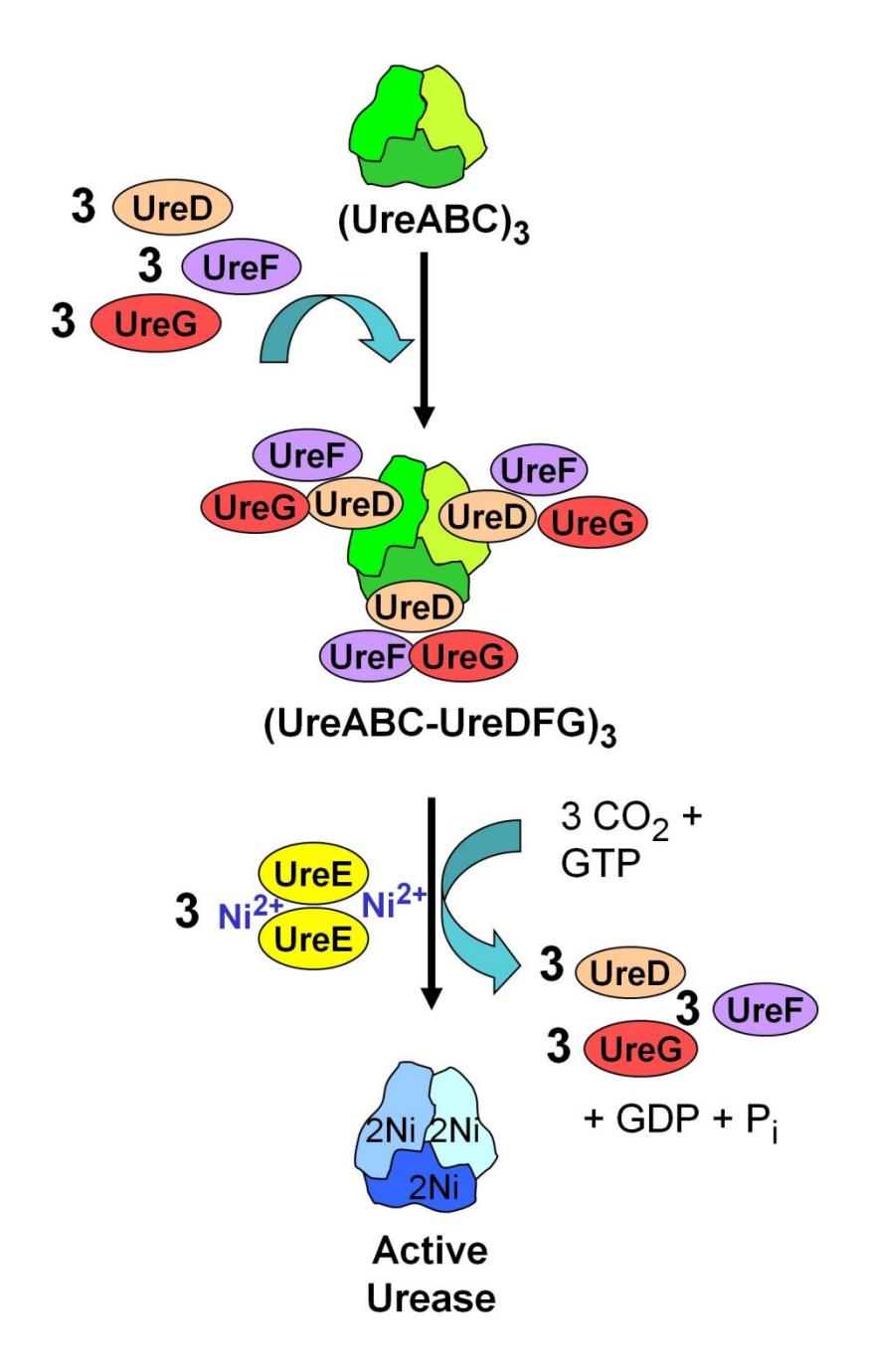


Figure 2.1: Simplified scheme of the urease activation process. Urease apoprotein (UreABC)₃ is synthesized with the nascent active site lacking nickel ions and with no carbamylation of its Lys217. Urease accessory proteins UreD, UreF, and UreG bind the apoprotein in a sequential manner to form the (UreABC—UreD—UreF—UreG)₃ activation complex (abbreviated further for simplicity in the figure). Urease activation requires carbamylation of Lys217 by CO₂, provision of nickel ions by the UreE metallochaperone, and GTP hydrolysis accompanied by release of the accessory proteins.

Studies of UreD are limited to the *K. aerogenes* system, along with a structure (3sf5) of the *H. pylori* UreD homolog UreH in complex with its cognate UreF (16). The *K. aerogenes* protein is insoluble when expressed alone, however a maltose binding protein (MBP)-UreD fusion is soluble and complements a $\Delta ureD$ urease cluster (17). Significantly, the UreD portion of MBP-UreD binds nickel (~2.5 Ni per protomer, K_d ~50 μ M) and this protein, when in the UreABC—UreD—UreF—UreG complex, is proposed to transfer the metal ion into the nascent urease active site.

K. aerogenes UreF, like UreD, is insoluble when synthesized separately from the other urease components; however, UreE-UreF and MBP-UreF fusion proteins are soluble and partially characterized (18, 19). In addition, two crystal structures of UreF from Helicobacter pylori (PDB codes 3cxn and 2wgl) were solved (20) along with the UreF-UreH complex (16). Computational studies of Bacillus pasteurii UreF led to a proposal that the protein functions as a GTPase activating protein (21), but no direct evidence for such a role has been reported in any system.

Purified recombinant UreG proteins (subunit M_r 22,000 - 23,000) of K. aerogenes, B. pasteurii, Mycobacterium tuberculosis, and H. pylori are soluble and contain motifs found in GTPases, although their GTPase activities are very low or non-detectable (13, 22-24). Mutation of Lys20 or Thr21 in the GXGKT P-loop motif (a GTPase motif) of the K. aerogenes protein abolishes its ability to activate urease (13). This region also is critical for in vitro activation of the (UreABC—UreD—UreF—UreG)3 complex (14). K. aerogenes UreG is reported to be

monomeric (13). In contrast, UreG proteins from B. pasteurii and M. tuberculosis are dimeric, with the subunits joined by a disulfide bridge involving Cys68 in the B. pasteurii protein and probably Cys90 in that from M. tuberculosis (23, 25). UreG from B. pasteurii binds two zinc ions per dimer (K_d 42 μ M) or four nickel ions per dimer (K_d 360 μ M), and this interaction was speculated to involve Glu64, Cys68 (i.e., the same residue as that participating in the disulfide), and His70 as metal ligands (22), although no experiments were performed to confirm these assignments. H. pylori UreG, a monomer as purified, dimerizes as it binds zinc ions (1.0 Zn per dimer, K_d 0.33 μ M) or remains a monomer as it binds nickel ions with lower affinity (2.0 Ni per monomer, K_d 10 μM) (24). Cys66 and His68 are proposed as ligands for the zinc ion-binding site, but the C66A, H68A, and C66A/H68A double mutant still binds zinc with only 10-fold lower affinity and these mutant proteins still dimerize upon addition of the metal ions. Furthermore, the presence of zinc, but not nickel, ions stabilizes a UreE-UreG complex using the H. pylori proteins (26). No crystal structure is available for any UreG; however, the crystal structure of the related protein HypB from Methanocaldococcus jannaschii is known (27). HypB is an accessory protein that participates in the metallocenter assembly of [NiFe] hydrogenases (8, 28). The crystal structure reveals two types of zinc binding sites: a mononuclear site in each subunit involving His100 and His104 (numbering derived from the HypB crystal structure; corresponding His residues are not located at these positions in UreG sequences) and a nonsymmetrical dinuclear binding site at the subunit interface. The metal-binding residues of the dinuclear site in M. jannaschii HypB (Cys95, His96, and Cys127) most likely correspond to Cys72, His74, and either Ser111 or Ser115 (although Ser is not a typical metal-binding residue) in K.

aerogenes UreG (or Cys68, His70, and Ser107 or Ser111 in the B. pasteurii protein) (Figure 2.2).

<i>Ka</i> UreG	10 20 MNSYKHPLRVGVGGPV <u>GSG<mark>K</mark>T</u> ALL	24
<i>Bp</i> UreG	MKTIHLGIGGPV <u>GSG<mark>K</mark>T</u> TLV	20
<i>мј</i> НурВ		50
<i>Ka</i> UreG	30 40 50 60 70 EALCKAMRDTWQLAVVTNDIYTKEDQRILTEAGALAPERIVGVETGGCPH	74
<i>Bp</i> UreG	KTL <mark>S</mark> EALK <mark>E</mark> EYSIAVITNDIYTRE <mark>D</mark> ANFLINENILEKDRIIGV <mark>E</mark> TGG <mark>C</mark> PH	70
<i>Мј</i> НурВ	EKL <mark>I</mark> DNLK <mark>D</mark> KYKIACIAGDVIAKF <mark>D</mark> AERMEKHGAKVVPL <mark>N</mark> TGK <mark>ECH</mark>	96
<i>Ka</i> UreG	80 90 100 110 120 TAIREDASMNLAAVEALSEKFGNLDLIFV <u>ESGG</u> DNL <mark>S</mark> ATF <mark>S</mark> PELADLTIY	124
<i>Bp</i> UreG	TAIRE <mark>D</mark> ASMNFEAIEELKNRFDDLEIILL <u>ESGG</u> DNL <mark>S</mark> ATF <mark>S</mark> PELV <mark>D</mark> AFIY	110
<i>Мј</i> НурВ	LDAHL <mark>V</mark> GHALEDLNLDEIDLLFI <u>ENVG</u> NLI <mark>C</mark> PAD <mark>F</mark> DLGT <mark>H</mark> KRIV	140
<i>Ka</i> UreG	130 140 150 160 170 VI <mark>D</mark> VAEGEKIPRKGGPGITKSDFLVI <u>NKTD</u> LAPYVGASLEVMASDTQRMR	174
<i>Bp</i> UreG	VI <mark>D</mark> VSEGGDIPRKGGPGVTRSDFLMV <u>NKTE</u> LAPYVGVDLDTMKNDTIKAR	160
<i>Мј</i> НурВ	VI <mark>S</mark> TTEGDDTIEKHPGIMKTADLIVI <u>NKID</u> LADAVGADIKKMENDAKRIN	190
<i>Ka</i> UreG	180 190 200 GDRPWTFTNLKQGDGLSTIIAFLEDKGMLGK	205
<i>Bp</i> UreG	NGRPFTFANIKTKKGLDEIIAWIKSDLLLEGKTNESASESK	201
<i>мј</i> Нурв	PDAEVVLLSLKTMEGFDKVLEFIEKSVKEVK	220

Figure 2.2: Multiple sequence alignment of *K. aerogenes* UreG, *B. pasteurii* UreG, and *M. jannaschii* HypB. Clustal W (44) was used to make the initial alignment, followed by manual modifications. Residues mutated in *K. aerogenes* UreG and the corresponding residues in the other sequences are highlighted in yellow. The P-loop motif, signature motif of the SIMBI G3E family, and guanine specificity loop are underlined.

UreE serves as a metallochaperone that delivers the nickel ions needed to form the urease active site (29, 30). The structures of a truncated version of UreE from K. aerogenes and

the full-length protein from *B. pasteurii* have been solved with bound copper and zinc, respectively (31, 32). The interaction of UreE with the other accessory proteins has not been well characterized; however, UreE and UreG from *H. pylori* were suggested to interact on the basis of yeast two-hybrid assays (33) and a UreE₂UreG₂ complex (formed with the isolated *H. pylori* proteins) was observed in the presence of zinc, but not nickel, ions (26).

In this study, I describe a new purification method for UreG that utilizes a *Strep*-tag. Using protein purified by this approach, I examine the metal binding capabilities of UreG_{Str} and a selection of its variants. Additionally, I assess the effects of those mutations on urease activation and exploit the *Strep*-tagged protein to examine its interactions with other urease components. These findings using the *K. aerogenes* urease activation system expressed in *E. coli* reveal significant new insights, many of which are likely to be more generally applicable to other urease systems.

EXPERIMENTAL PROCEDURES

Vector Construction, Cell Growth, and Purification of Strep-Tagged UreG. The ureG sequence was cloned into pASK-IBA3plus and pASK-IBA5plus plasmids (IBA GmbH, Göttingen, Germany) to create vectors pIBA3+G and pIBA5+G (Table 2.1) encoding UreG with a Strep-tag II (a WSHPQFEK peptide; subsequently referred to as a Strep-tag) at the C- or N-termini, respectively. First, a polymerase chain reaction (PCR) was performed using *Pfu*Turbo[®] Hotstart PCR Master Mix (Stratagene, USA), the plasmid pKAUG-1 as a template, and the primers 5'-TA CTG TCC CGC GGG ATG AAC TCT TAT AAA CAC-3' and 5'-T ACT GTC CTG CAG TTT GCC AAG CAT GCC TTT-3'. The first primer contains a SacII restriction site and the second a PstI restriction site (shown in italics) used to clone the fragment into pASK-IBA3plus. In a similar manner, the primers 5'-T ACT GTC CCG CGG GG AAC TCT TAT AAA CAC CCG-3' and 5'- T ACT GTC GGA TCC CTA TTT GCC AAG CAT GCC-3', containing restriction sites for SacII and BamHI respectively, were used to clone the fragment into pASK-IBA5plus. The plasmids and PCR products were digested with the corresponding restriction enzymes (New England Biolabs) and ligated to produce plasmids pIBA3+G and pIBA5+G. These constructions were confirmed by sequencing (Davis sequencing, Davis, CA, USA).

Table 2.1: Plasmids and *E. coli* strains used in this study

Plasmid	Description	<i>E. coli</i> strain	Reference
pASK-IBA3plus	Plasmid for creating fusion proteins with a <i>Strep</i> -tag II (WSHPQFEK) at the C-terminus	<u> </u>	IBA
pASK-IBA5plus	Plasmid for creating fusion proteins with a <i>Strep</i> -tag II at the N-terminus		IBA
pEC007	Modified pACT3 to encode UreE	DH5 α	(17)
pIBA3+G	Modified pASK-IBA3plus to encode	DH5α or BL21 (DE3)	This work
IDAE O	UreG _{Str}	, ,	- 1 · 1
pIBA5+G	Modified pASK-IBA5plus to encode	DH5 α or	This work
	UreG _{Str}	BL21 (DE3)	
pIBA3+GK20A, pIBA3+GE25A, pIBA3+GC28A,	Modified pIBA3+G to encode the K20A, E25A, C28A, D33A, D49A, E68A, C72A, H74A, D80A, S111A, S115A,	BL21 (DE3)	This work
pIBA3+GD33A, pIBA3+GD49A, pIBA3+GE68A, pIBA3+GC72A, pIBA3+GH74A, pIBA3+GD80A, pIBA3+GS111A, pIBA3+GS115A,	D120A and D127A variants of UreG _{Str}		
pIBA3+GD120A			
plBA3+GD127A			(0.0)
pKAU17	K. aerogenes urease gene cluster in pUC8		(34)
pKAUD2	pKAU17 modified to overexpress ureD		(11)
pKAUG-1	Modified pKAUD2 containing only <i>K.</i> aerogenes ureG.	BL21 (DE3)	(35)
pKK17	K. aerogenes ureDABCEFG gene cluster inserted into pKK223-3	DH5α	(36)
pKKG	Modified pKK17 encoding UreG _{Str}	DH5α	This work
pKKGK20A, pKKGE25A, pKKGC28A, pKKGD33A, pKKGD49A, pKKGE68A, pKKGC72A, pKKGH74A, pKKGD80A, pKKGS111A,	Modified pKKG encoding the K20A, E25A, C28A, D33A, D49A, E68A, C72A, H74A, H74C, H74N, D80A, S111A, S115A, and D127A variants of UreG _{Str}	DH5α	This work

Isolated colonies of E. coli BL21(DE3) (Stratagene) were transformed with the plasmids and grown at 37 °C overnight in lysogeny broth (LB, or Lennox broth, Fisher Scientific) supplemented with 300 $\mu g \ mL^{-1}$ of ampicillin. These cultures were used to inoculate 1 L of LB supplemented with 300 μg mL⁻¹ of ampicillin. The cultures were grown at 37 °C with shaking for 4 h and induced overnight with 0.2 $\mu g \; mL^{-1}$ anhydrotetracycline. The cells were harvested by centrifugation and resuspended in 1 mL of buffer W (100 mM Tris-HCl, pH 8.0, containing 150 mM NaCl and 1 mM EDTA) per gram of cells and supplemented with 1 mM phenylmethylsulphonyl fluoride as a protease inhibitor before sonication (Branson 450 sonifier, 5 repetitions, each of 2 min, at 3 W output power and 50% duty cycle). The disrupted cells were centrifuged at 100,000 x g at 4 °C for 45 min and the cell-free supernatant was loaded onto a 1 mL Strep-Tactin column (IBA, Germany) previously equilibrated in buffer W. This column has an engineered streptavidin ligand that binds to the Strep-tag with high affinity. The Strep-tagged UreG protein (UreG_{Str}) was eluted with desthiobiotin according to the manufacturer's instructions. For comparative studies, native UreG was purified as previously described (13). For further purification and to provide assurance that samples were completely reduced, the proteins were chromatographed at 1 mL min ⁻¹ on a preparative Superdex-75 column (65 cm x 2.0 cm diam., GE Healthcare) equilibrated in 50 mM HEPES buffer, pH 7.4, containing 200 mM NaCl, 1 mM EDTA and 1 mM dithiothreitol (DTT).

Fractions containing $UreG_{Str}$, UreG, or mutant forms of these proteins were analyzed by sodium dodecyl sulfate polyacrylamide gel electrophoresis (SDS-PAGE) (37) using gels prepared

with 12% running and 5% stacking acrylamide sections and stained with Coomassie brilliant blue. The calculated molecular weights of UreA (11.1-kDa), UreB (11.7-kDa), UreE (17.6-kDa), UreG (21.9-kDa), UreG $_{Str}$ (23.1-kDa), UreF (25.2-kDa), UreD (29.8-kDa), and UreC (60.3-kDa) generally migrate during electrophoresis as expected with the exception of UreG and UreG $_{Str}$ which behave as if they are larger than UreF. Molecular weight markers were obtained from Bio-Rad (Hercules, CA). Protein concentrations were determined by using a commercial dye-binding assay (Bio-Rad, Hercules, CA) with bovine serum albumin as the standard.

UreE Purification. E. coli DH5 α cells containing pEC007 (*17*), expressing full length UreE, were grown overnight in 10 mL LB supplemented with 50 μg mL⁻¹ chloramphenicol. These cultures were used to inoculate 1L of LB supplemented with 50 μg mL⁻¹ chloramphenicol and grown to an optical density at 600 nm (O.D.600) of 0.4, induced with 0.5 mM isopropyl β-D-1-thiogalactopyranoside (IPTG), and grown overnight at 37 °C. UreE was purified by using previously published protocols (*38*).

Site-Directed Mutagenesis. pIBA3+G was mutated by using overlapping oligonucleotides containing the desired mutation (see Table 2.2) during PCR performed with PfuTurbo[®] Hotstart PCR Master Mix. The products were digested with DpnI for 1 h at 37 °C and used to transform chemically competent E. coli DH5 α cells. After confirmation by sequencing, the mutated plasmids were transformed into E. coli BL21(DE3) competent cells (Stratagene, USA). All mutant Ure G_{Str} proteins were expressed and purified as described for Ure G_{Str} .

Table 2.2: Oligonucleotides used to generate UreG mutations

Purpose	Sequence
UreG mutation E25A	5' GTA AAA CCG CTC TGC TGG <i>CGG</i> CGC TGT GTA AAG CGA TG 3'
	5' CAT CGC TTT ACA CAG CGC <i>CGC</i> CAG CAG AGC GGT TTT AC 3'
UreG mutation C28A	5' CT CTG CTG GAA GCG CTG <u>GCA</u> AAA GCG ATG CGC GAT AC 3'
	5' GT ATC GCG CAT CGC TTT <u>TGC</u> CAG CGC TTC CAG CAG AG 3'
UreG mutation D33A	5' GTA AAG CGA TGC GCG <i>CGA</i> CCT GGC AGC TGG C 3'
	5' G CCA GCT GCC AGG <u>TCG</u> CGC GCA TCG CTT TAC 3'
UreG mutation D49A	5' GAC ATC TAT ACC AAA GAA <i>GCG</i> CAG CGC ATC CTC ACC GAA 3'
UreG mutation E68A	5' GAA CGC ATC GTC GGT GTG <u>GCG</u> ACC GGC GGC TGC CCG CAT 3'
UreG mutation C72A	5' GTC GGT GTG GAA ACC GGC GGC <u>GCG</u> CCG CAT ACG GCG ATC
	CGC GAA 3'
UreG mutation H74A	5' GAA ACC GGC GGC TGC CCG <u>GCA</u> ACG GCG ATC CGC GAA GAT 3'
UreG mutation H74C	5' GAA ACC GGC GGC TGC CCG <u>TGC</u> ACG GCG ATC CGC GAA GAT 3'
UreG mutation H74N	5' GAA ACC GGC GGC TGC CCG <u>AAT</u> ACG GCG ATC CGC GAA GAT 3'
UreG mutation D80A	5' CAT ACG GCG ATC CGC GAA <u>GCG</u> GCC TCA ATG AAC CTC GCC 3'
UreG mutation S111A	5' GAA AGC GGC GGC GAT AAC CTG <u>GCC</u> GCC ACC TTC AGC CCG GAG
	CTG 3'
	5' CAG CTC CGG GCT GAA GGT GGC <i>GGC</i> CAG GTT ATC GCC GCC GCT
	TTC 3'
UreG mutation S115A	5' AAC CTG AGC GCC ACC TTC <i>GCC</i> CCG GAG CTG GCG GAT CTG 3'
	5' CAG ATC CGC CAG CTC CGG <i>GGC</i> GAA GGT GGC GCT CAG GTT 3'
UreG mutation D120A	5' C CGG AGC TGG CGG <i>CGC</i> TGA CCA TCT AC 3'
	5' GT AGA TGG TCA <i>GCG</i> CCG CCA GCT CCG G 3'
UreG mutation D127A	5' CA TCT ACG TCA TCG <u>CGG</u> TGG CCG AAG GGG AG 3'
	5' CT CCC CTT CGG CCA <u>CCG</u> CGA TGA CGT AGA TG 3'

Circular Dichroism (CD). Wild-type and Strep-tagged UreG proteins were purified and concentrated up to 0.2 mg mL $^{-1}$ in 15 mM potassium phosphate buffer, pH 7.6, containing 1 mM DTT. A 100 μ L sample was placed into a 1 cm path length cell and scanned using a Jasco J-710 spectropolarimeter between 180 and 300 nm. The data were analyzed with the DICHROWEB server (39), and the best fit was obtained by using CDSSTR and set 4.

Analytical Gel Filtration Chromatography. Analytical hydrodynamic radius assays used Sephacryl 300 HR (65 cm x 2.0 cm diam., Sigma). The buffer contained 50 mM HEPES, pH 7.4, with 200 mM NaCl and other additives as indicated, using a flow rate of 1 mL min⁻¹.

In vivo Expression of UreG_{Str} Variants in the Context of the Urease Operon. Plasmid pKK17 (29), which contains the entire ureDABCEFG urease gene cluster under the control of the tac promoter, was modified to encode UreG_{Str} and its mutant forms by replacing a Psil/KpnI fragment to create plasmid pKKG and variants. For analysis of urease activity in cell extracts, E. coli DH5α containing the desired plasmid was inoculated into 1 mL of LB supplemented with 300 μg mL⁻¹ of ampicillin and 1 mM NiCl₂ (unless noted) and grown overnight at 37 °C with agitation. A 0.25 mL aliquot of the culture was used to inoculate 25 mL of LB containing 100 μg mL⁻¹ ampicillin plus 1 mM NiCl₂ (unless noted) and grown for 2.5 h at 37 °C with agitation. IPTG added to 0.1 mM was used to induce the expression of the operon overnight at 37 °C. Cells were harvested by centrifugation for 10 min at 5,000 x q and 4 °C and resuspended in either 1 mL of 25 mM HEPES buffer, pH 7.4, if performing urease activity assays or 750 µl of buffer W if used for pull-down assays. Phenylmethylsulphonyl fluoride was added to 0.1 mM, the cells were sonicated (Branson 450 sonifier, 5 repetitions, each of 45 sec, at 1 W output power and 50% duty cycle), and the disrupted cells were centrifuged 10 min at 4 °C and 16,000 x g in a microcentrifuge. The soluble, cell-free extracts were used to test urease activity and perform pull-down assays.

Urease Activity Assays. Urease activities were measured by quantifying the rate of ammonia release from urea by formation of indophenol, which was monitored at 625 nm (40). One unit of urease activity was defined as the amount of enzyme required to hydrolyze 1 µmole of urea per min at 37 °C. The standard assay buffer consisted of 50 mM HEPES, pH 7.8, and 50 mM urea.

Metal Quantification. The metal contents of freshly purified UreG and UreG $_{Str}$ were assessed by using inductively coupled plasma-emission spectrometry at the University of Georgia Chemical Analysis Laboratory.

Metal Binding Analyses. Purified proteins were dialyzed overnight against 50 mM HEPES buffer, pH 7.4, containing 200 mM NaCl, 1 mM EDTA, and 1 mM DTT, followed by dialysis against 50 mM HEPES buffer, pH 7.4, containing 200 mM NaCl until the EDTA and DTT concentrations were negligible. Non-radioactive equilibrium dialysis experiments were performed by using an equilibrium micro-volume dialyzer (Hoefer Scientific instruments). Purified protein (400 μL of 10 μM) was dialyzed against 400 μL of various concentrations of NiCl₂ or ZnCl₂ overnight at 4 °C by using a 3,500 Da molecular weight cut off membrane (MWCO, Spectra-Por). Metal concentrations on both sides of the membrane were determined by adding 100 μL of these solutions to 900 μL of 100 μM 4-(2-pyridylazo) resorcinol (PAR) made in 50 mM HEPES (pH 7.4) with 200 mM NaCl, incubating for 10 min, and monitoring the absorbance at 500 nm (41). The data were plotted and analyzed in Sigma Plot (Systat Software, Inc.) by using Eq. 1, appropriate for samples containing a single type of binding site, where Y is the number of metal ions bound per UreG subunit, B_{max} is the maximum number of metal ions bound per UreG peptide, [M_f] is the concentration of free metal ions, and K_d is the dissociation constant.

$$Y = B_{\text{max}}[M_f]/(K_d + [M_f]) \tag{1}$$

Metal competition experiments were performed in a Rapid Equilibrium Dialysis plate (Pierce

Biotechnology, Rockford, IL). Purified UreG $_{Str}$ (300 μ L of 25 μ M) was dialyzed against 500 μ L of varying concentrations of nickel ions containing 63 Ni and the indicated concentrations of ZnCl $_2$, with shaking overnight at 5 °C and 300 rpm. Aliquots of the resulting samples (200 μ L) were added to 10 mL of Safety Solve (Research Products International Corp.) and 63 Ni contents were determined by using a Beckman-Coulter LS6500 liquid scintillation counter. The data were fit by using the following equation for competitive binding to a single type of binding site:

$$Y = B_{max}[Ni]/\{K_{d}(1 + [Zn]/K_{i}) + [Ni]\}$$
 (2)

The constants are as indicated above, and K_i is the inhibition constant for Zn.

 $UV/Visible\ Spectroscopy.$ Samples (1 mL) of the indicated concentrations of $UreG_{Str}$, C28A $UreG_{Str}$, and C72A $UreG_{Str}$ in 50 mM HEPES, pH 7.4, containing 200 mM NaCl were titrated with aliquots of 1-5 μ L of 1 mM NiCl₂. Absorption spectra were obtained after each addition, and these were corrected for dilution.

Pull-Down Assays. Soluble cell-free extracts from *E. coli* DH5α containing pKKG grown with and without supplemented Ni were loaded onto a 0.3 mL *Strep*-Tactin column equilibrated in buffer W. Proteins were eluted according to the manufacturer's instructions and analyzed by using 13.5% SDS-PAGE.

For *in vitro* pull-down assays, UreE and Ure G_{Str} or variants were mixed in a final concentration of 16 μ M for each protomer with varying concentrations of NiCl₂ or ZnCl₂, incubated on ice as indicated, applied to a 0.5 mL *Strep*-Tactin column, washed, and eluted

according to the manufacturer's instructions. Eluted fractions were analyzed by using 12% SDS-PAGE. Further analysis of the interaction between UreE and UreG $_{Str}$ was carried out by mixing equal concentrations of each protein (40 or 150 μ M protomer) and subjecting the mixture to chromatography on Sephacryl S-300 in buffer containing or lacking 60 μ M NiCl $_2$.

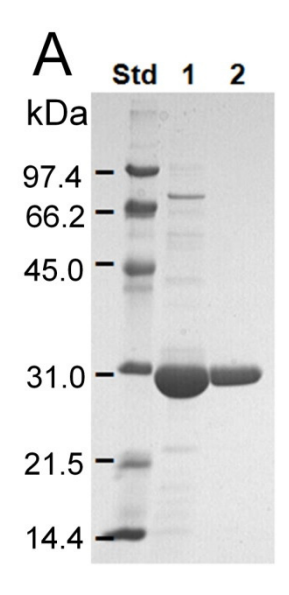
Western Blot. Proteins were resolved by SDS-PAGE and transferred to an Immobilon-P polyvinylidene difluoride membrane (Millipore, USA). ExtrAvidin®—alkaline phosphatase conjugate (1:2500 dilution, Sigma, USA) was used as a probe to bind to *Strep*-tagged forms of UreG. BCIP®/NBT-Blue Liquid Substrate (Sigma, USA) was added to develop the color. To detect UreE or urease, the membranes were incubated for 45 min with anti-UreE IgG (1:10,000 dilution) (*38*) or anti-urease antibody (1:5,000 dilution) (*34*) in TBS buffer (150 mM NaCl, 100 mM Tris, pH 7.4) containing 1% Tween 20. After washing the membranes four times with TBS buffer, they were incubated for 45 min with anti-rabbit IgG conjugated to alkaline phosphatase (Sigma, USA) that was diluted 30,000-fold. The membranes were washed again and BCIP®/NBT-Blue Liquid Substrate was added to develop the color. Prestained molecular weight markers were obtained from Bio-Rad (Hercules, CA).

RESULTS

Characterization of Strep-Tagged UreG. The native form of K. aerogenes UreG was previously purified from recombinant E. coli cells by sequential use of two Mono-Q columns in different buffers followed by gel filtration chromatography (13); however, the tendency of the protein to elute from ion exchange resins over a large number of fractions led to low overall yields. To overcome this problem and to facilitate a single-step purification of UreG variants, we developed a new purification system exploiting a fusion peptide sequence that binds with high affinity to Strep-Tactin resin. The Strep-tag II (42, 43) was designed specifically to allow affinity purification without introduction of metal-binding residues as in the commonly used His6-tag. The ureG sequence was cloned into plasmids pASK-IBA3plus and pASK-IBA5plus to encode UreG fused with a Strep-tag at the C- and N-terminus, respectively. E. coli BL21(DE3) cells transformed with the plasmid derived from the pASK-IBA3plus vector produced more recombinant protein, so this plasmid was selected for further experiments. For comparative analyses, native UreG also was obtained by using the previously described protocol (13).

Highly purified $UreG_{Str}$ was obtained by single-step chromatography on a Strep-Tactin column and essentially homogeneous protein was available after subsequent gel filtration chromatography in buffer containing 1 mM DTT (Figure 2.3A). The elution profile (Figure 2.3B) was consistent with $UreG_{Str}$ being monomeric with a very small shoulder suggesting a trace of dimeric protein. Significantly, the monomeric nature of this protein was retained regardless of the presence or absence of nickel or zinc ions. By contrast to these metal ion-independent results, the inclusion of nickel ions caused the C28A $UreG_{Str}$ variant to chromatograph primarily

as a dimer (Figure 2.3B, gray trace), as described further in a later section. For comparison to $UreG_{Str}$, native UreG exhibited a major monomeric species as well as a minor dimeric feature by size exclusion chromatography (data not shown), with the dimer peak disappearing after overnight dialysis in a buffer containing DTT. These results are consistent with the dimer being an artifact of oxidation that occurs much more readily in the wild-type protein than in $UreG_{Str}$.



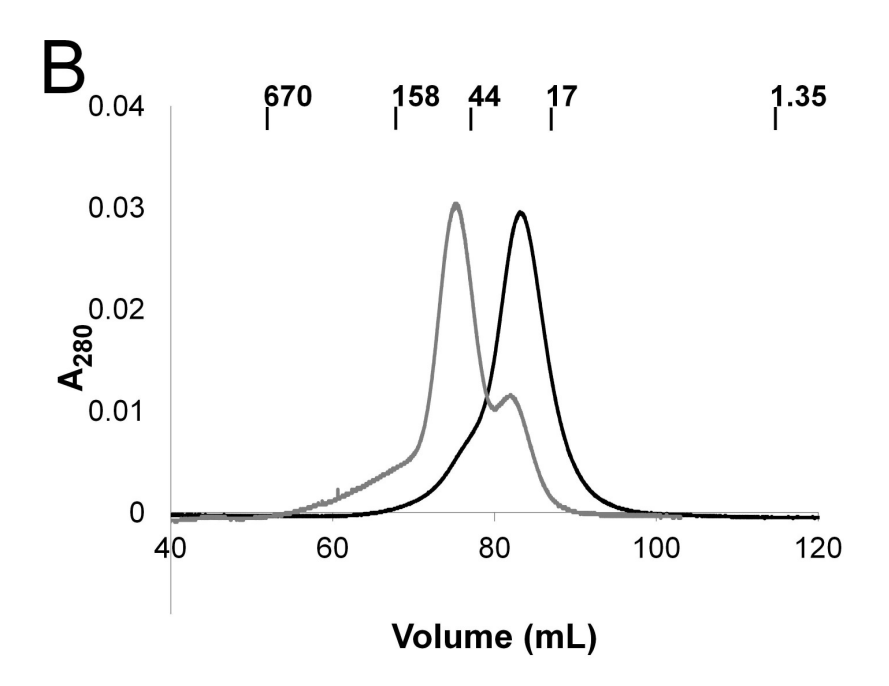


Figure 2.3: Purification of $UreG_{Str}$ and size exclusion chromatography native size analysis. (A) Purification of $UreG_{Str}$. Lane 1: $UreG_{Str}$ after Strep-Tactin column purification. Lane 2: $UreG_{Str}$ after Superdex-75 gel filtration chromatography. (B) Sephacryl S300HR size exclusion chromatography. $UreG_{Str}$ (1.0 mL) was loaded onto a 130 mL Sephacryl S-300 column equilibrated with 50 mM HEPES buffer, pH 7.4, containing 200 mM NaCl plus 15 μ M NiCl₂ and chromatographed at a flow rate of 1 mL min $^{-1}$. Black: $UreG_{Str}$. Gray: C28A $UreG_{Str}$. The positions of molecular weight standards (BioRad) are indicated in kDa.

The presence of the *Strep*-tag did not affect folding of UreG according to CD spectroscopy (spectra not shown). Fitting of the spectra indicated UreG_{Str} (60% α helix, 18% β strands, 4% turns, and 18% random coil for UreG_{Str}) possessed essentially the same secondary structure as native UreG (65% α helix, 15% β strands, 5% turns and 15% random coil for native UreG), each with a normalized root mean square deviation of 0.001).

Targeting Residues for Mutagenesis. Several criteria were used to select UreG_{Str} residues for mutagenesis. First, we identified highly conserved residues by creating an alignment using Clustal W (44) of the most diverse UreG and HypB sequences found in the NCBI database along with other UreG sequences of interest. The hydrogenase-activating GTPases are ~25% identical in sequence to UreG and both of these protein families function in assembly of nickel metallocenters. Notably, residues conserved in these two protein families constitute a much smaller number than the residues conserved in just UreG proteins (where the identities typically are over 50%; see UreG sequence comparisons in (22, 23)). The UreG/HypB sequence comparison highlights the P-loop motif (GSGKT at positions 17-21 in K. aerogenes UreG), the signature motif (ESGG at positions 104-107 of UreG) for the SIMBI G3E family of GTPases (45), and the guanine specificity loop (NKTD at positions 151-154 of UreG) (Figure 2.2). Second, we examined the crystal structure of M. jannaschii HypB (27) which uses Cys95, His96, and Cys127 to coordinate a dinuclear zinc binding site; counterparts were identified in K. aerogenes UreG (Cys72, His74, and perhaps either Ser111 or Ser115, although Ser is rarely observed as a metal ligand). In addition, the HypB structure indicated multiple residues involved in MgGTP binding, hinting at the comparable residues in UreG. Finally, we identified K. aerogenes UreG residues

corresponding to those hypothesized to be metal ligands in *B. pasteurii* UreG (22), as well as some residues that were not as highly conserved but seemed likely choices for metal binding.

On the basis of these criteria, the following residues were targeted for mutagenesis. Lys20, previously shown to be a critical P-loop residue (13), was changed to form K20A Ure G_{Str} . Asp49, equivalent to the Mg⁺²-coordinating Asp75 in *M. jannaschii* HypB (27), was changed to generate D49A UreG_{Str}. Glu68, the residue corresponding to a suggested metal ligand of the B. pasteurii protein (22), was changed to obtain the E68A protein. Cys72, likely to correspond to the Cys95 metal ligand at the dinuclear site of M. jannaschii HypB (27) and whose equivalent was speculated to be a metal ligand in B. pasteurii UreG (22), was changed to create the C72A variant. His74, likely to correspond to the His96 dinuclear center ligand of HypB (27) and equivalent to the postulated His70 metal ligand in B. pasteurii UreG (22), was changed to produce the H74A mutant protein. Asp80, corresponding to Asp98 of HypB (where it is positioned between the dinuclear center and the GTP-binding site) and highly conserved in both proteins, was changed to make D80A UreG_{Str}. Ser111 and Ser115 that approximate the Cys127 ligand of the dinuclear site in HypB were changed to fashion the S111A and S115A proteins. In addition, Cys28, the only other cysteine residue in the K. aerogenes UreG sequence, along with Glu25 and Asp33, the two acidic residues closest to that cysteine, and Asp120 and Asp127, two highly conserved aspartic acid residues, were all changed to alanine residues.

Effect of UreG_{Str} Variants on Urease Activity in Cell Extracts. The selected ureG mutants

were expressed as part of the urease operon, and the levels of the encoded $UreG_{Str}$ variants were shown to be indistinguishable by Western blot (data not shown). The urease activities measured in soluble extracts of cells producing $UreG_{Str}$ were essentially identical to those of extracts from cells containing native UreG (Table 2.3). Similarly, cell-free extracts containing D33A and E68A $UreG_{Str}$ possessed about 80% of the activity observed for extracts containing the non-mutant $UreG_{Str}$. The E25A, C28A, S115A, and D127A forms of $UreG_{Str}$ exhibited somewhat diminished activities (5%, 13%, 30%, and 33%, respectively, of wild type urease activity). In contrast, the cells producing K20A, D49A, C72A, H74A, D80A, and S111A variants of $UreG_{Str}$ exhibited nearly undetectable levels of urease activity. For unidentified reasons, the gene encoding D120A $UreG_{Str}$ was unable to be cloned into the urease gene cluster despite repeated attempts.

Table 2.3: Effects of UreG Mutations on the Urease Activity in Soluble Cell-free Extracts

Sample	Specific activity	Specific activity
	$(U mg^{-1})^a$	(% of wild type)
UreG	129.6 ± 10.4	100
UreG _{Str}	122.6 ± 9.8	94.6
K20A UreG _{Str}	0.09 ± 0.01	0.07
E25A UreG _{Str}	6.4 ± 1.9	4.94
C28A UreG _{Str}	16.6 ± 1.3	12.8
D33A UreG _{Str}	105.4 ± 10.5	81.3
D49A UreG _{Str}	0.19 ± 0.04	0.15
E68A UreG _{Str}	107.4 ± 8.6	82.9
C72A UreG _{Str}	0.14 ± 0.02	0.11
H74A UreG _{Str}	0.14 ± 0.04	0.11
D80A UreG _{Str}	0.24 ± 0.15	0.19
S111A UreG _{Str}	0.09 ± 0.01	0.07
S115A UreG _{Str}	39 ± 10	30.1
D127A UreG _{Str}	42.6 ± 6.2	32.9

^a Error values are standard deviation from triplicate biological samples, including a minimum error associated with protein assays.

Metal Binding to UreG, UreG_{Str}, and UreG_{Str} Variants. Based on published metal-binding studies of UreG from other sources (22-25) and the dinuclear zinc metallocenter structure of HypB, we tested whether UreG from K. aerogenes would bind nickel or zinc ions. Freshly purified UreG and UreG_{Str} were free of metal according to inductively coupled plasma-emission spectrometry. The nickel and zinc ion binding properties of UreG, UreG_{Str}, and the site-directed mutants were examined by using PAR, a colorimetric indicator (41), to monitor metal concentrations after equilibrium dialysis (Table 2.4). As shown in Figure 2.4, UreG_{Str} and native UreG each bound approximately one nickel ion per monomer (1.0 \pm 0.08 and 0.95 \pm 0.09

per monomer, respectively), with $UreG_{Str}$ also binding 1.1 \pm 0.08 Zn (zinc ion binding to native UreG could not be reliably determined due to protein precipitation). Surprisingly, $UreG_{Str}$ bound nickel ions with greater affinity ($K_d = 5.0 \pm 1.8 \, \mu M$) than native UreG ($K_d = 16 \pm 3.1 \, \mu M$) (Figure 2.4A). The basis of this lower K_d is unclear and this difference in K_d could be a point of potential concern; however, $UreG_{Str}$ is able to activate urease to wild-type levels (Table 2.3), so the tagged version of the protein was used for further studies. The nickel-binding properties of the variant proteins were studied by using the tagged constructs and selected results were confirmed by using the non-tagged version.

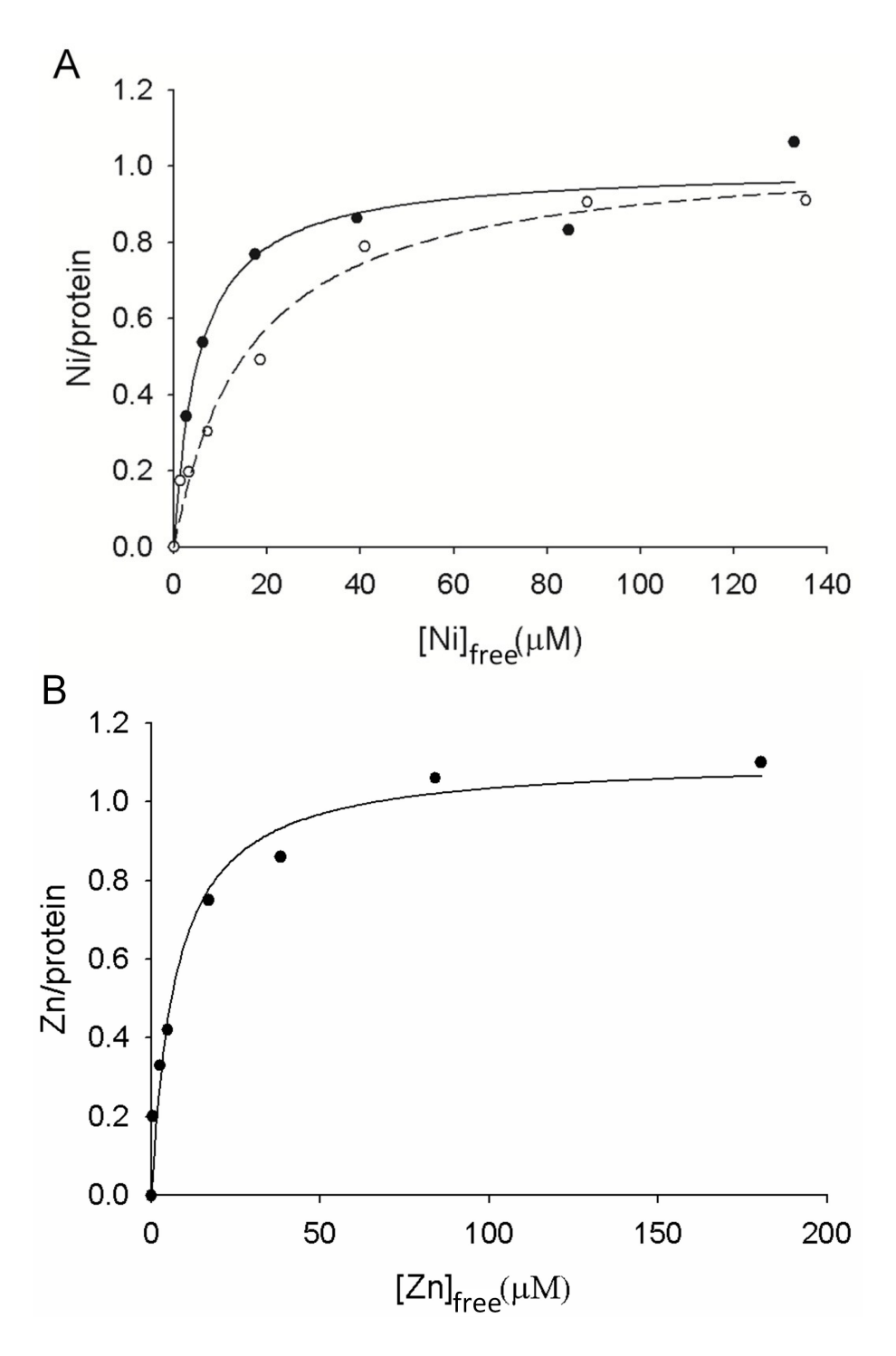


Figure 2.4: Equilibrium dialysis analysis of metal binding to wild type and Strep-tagged UreG. (A) Nickel ion binding to $UreG_{Str}$ (filled circles) and UreG (open circles). (B). Zinc ion binding to $UreG_{Str}$. The concentrations of metal ions in dialysis chambers containing protein and buffer were assessed by reaction with PAR, and the differences of these values were used to calculate the amounts of metal:protein complexes. Ligand binding fits to a single type of binding site are indicated.

In order to examine whether nickel and zinc ions compete for the same metal binding site of $UreG_{Str}$, additional equilibrium dialysis experiments used ^{63}Ni . When dialyzed against varying concentrations of nickel ions containing 63 Ni, UreG_{Str} (25 μ M) bound 1.15 \pm 0.07 nickel ions per monomer with a K_d of 2.7 \pm 0.2 μM (Figure 2.5 A), in very reasonable agreement with the PAR data. Using these baseline data, two types of competitive binding assays were performed. First, UreG_{Str} was dialyzed against varying concentrations of nickel ions containing 63 Ni and a constant concentration of zinc ions (10 μ M) (Figure 2.5 A, dashed line). These results clearly demonstrate competition between the metal ions; equation 2 provided a zinc ion K_i of $3.9 \pm 0.3 \,\mu\text{M}$. Second, UreG_{Str} was dialyzed against a constant concentration of nickel ions (25 μ M) containing 63 Ni along with varied concentrations of zinc ions (Figure 2.5 B). A zinc ion K_i of $2.7 \pm 0.2 \,\mu\text{M}$ was determined, in close agreement with the first method. The K_i for zinc ion competition of nickel ion binding is in good agreement with the K_d for Zn determined by the PAR method (Figure 2.4 B).

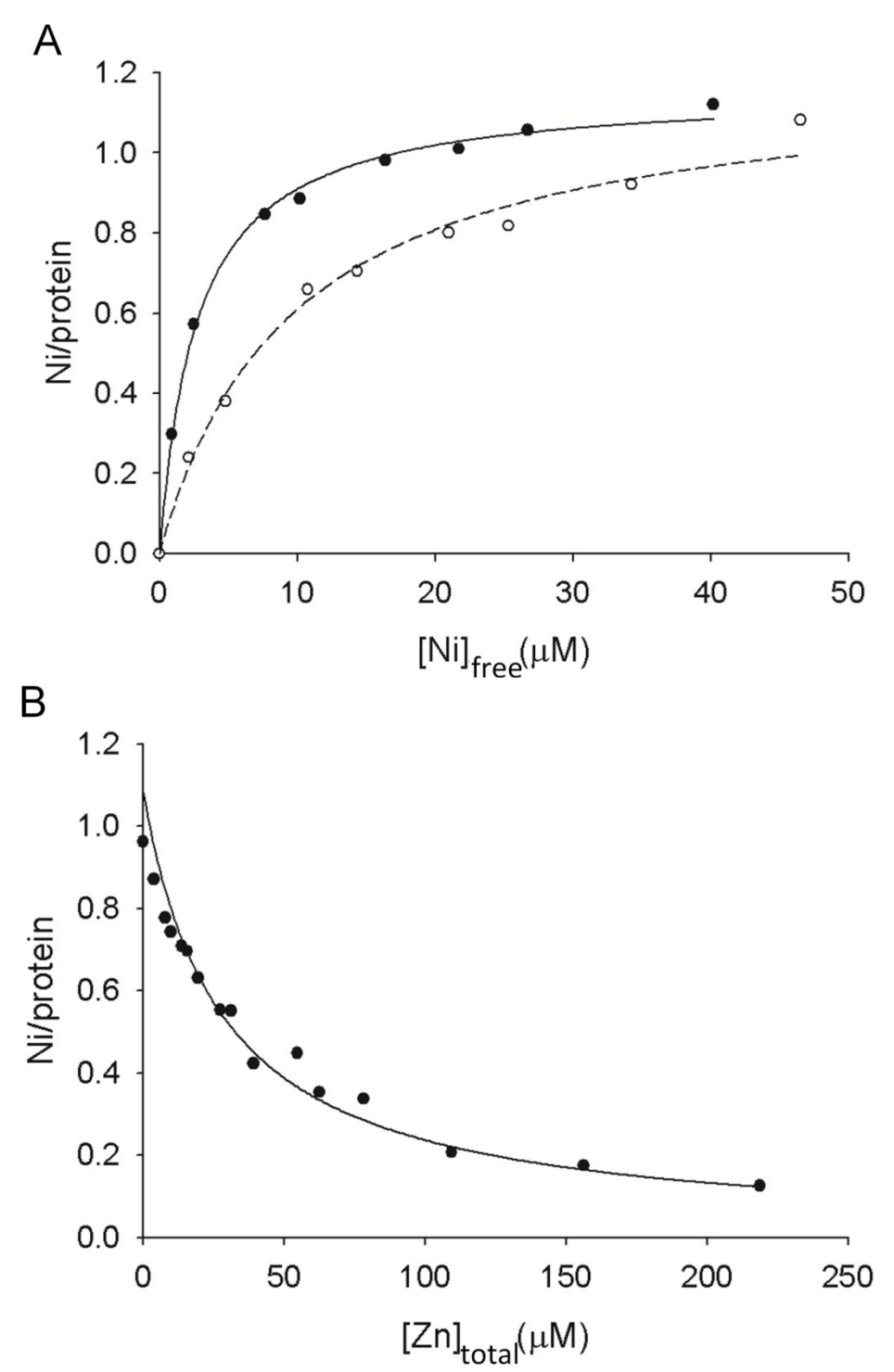


Figure 2.5: Equilibrium dialysis analyses to assess the competition of nickel and zinc ions. (A) Varying concentrations of nickel ions containing ⁶³Ni were examined for binding to 25 μ M UreG_{Str} in the absence of added zinc ions (filled circles) or in competition with 10 μ M ZnCl₂ (open circles). (B) 25 μ M UreG_{Str} was mixed with 25 μ M nickel ions containing ⁶³Ni and varied concentrations of zinc ions. The data were fit by using Eq. 3.

PAR-based equilibrium dialysis experiments were carried out with all site-directed variants. Unfortunately, zinc ions caused protein precipitation at concentrations higher than 100 μ M with nearly all of the mutant UreG_{Str} proteins, thus precluding their detailed thermodynamic analyses. In contrast, the mutant proteins exhibited well-behaved nickel ion binding curves. Table 2.4 provides the nickel ion K_d and B_{max} for each mutant protein. Most UreG_{Str} variants behaved much like the control protein in terms of their thermodynamics of nickel ion binding. That is, their Kd values were the same or only slightly larger than that of UreG_{Str} and they bound a single nickel ion per protomer. Nearly 4-fold increases in K_d were measured with the E25A and D80A variants. The largest change in thermodynamic properties was measured in the case of the C72A UreG_{Str} variant, which exhibited a nickel ion K_d of 61 ± 13 μ M, consistent with its involvement in metal binding. Parallel to the large increase in K_d for C72A UreG_{Str} compared to UreG_{Str}, a similar large increase in K_d was demonstrated in the mutant protein lacking the Strep-tag (59 ± 24 μM, data not tabulated). By contrast to the results related to substitution of Cys72, the mutation affecting the only other Cys in the protein (i.e., C28A UreG_{Str}) behaved much like the control protein in terms of its thermodynamic properties. Nevertheless, this protein did exhibit anomalous behavior. In particular, the C28A variant formed predominantly a dimer in the presence of nickel ions as identified by gel filtration chromatography experiments (Figure 2.3 B).

Table 2.4: Thermodynamics of Nickel Ion Binding to UreG, UreG_{Str}, and its Variants

Protein	<i>K</i> _d (μM)	B_{max}
UreG	16 ± 3.1	1.0 ± 0.08
UreG _{Str}	5.0 ± 1.8	0.95 ± 0.09
E25A UreG _{Str}	18 ± 5	0.75 ± 0.08
C28A UreG _{Str}	8.5 ± 1.9	0.81 ± 0.06
D49A UreG _{Str}	11 ± 2	0.94 ± 0.08
E68A UreG _{Str}	7.7 ± 3.3	0.82 ± 0.09
C72A UreG _{Str}	61 ± 13	1.21 ± 0.1
H74A UreG _{Str}	12 ± 4	1.2 ± 0.1
D80A UreG _{Str}	20 ± 9	1.1 ± 0.1
S111A UreG _{Str}	6.6 ± 2.4	0.97 ± 0.1
S115A UreG _{Str}	12 ± 4	1.1 ± 0.1
D120A UreG _{Str}	10 ± 2	0.92 ± 0.06
D127A UreG _{Str} a	10 ± 5	1.5 ± 0.2

Data were obtained for this sample using a 15,000 MWCO membrane, whereas all other data used a 3,500 MWCO membrane.

To further investigate the nature of the nickel ion-binding site in UreG, NiCl₂ was titrated into solutions of UreG_{Str} and the two UreG_{Str} cysteine variants while monitoring their UV-visible spectra. For UreG_{Str}, a peak at 330 nm appeared with increasing Ni²⁺ concentrations (Figure 2.6 A). This feature is consistent with a thiolate-to-Ni²⁺ charge-transfer transition (46); however, the changes in intensity of this peak versus the concentrations of added nickel ions (Figure 2.7 A) were inconsistent with the K_d obtained by equilibrium dialysis analysis indicating that the two techniques are not reporting on the same event. No absorption feature was detected when nickel ions were added to the C72A protein (data not shown), indicating that

Cys72 is primarily responsible for the ligand-to-metal charge-transfer band noted for $UreG_{Str}$. Titration of nickel ions into the C28A $UreG_{Str}$ protein yielded a feature at 303 nm (Figure 2.6 B). The perturbation of the peak maximum compared to that of the non-mutated protein could be indicative of a different ligand environment for the metal ion in the primarily dimeric C28A $UreG_{Str}$. The intensity changes observed for the C28A variant with varied nickel ion concentrations (Figure 2.7 B) do not reflect the expectations from equilibrium dialysis, again consistent with the two methods measuring non-equivalent nickel ion-binding events. Regardless, it is clear that a Cys residue binds nickel ions in the C28A and native proteins, but not in the C72A variant.

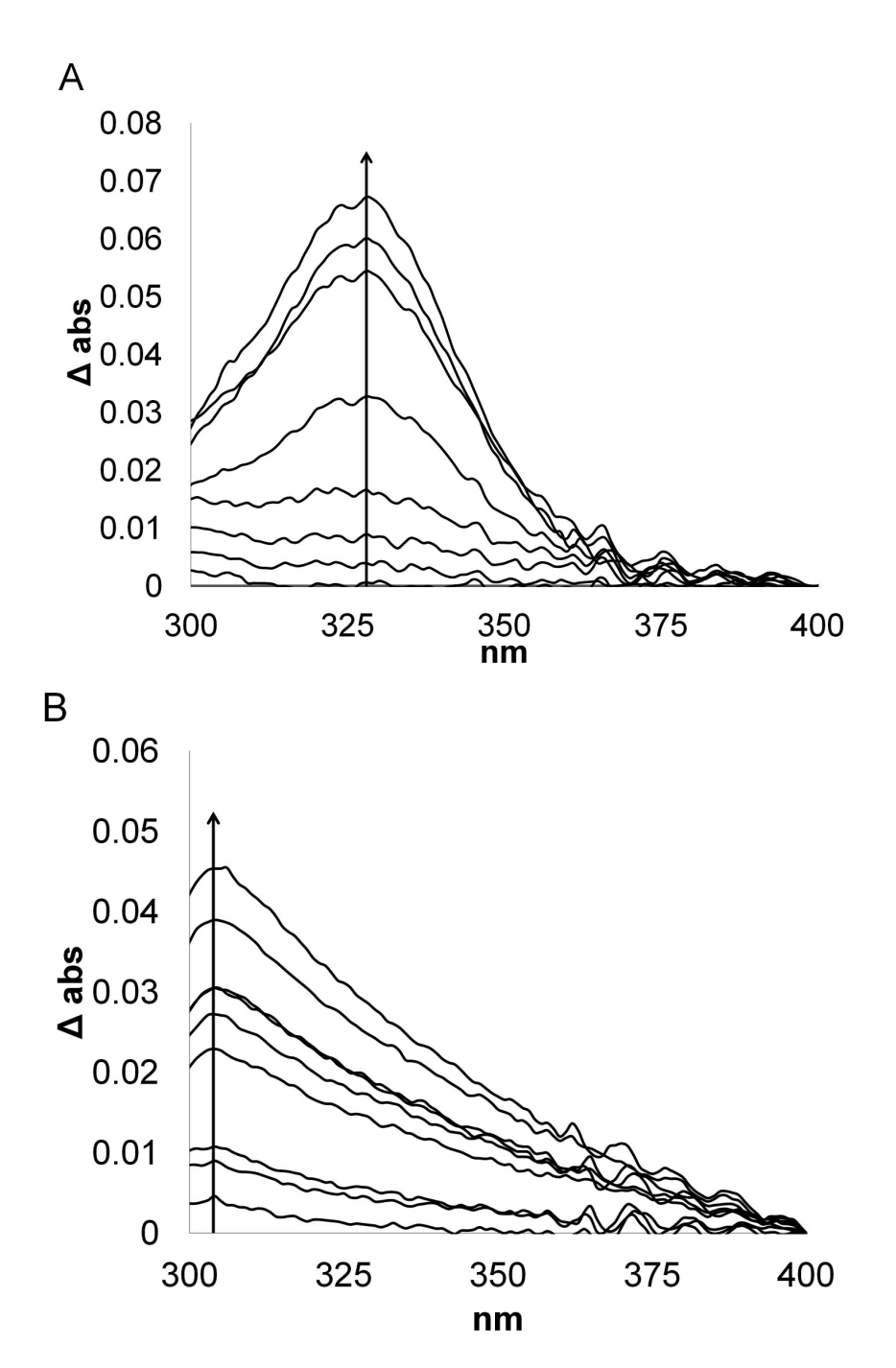


Figure 2.6: UV-visible spectral titrations of $UreG_{Str}$ and its C28A variant with $NiCl_2$. (A) Difference spectra obtained for 58 μ M $UreG_{Str}$ titrated with nickel ions in 50 mM HEPES buffer, pH 7.4, containing 200 mM NaCl. (B) Difference spectra of 26 μ M C28A $UreG_{Str}$ titrated with nickel ions in the same manner.

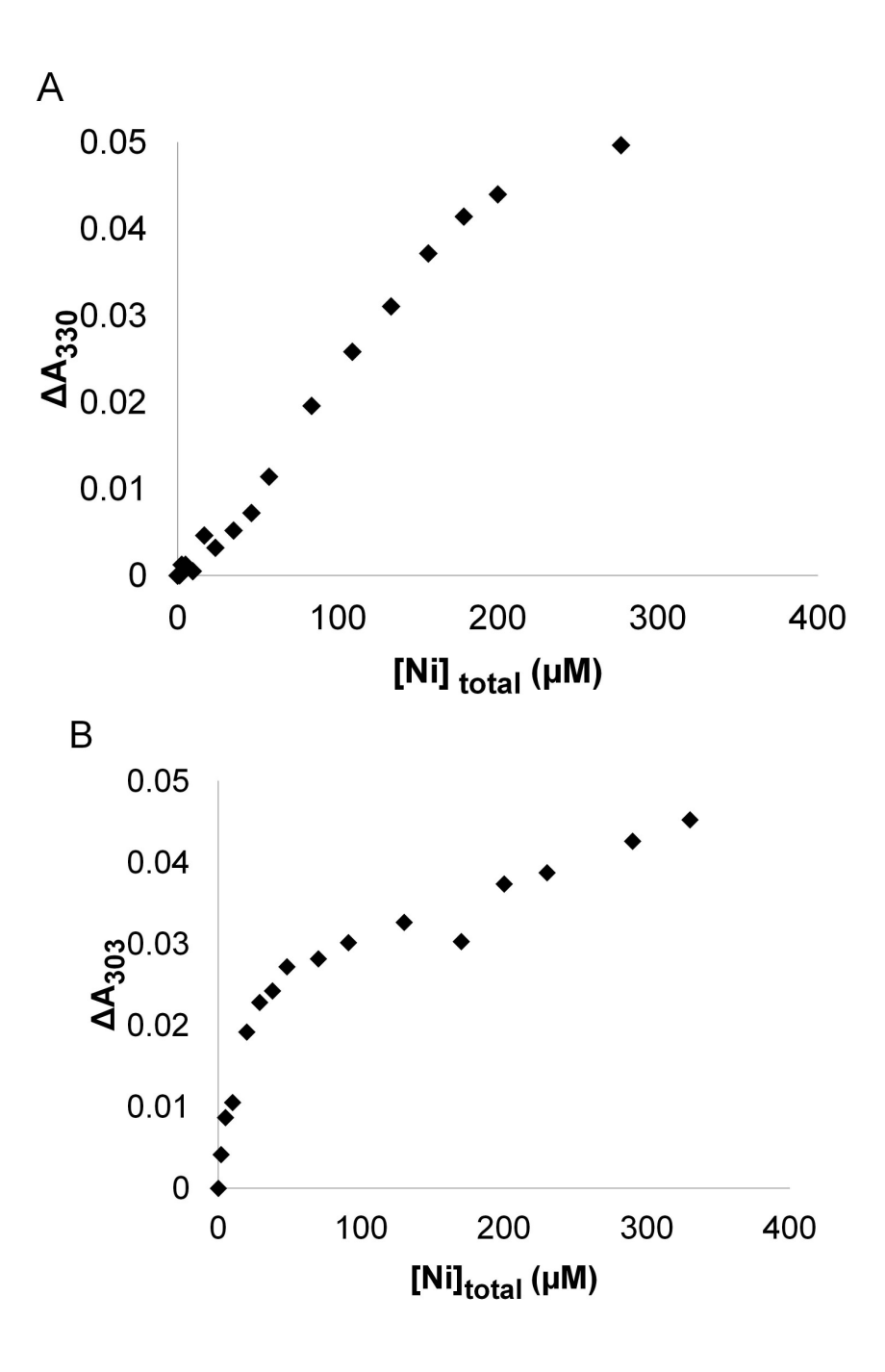


Figure 2.7: Difference in UV-visible absorbance spectra according to Ni concentration (A) Difference in absorbance at 330 nm for $UreG_{Str}$ plotted against the total nickel ion concentration. (B) Difference in absorbance at 303 nm for C28A $UreG_{Str}$ plotted against total nickel ion concentration.

Pull-down Assays. We exploited the Strep-tag on UreG_{Str} to examine the interactions of UreG with other cellular proteins and to identify complexes that form in vivo. E. coli DH5α cells containing the modified urease operon expressing UreG_{Str} or mutants of this protein were grown with or without added nickel ions, then soluble cell-free extracts were chromatographed on Strep-Tactin columns and the proteins eluted with desthiobiotin-containing buffer. The resulting samples were examined by SDS-PAGE, with three key results illustrated (Figure 2.8). For most samples, UreG_{Str} (the expected major band) associated with the urease structural subunits (identified by their characteristic sizes and by Western blot analysis using anti-urease antibodies, data not shown) along with bands migrating at positions expected for the UreD and UreF accessory proteins. In addition, Western blot analysis using anti-UreE antibodies (data not shown) identified UreE in all samples, but this protein was present in much smaller amounts for cells grown in the absence of added nickel ions. In contrast to the other samples, added nickel ions led to the D80A UreG_{Str} forming a complex only with UreE and not associating with urease, UreD, or UreF (Figure 2.8 A).

To further investigate the interaction between $UreG_{Str}$ and UreE, *in vitro* pull-down studies were performed with the purified proteins. $UreG_{Str}$ and UreE (1:1 molar ratio of protomers, 16 μ M each) were mixed in buffer containing various concentrations of nickel or zinc ions. After incubating approximately 10 min on ice, the samples were loaded onto Strep-Tactin columns, washed, and the bound proteins were eluted with desthiobiotin and examined by SDS-PAGE. An increasing ratio of UreE bound to $UreG_{Str}$ as the nickel or zinc ion

concentrations increased, with approximately 0.5 UreE protomer per UreG observed for 60 µM or higher metal ion concentration according to densitometry measurements (Figure 2.8 B). To test whether the amount of complex formation increased over time, a mixture of UreG_{Str}, UreE, and nickel ions was incubated on ice for up to 4 h before performing the pull-down experiment; all incubation times exhibited the same amount of complex (data not shown). The resulting UreG_{Str}:UreE complex was further investigated by using gel filtration chromatography. When equal protomer concentrations of the two proteins were combined and chromatographed on a Sephacryl S-300 column in the absence of metal ions (Figure 2.9 A), a single feature was observed corresponding to overlapping peaks of the monomer of $UreG_{Str}$ ($M_r = 23.1$ kDa) and the dimer of UreE (M_r = 35.1 kDa). By contrast, when the experiment was repeated with 60 μ M NiCl₂ added to the buffer a second peak with an apparent molecular weight of 168 kDa appeared. Analysis of fractions from that peak by using SDS-PAGE revealed an approximate 1:2 UreG_{Str}:UreE protomer ratio as calculated by using densitometry measurements (Figure 2.9 B). Significantly, the ratio obtained here reflects the actual protomer ratio in the isolated complex, whereas the ratio described above includes a combination of UreE that reversibly associated with UreG_{Str} as well as free UreG_{Str}. The second peak eluting from this column was comprised of predominantly UreG_{Str} and chromatographed as the expected monomer. UreE alone forms an even larger complex with an apparent molecular weight of more than 330 kDa when 60 µM NiCl₂ is present (data not shown).

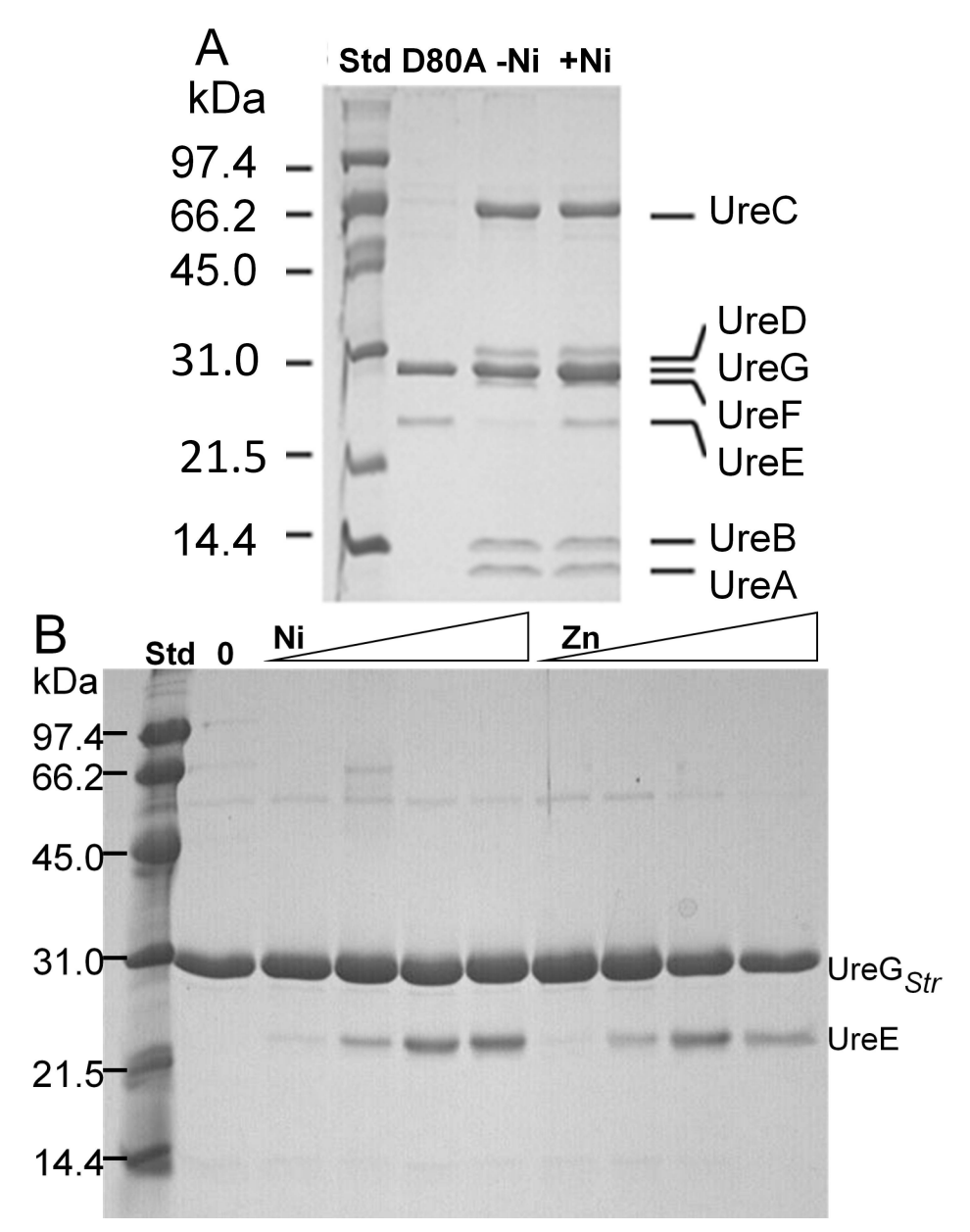


Figure 2.8: Interactions of $UreG_{Str}$ with urease proteins using cell-free extracts and $in\ vitro$ interactions between $UreG_{Str}$ and UreE. (A) $In\ vivo$ complexes formed with selected $UreG_{Str}$ samples in $E.\ coli\ DH5\alpha$ cells. Soluble cell-free extracts were generated from cells grown in medium lacking (-Ni) or containing (+Ni) nickel ions and expressing the urease operon encoding non-mutated $UreG_{Str}$ or for cells expressing the operon encoding D80A $UreG_{Str}$ (+Ni). The extracts were applied to Strep-Tactin columns, and the proteins eluted with desthiobiotin were subjected to SDS-PAGE. (B) $In\ vitro$ pull-down assays using purified $UreG_{Str}$ and UreE. The two proteins (1:1 molar ratio of protomers, $16\ \mu M$ each) were incubated with varying concentrations of nickel or zinc ions (0 to $100\ \mu M$), loaded onto Strep-Tactin columns, eluted with desthiobiotin, and subjected to SDS-PAGE.

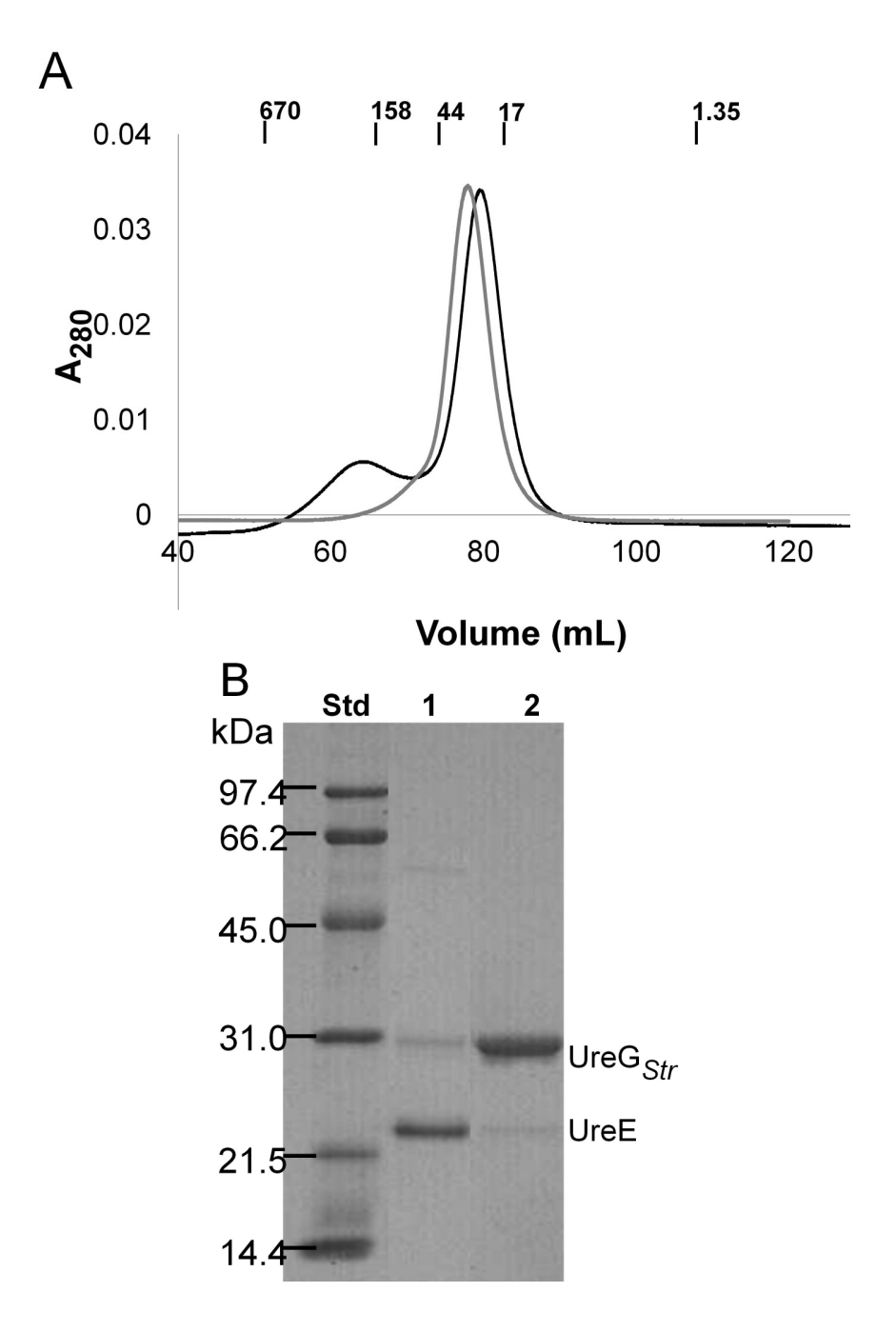


Figure 2.9: Chromotography of $UreG_{Str}$: UreE complex. (A) Sephacryl S-300 chromatography of a mixture of $UreG_{Str}$ and UreE (1:1 molar ratio of protomers) in 50 mM HEPES buffer, pH 7.4, containing 200 mM NaCl with (black) and without (gray) 60 μ M NiCl₂. Molecular weight standards (BioRad) are indicated in kDa. (B) SDS-PAGE analysis of the two peak fractions from panel C from the chromatograph including nickel ions.

The $UreG_{Str}$ variants also were mixed with UreE and subjected to pull-down experiments. None of the $UreG_{Str}$ variants exhibited deficiencies in their abilities to form a complex with UreE when $60~\mu M$ nickel ions were present, nor did any of the mutations form a complex with UreE in the absence of metal.

DISCUSSION

Using a new procedure to purify *K. aerogenes* UreG, we generated significant findings related to the protein's functional quaternary structure, its metal ion binding properties, the effects of selected mutations on activity and metal binding, and the formation of a complex between this protein and its cognate UreE in a manner induced by metal ions. Notably, some of these results obtained using *K. aerogenes* UreG exhibit stark differences compared to those reported for UreG proteins from other organisms (22-24).

The use of a *Strep*-tag on UreG facilitated purification and allowed for protein interaction studies via pull-down assays. While designed to not interfere with metal binding analyses (42, 43), a major concern for the more widely used His_6 -tag, we found the *Strep*-tagged version of UreG bound nickel ions more tightly than the wild type protein. The basis of the three-fold difference in K_d is unclear, but we note that the *Strep*-tag contains a His residue which could play some role in metal binding or in slightly perturbing the protein conformation. These results demonstrate that any tag might have unexpected effects. Significantly, the tag on UreG does not interfere with its function in urease activation as shown by the ability of $UreG_{Str}$ to activate urease apoprotein within cells to 95% of that of the wild-type protein, signifying that the difference in the K_d doesn't affect the role of UreG *in vivo*.

CD measurements confirmed that the *Strep*-tag did not interfere with the overall fold of the UreG protein. Furthermore, both wild-type UreG and UreG $_{Str}$ were found to be highly structured (only 18% and 15% random coil, respectively) compared to the intrinsically

adisordered structures of the *B. pasteurii*, *M. tuberculosis*, and *H. pylori* proteins (30%, 45%, and ~50% random coil, respectively) (23-25). This result might imply that *K. aerogenes* UreG is better suited for structural characterization efforts than UreG from other sources.

UreG_{Str} is monomeric according to gel filtration experiments, and this state is unaffected by the addition of nickel or zinc ions. This quaternary structure differs from the dimeric UreG proteins of *B. pasteurii* or *M. tuberculosis* (23, 25) and from *H. pylori* UreG which dimerizes in the presence of zinc, but not nickel ions (24). Several other members of the SIMBI G3E family of small GTPases possess dimeric structures, while others are monomeric. For example, HypB and MeaB (an editor for transferring vitamin B₁₂ into methylmalonyl-CoA mutase), crystallized as dimers, although - of potential interest - their dimer interfaces are distinct, whereas YjiA (a protein of undefined function) is a monomer (27, 47-49). Our conclusion that UreG functions as a monomeric protein in *K. aerogenes* coincides with earlier results indicating stoichiometric levels of UreD, UreF, and UreG in various urease complexes generated in this system and with data demonstrating that UreD and UreF are stoichiometric with the urease subunits (11-13, 17, 50).

The metal binding properties of K. aerogenes $UreG_{Str}$ also differ significantly from those of UreG proteins isolated from other species. Equilibrium dialysis studies demonstrated that nickel and zinc ions compete with similar affinities for a single metal ion-binding site on $UreG_{Str}$. While the dimeric B. pasteurii UreG similarly binds 1 zinc ion per protomer, it binds 2 nickel ions per protomer with the affinities for the two metal ions differing by an order of magnitude (and these affinities are approximately 10- and 100-fold less than for K. aerogenes $UreG_{Str}$) (22). H.

pylori UreG binds only 0.5 zinc ions per protomer leading to dimerization, whereas it binds two nickel ions per monomer without dimerization and with 20-fold lower affinity (24). In comparison to the B. pasteurii and H. pylori proteins, the small nickel ion K_d of UreG_{Str} may be compatible with its functional significance in transferring nickel ions to UreD in the UreABC-UreDFG activation complex; however, one must be cautious in interpreting these thermodynamic results since urease metallocenter assembly is, at least in part, a kinetic process linked to GTP hydrolysis. Furthermore, we cannot rule out that the physiologically significant metal binding site is comprised of residues from UreG and another urease-related protein.

We identified Cys72 as a nickel ion ligand in $UreG_{Str}$. Replacing this residue with Ala led to a 12-fold increase in the nickel ion K_d , consistent with its participation in the metal binding site. In addition, titration of nickel ions into $UreG_{Str}$ led to the formation of a 330 nm absorption attributed to a thiolate-to- Ni^{2+} charge-transfer transition which was not generated when Cys72 was absent, implicating this residue as a nickel-coordinating ligand. The corresponding Cys68 residue in B. pasteurii UreG also was proposed as a metal ion-binding residue; however, the same residue was identified as forming a disulfide bond that stabilized the dimeric form of that protein (22, 25). Simultaneous function as a disulfide and as a metal ion ligand is unlikely. The corresponding Cys66 residue in H. pylori UreG was proposed to be involved in zinc ion binding on the basis of a 10-fold decreased affinity in the C66A variant (24), but curiously the effects of this mutation on nickel ion binding were not examined. Our studies

of *K. aerogenes* UreG confirm that this conserved cysteine is involved in nickel ion binding and show it does not form an essential disulfide bond.

Other residues comprising the metal ion-binding site of K. aerogenes UreG_{Str} were not identified with certainty by our mutagenesis and equilibrium dialysis studies, but some inferences are possible. The E25A and D80A variants exhibited four-fold increases in nickel ion K_d , and other substitutions had even smaller effects, consistent with nearby residues compensating for the loss of some ligands. Nevertheless, it is notable that mutants expressing the K20A, D49A, C72A, H74A, D80A, and S111A UreG_{Str} proteins in the context of the complete urease gene cluster were essentially inactive. Lys20 is in the P-loop and Asp49 corresponds to the Mg²⁺ coordinating residue of HypB, thus likely accounting for their essential roles. Based on homology to the HypB structure, we propose that His74 and Ser111 are located close to Cys72 and the former residue is likely to participate in metal binding (while we cannot eliminate the possibility, Ser is much less likely to serve as a metal ligand). The residue corresponding to His74 was mutated in H. pylori UreG, and the resulting H68A protein bound zinc ions with lower affinity by an order of magnitude (24), again without analysis of the effects on nickel ion binding. For B. pasteurii UreG, the metal-binding ligands were proposed to be Glu64, Cys68, and His70, corresponding to Glu68, Cys72, and His74 of the K. aerogenes protein (22). The lack of effect on urease activity for cells containing E68A UreG_{Str} effectively rules out this Glu residue as an essential metal-binding residue.

The only other cysteine in K. aerogenes UreG_{Str}, Cys28, is not essential for urease

activation, but the urease activity decreased to 13% of non-mutant samples in cells containing the C28A variant. Titration of nickel ions into the C28A variant generated a perturbed UV spectrum, with nearly a two-fold increase in intensity and a shift of about 30 nm in the absorption feature, indicating a slightly different metal coordinating environment. This change may be associated with the protein's ability to form a dimer in the presence of nickel ions.

In addition to the above new results obtained with purified $UreG_{Str}$, we investigated the interaction of this protein with other urease-related proteins. Soluble extracts of cells expressing the urease gene cluster with ureG modified to encode $UreG_{Str}$ were analyzed by pull-down assays. The Strep-tagged version of UreG formed a complex that included all other urease components, with the amount of bound UreE enhanced by the presence of nickel ions. A similar UreABC—UreD—UreF—UreG—UreE complex was previously described for a sample in which a hinge-like region of UreB was mutated, resulting in the trapping of this complex (50). Those studies led to a model in which the accessory proteins function, in part, to shift the position of the main domain of UreB to allow nickel ions and bicarbonate to gain access to the nascent active site.

When cells expressing the UreG_{Str} variants were examined in the context of the other urease components, Asp80 was identified as being essential for stabilizing the binding of UreG to the UreABC—UreD—UreF complex. Significantly, the D80A variant failed to generate the UreABC—UreD—UreF—UreG—UreE complex; instead, it only interacted with UreE. Asp80 is likely to be positioned at the interface between UreG and the UreABC—UreD—UreF complex. On the basis of prior studies examining urease-related complexes formed with the *K. aerogenes*

proteins, UreG most likely binds to UreF (12-14, 17). The D80A UreG_{Str}:UreE complex indicates that UreE binds to UreG within the UreABC—UreD—UreF—UreG—UreE complex. An interaction between UreG and UreE was previously suggested by two-hybrid analyses of the *H. pylori* proteins (33) and by direct biochemical analysis of these proteins from the same microorganism (26).

Further investigation of the interaction between UreG_{Str} and UreE used purified proteins and in vitro pull-down assays to reveal stabilization of the complex by either nickel or zinc ions. Zinc ion-dependent stabilization of a complex between these proteins was seen previously with the H. pylori proteins (26), but in that case nickel ions were ineffective for generating the complex. Moreover, the protein stoichiometries of the two complexes differed. Whereas the H. pylori proteins formed a zinc-stabilized (UreG)₂(UreE)₂ complex, with a dimeric UreG binding to the dimeric UreE, the K. aerogenes proteins formed a nickel- or zinc-stabilized complex with one UreE dimer per UreG_{Str} protomer, aggregated into a [UreG_{Str}(UreE)₂]₃ complex of ~168 kDa. The Ni-stabilized interaction between K. aerogenes UreG_{Str} and UreE, coupled with the Ni-binding capabilities of UreG and UreD (17), support a model in which UreE delivers nickel ions to UreG within the UreABC-UreD-UreF-UreG complex (Figure 2.10), with the metal ion subsequently passed from UreG to UreD and then into the nascent active site of urease. One or more of the sequential metal ion transfer steps is likely driven by GTP hydrolysis, and the overall process, but not the individual proteins, is specific for nickel ions.

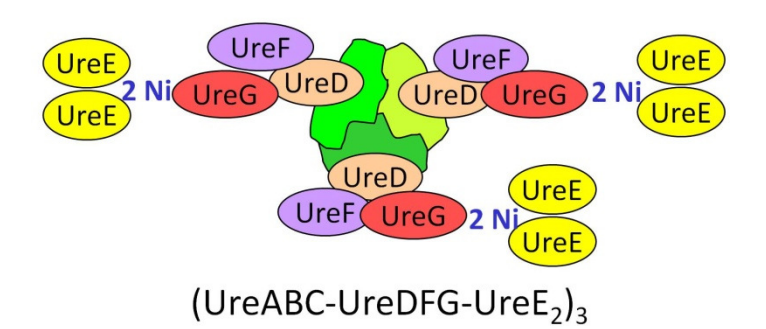


Figure 2.10: Model of UreG:UreE interaction in the urease activation process. UreE binds Ni and delivers it to UreG.

In conclusion, this work describes a new approach to purify *K. aerogenes* UreG using a *Strep*-tag, provides critical new insights into the interactions between this protein and nickel and zinc ions, identifies Cys72 as a nickel ligand, demonstrates the necessity of Asp80 for stabilizing UreG binding to UreABC—UreD—UreF, establishes UreG as the site of binding for UreE, and supports a model for sequential metal ion transfer from UreE to UreG to UreD to the urease active site.

REFERENCES

REFERENCES

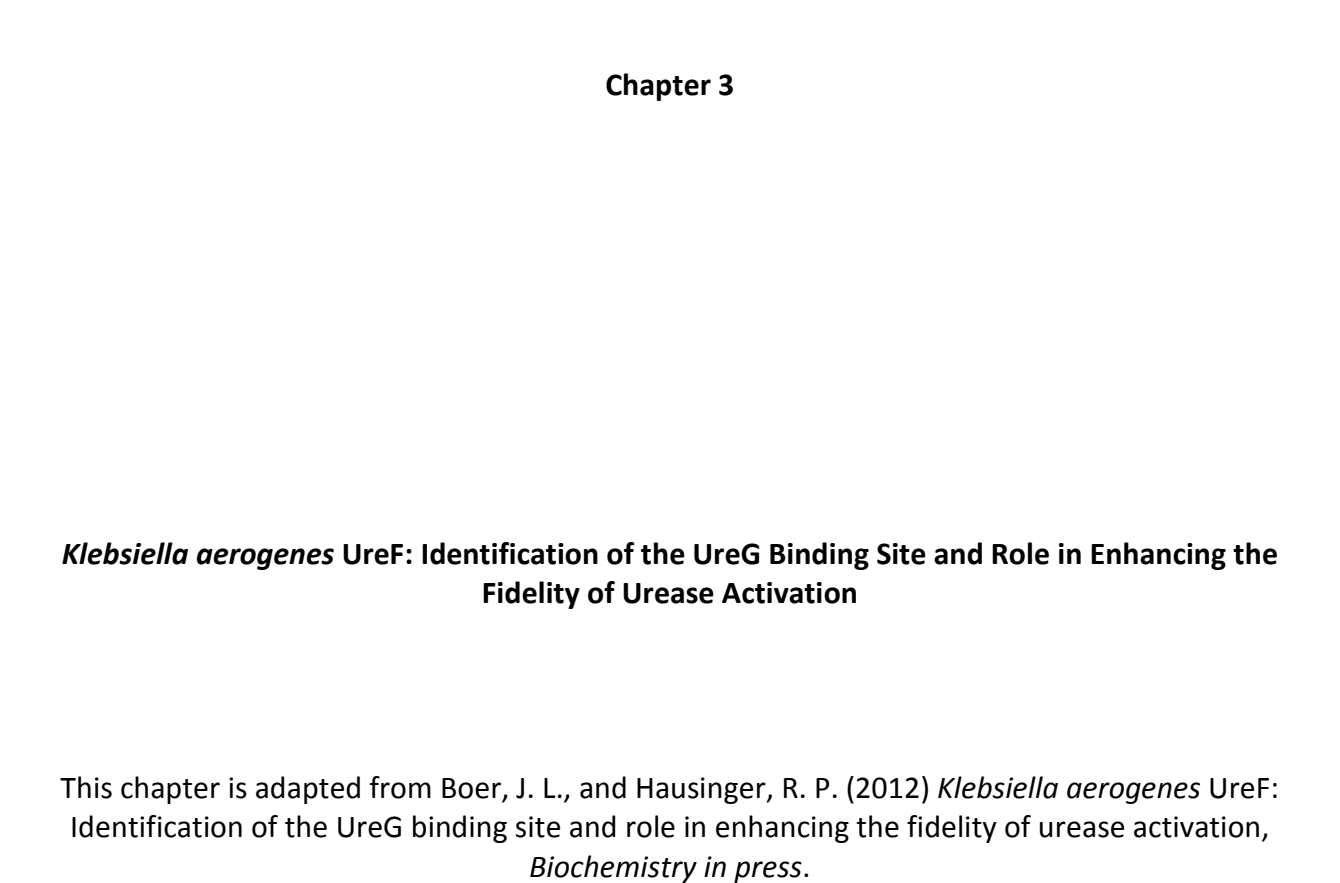
- 1. Carter, E. L., Flugga, N., Boer, J. L., Mulrooney, S. M., and Hausinger, R. P. (2009) Interplay of metal ions and urease, *Metallomics* 1, 207-221.
- 2. Krajewska, B. (2009) Ureases I. Functional, catalytic and kinetic properties: A review, *J. Mol. Catal. B: Enzym. 59*, 9-21.
- 3. Jabri, E., Carr, M. B., Hausinger, R. P., and Karplus, P. A. (1995) The crystal structure of urease from *Klebsiella aerogenes*, *Science 268*, 998-1004.
- 4. Benini, S., Rypniewski, W. R., Wilson, K. S., Miletti, S., Ciurli, S., and Mangani, S. (1999) A new proposal for urease mechanism based on the crystal structures of the native and inhibited enzyme from *Bacillus pasteurii*: why urea hydrolysis costs two nickels, *Structure* 7, 205-216.
- 5. Ha, N. C., Oh, S. T., Sung, J. Y., Cha, K. A., Lee, M. H., and Oh, B. H. (2001) Supramolecular assembly and acid resistance of *Helicobacter pylori* urease, *Nat. Struct. Biol. 8*, 505-509.
- 6. Sheridan, L., Wilmot, C. M., Cromie, K. D., van der Logt, P., and Phillips, S. E. V. (2002) Crystallization and preliminary X-ray structure determination of jack bean urease with a bound antibody fragment, *Acta Crystallogr., Sec. D: Biol. Crystallogr.* 58, 374-376.
- 7. Kim, J. K., Mulrooney, S. B., and Hausinger, R. P. (2005) Biosynthesis of active *Bacillus subtilis* urease in the absence of known urease accessory proteins, *J. Bacteriol.* 187, 7150-7154.
- 8. Quiroz, S., J. K. Kim, S. B. Mulrooney, and R. P. Hausinger. (2007) Chaperones of nickel metabolism, in *Nickel and Its Surprising Impact on Nature* (Sigel, A., H. Sidel, R. K. O. Sigel, Ed.), pp 519-544, John Wiley & Sons, Ltd., Chichester, UK.
- 9. Lee, M. H., Mulrooney, S. B., and Hausinger, R. P. (1990) Purification, characterization, and *in vivo* reconstitution of *Klebsiella aerogenes* urease apoenzyme, *J. Bacteriol.* 172, 4427-4431.
- 10. Jabri, E., and Karplus, P. A. (1996) Structures of the *Klebsiella aerogenes* urease apoenzyme and two active-site mutants, *Biochemistry 35*, 10616-10626.
- 11. Park, I. S., Carr, M. B., and Hausinger, R. P. (1994) In vitro activation of urease apoprotein and role of UreD as a chaperone required for nickel metallocenter assembly, *Proc. Natl. Acad. Sci. U.S.A.* 91, 3233-3237.
- 12. Moncrief, M. B. C., and Hausinger, R. P. (1996) Purification and activation properties of UreD-UreF-urease apoprotein complexes, *J. Bacteriol.* 178, 5417-5421.

- 13. Moncrief, M. B. C., and Hausinger, R. P. (1997) Characterization of UreG, identification of a UreD-UreF-UreG complex, and evidence suggesting that a nucleotide-binding site in UreG is required for in vivo metallocenter assembly of *Klebsiella aerogenes* urease, *J. Bacteriol.* 179, 4081-4086.
- 14. Soriano, A., and Hausinger, R. P. (1999) GTP-dependent activation of urease apoprotein in complex with the UreD, UreF, and UreG accessory proteins, *Proc. Natl. Acad. Sci. U.S.A. 96*, 11140-11144.
- 15. Soriano, A., Colpas, G. J., and Hausinger, R. P. (2000) UreE stimulation of GTP-dependent urease activation in the UreD-UreF-UreG-urease apoprotein complex, *Biochemistry 39*, 12435-12440.
- 16. Fong, Y. H., Wong, H. C., Chuck, C. P., Chen, Y. W., Sun, H., and Wong, K.-B. (2011) Assembly of preactivation complex for urease maturation in *Helicobacter pylori*, *J. Biol. Chem.* 286, 43241-43249.
- 17. Carter, E. L., and Hausinger, R. P. (2010) Characterization of *Klebsiella aerogenes* urease accessory protein UreD in fusion with the maltose binding protein, *J. Bacteriol.* 192, 2294-2304.
- 18. Kim, J. K., Mulrooney, S. B., and Hausinger, R. P. (2006) The UreEF fusion protein provides a soluble and functional form of the UreF urease accessory protein, *J. Bacteriol.* 188, 8413-8420.
- 19. Kim, K. Y., Yang, C. H., and Lee, M. H. (1999) Expression of the recombinant *Klebsiella aerogenes* UreF protein as a MalE fusion, *Arch. Pharm. Res. 22*, 274-278.
- 20. Lam, R., Romanov, V., Johns, K., Battaile, K. P., Wu-Brown, J., Guthrie, J. L., Hausinger, R. P., Pai, E. F., and Chirgadze, N. Y. (2010) Crystal structure of a truncated urease accessory protein UreF from *Helicobacter pylori*, *Proteins 78*, 2839-2848.
- 21. Salomone-Stagni, M., Zambelli, B., Musiani, F, and Ciurli, S. (2007) A model-based proposal for the role of UreF as a GTPase-activating protein in the urease active site biosynthesis, *Proteins 68*, 749-761.
- 22. Zambelli, B., Stola, M., Musiani, F., De Vriendt, K., Samyn, B., Devreese, B., Van Beeumen, J., Turano, P., Dikiy, A., Bryant, D. A., and Ciurli, S. (2005) UreG, a chaperone in the urease assembly process, is an intrinsically unstructured GTPase that specifically binds Zn²⁺, *J. Biol. Chem. 280*, 4684-4695.
- 23. Zambelli, B., Musiani, F., Savini, M., Tucker, P., and Ciurli, S. (2007) Biochemical studies on *Mycobacterium tuberculosis* UreG and comparative modeling reveal structural and functional conservation among the bacterial UreG family, *Biochemistry 46*, 3171-3182.

- 24. Zambelli, B., Turano, P., Musiani, F., Neyroz, P., and Ciurli, S. (2009) Zn²⁺-linked dimerization of UreG from *Helicobacter pylori*, a chaperone involved in nickel trafficking and urease activation, *Proteins 74*, 222-239.
- 25. Neyroz, P., Zambelli, B., and Ciurli, S. (2006) Intrinsically disordered structure of *Bacillus pasteurii* UreG as revealed by steady-state and time-resolved fluorescence spectroscopy, *Biochemistry 45*, 8918-8930.
- 26. Bellucci, M., Zambelli, B., Musiani, F., Turano, P., and Ciurli, S. (2009) *Helicobacter pylori*UreE, a urease accessory protein: specific Ni²⁺- and Zn²⁺-binding properties and interaction with its cognate UreG, *Biochem. J. 422*, 91-100.
- 27. Gasper, R., Scrima, A., and Wittinghofer, A. (2006) Structural insights into HypB, a GTP-binding protein that regulates metal binding, *J. Biol. Chem.* 281, 27492-27502.
- 28. Leach, M. R., and Zamble, D. B. (2007) Metallocenter assembly of the hydrogenase enzymes, *Curr. Opin. Chem. Biol.* 11, 159-165.
- 29. Colpas, G. J., Brayman, T. G., Ming, L. J., and Hausinger, R. P. (1999) Identification of metal-binding residues in the *Klebsiella aerogenes* urease nickel metallochaperone, UreE, *Biochemistry 38*, 4078-4088.
- 30. Musiani, F., Zambelli, B., Stola, M., and Ciurli, S. (2004) Nickel trafficking: insights into the fold and function of UreE, a urease metallochaperone, *J. Inorg. Biochem. 98*, 803-813.
- 31. Song, H. K., Mulrooney, S. B., Huber, R., and Hausinger, R. P. (2001) Crystal structure of *Klebsiella aerogenes* UreE, a nickel-binding metallochaperone for urease activation, *J. Biol. Chem.* 276, 49359-49364.
- 32. Remaut, H., Safarov, N., Ciurli, S., and Van Beeumen, J. (2001) Structural basis for Ni²⁺ transport and assembly of the urease active site by the metallochaperone UreE from *Bacillus pasteurii*, *J. Biol. Chem. 276*, 49365-49370.
- 33. Rain, J. C., Selig, L., De Reuse, H., Battaglia, V., Reverdy, C., Simon, S., Lenzen, G., Petel, F., Wojcik, J., Schachter, V., Chemama, Y., Labigne, A. S., and Legrain, P. (2001) The protein-protein interaction map of *Helicobacter pylori Nature 409*, 211-215.
- 34. Mulrooney, S. B., Pankratz, H. S., and Hausinger, R. P. (1989) Regulation of geneexpression and cellular-localization of cloned *Klebsiella aerogenes* (*Klebsiella pneumoniae*) urease, *J. Gen. Microbiol.* 135, 1769-1776.
- 35. Park, I. S. (1994) Thesis, in *Microbiology*, Michigan State University, East Lansing, MI.

- 36. Colpas, G. J., Brayman, T. G., Ming, L.-J., and Hausinger, R. P. (1999) Identification of metal-binding residues in the *Klebsiella aerogenes* urease nickel metallochaperone, UreE, *Biochemistry 38*, 4078-4088.
- 37. Laemmli, U. K. (1970) Cleavage of structural proteins during assembly of head of bacteriophage-T4, *Nature 227*, 680.
- 38. Lee, M. H., Pankratz, H. S., Wang, S., Scott, R. A., Finnegan, M. G., Johnson, M. K., Ippolito, J. A., Christianson, D. W., and Hausinger, R. P. (1993) Purification and characterization of *Klebsiella aerogenes* UreE protein: a nickel-binding protein that functions in urease metallocenter assembly, *Prot. Sci. 2*, 1042-1052.
- 39. Whitmore, L., and Wallace, B. A. (2004) DICHROWEB, an online server for protein secondary structure analyses from circular dichroism spectroscopic data, *Nuc. Acids Res.* 32, W668-W673.
- 40. Weatherburn, M. W. (1967) Phenol-hypochlorite reaction for determination of ammonia, *Anal. Chem. 39*, 971-974.
- 41. Hunt, J. B., Sue H. Neece, and Ann Ginsburg. (1985) The use of 4-(2-pyridylazo) resorcinol in studies of zinc release from *Escherichia coli* aspartate transcarbamoylase, *Anal. Biochem.* 146, 150-157.
- 42. Skerra, A., and Schmidt, T. G. M. (2000) Use of the Strep-tag and streptavidin for detection and purification of recombinant proteins, in *Applications of Chimeric Genes and Hybrid Proteins*, Pt A, pp 271-304, Academic Press Inc, San Diego.
- 43. Maier, T., Drapal, N., Thanbichler, M., and Böck, A. (1998) Strep-Tag II affinity purification: An approach to study intermediates of metalloenzyme biosynthesis, *Anal. Biochem. 259*, 68-73.
- 44. Larkin, M. A., Blackshields, G., Brown, N. P., Chenna, R., McGettigan, P. A., McWilliam, H., Valentin, F., Wallace, I. M., Wilm, A., Lopez, R., Thompson, J. D., Gibson, T. J., and Higgins, D. G. (2007) Clustal W and clustal X version 2.0, *Bioinformatics 23*, 2947-2948.
- 45. Leipe, D. D., Wolf, Y. I., Koonin, E. V., and Aravind, L. (2002) Classification and evolution of P-loop GTPases and related ATPases, *J. Mol. Biol.* 317, 41-72.
- 46. Kozlowski, H., Révérend, B. D.-L., Ficheux, D., Loucheux, C., and Sovago, I. (1987) Nickel(II) complexes with sulfhydryl containing peptides. Potentiometric and spectroscopic studies, *J. Inorg. Biochem.* 29, 187-197.
- 47. Hubbard, P. A., Padovani, D., Labunska, T., Mahlstedt, S. A., Banerjee, R., and Drennan, C. L. (2007) Crystal structure and mutagenesis of the metallochaperone MeaB: Insight into the causes of methylmalonic aciduria, *J. Biol. Chem. 282*, 31308-31316.

- 48. Khil, P. P., Obmolova, G., Teplyakov, A., Howard, A. J., Gilliland, G. L., and Camerini-Otero, R. D. (2004) Crystal structure of the *Escherichia coli* YjiA protein suggests a GTP-dependent regulatory function, *Proteins 54*, 371-374.
- 49. Padovani, D., and Banerjee, R. (2009) A G-protein editor gates coenzyme B-12 loading and is corrupted in methylmalonic aciduria, *Proc. Natl. Acad. Sci. U.S.A.* 106, 21567-21572.
- 50. Quiroz-Valenzuela, S., Sukuru, S. C. K., Hausinger, R. P., Kuhn, L. A., and Heller, W. T. (2008) The structure of urease activation complexes examined by flexibility analysis, mutagenesis, and small-angle X-ray scattering, *Arch. Biochem. Biophys* 480, 51-57.



ABSTRACT

The Ni-containing active site of Klebsiella aerogenes urease is assembled through the concerted action of the UreD, UreE, UreF, and UreG accessory proteins. UreE functions as a metallochaperone that delivers Ni to a complex of UreD-UreF-UreG bound to urease apoprotein, with UreG serving as a GTPase during enzyme activation. The present study focuses on the role of UreF, previously proposed to act as a GTPase activating protein (GAP) of Sixteen conserved UreF surface residues that may play roles in protein:protein UreG. interactions were independently changed to Ala. When produced in the context of the entire urease gene cluster, cell-free extracts of nine site-directed mutants had less than 10% of the wild-type urease activity. Enrichment of the variant forms of UreF, as the UreE-F fusion proteins, uniformly resulted in co-purification of UreD and urease apoprotein; whereas UreG bound to only a subset of the species. Notably, reduced interaction with UreG correlated with the low activity mutants. The affected residues in UreF map to a distinct surface on the crystal structure, defining the UreG binding site. In contrast to the hypothesis that UreF is a GAP, the UreD—UreF—UreG—urease apoprotein complex containing K165A UreF exhibited significantly greater levels of GTPase activity than that containing the wild-type protein. Additional studies demonstrated the UreG GTPase activity was largely uncoupled from urease activation for the complex containing this UreF variant. Further experiments with these complexes provided evidence that UreF gates the GTPase activity of UreG to enhance the fidelity of urease metallocenter assembly, especially in the presence of the non-cognate metal Zn.

INTRODUCTION

Urease, an enzyme that is widely found in bacteria, plants, and fungi, hydrolyzes urea into ammonia and carbonic acid, with the resulting ammonification and increase in pH having important implications in medicine and agriculture (1-4). The best-studied urease system is produced by recombinant Escherichia coli expressing the Klebsiella aerogenes urease genes, ureDABCEFG. K. aerogenes urease contains three subunits, UreA, UreB, and UreC, that form a trimer of trimers in the supramolecular structure (5). The three active sites in the native enzyme each contain two Ni atoms bridged by a lysine carbamate and are deeply buried in the protein. Assembly of these active sites requires nickel, bicarbonate, GTP hydrolysis, and products of the other four *ure* genes (2, 4). The (UreABC)₃ apoprotein can be purified alone (6) or with combinations of the UreD, UreF, UreG, and UreE accessory proteins (7-11). With each additional accessory protein, (UreABC)₃ is more primed for activation, leading to greater in vitro activity after incubation with Ni, bicarbonate, and GTP when UreG is present (Figure 3.1). As summarized below, some properties of these complexes and the individual urease accessory proteins have been discerned (these comments refer to the K. aerogenes urease components unless stated otherwise); however, their exact roles remain unclear.

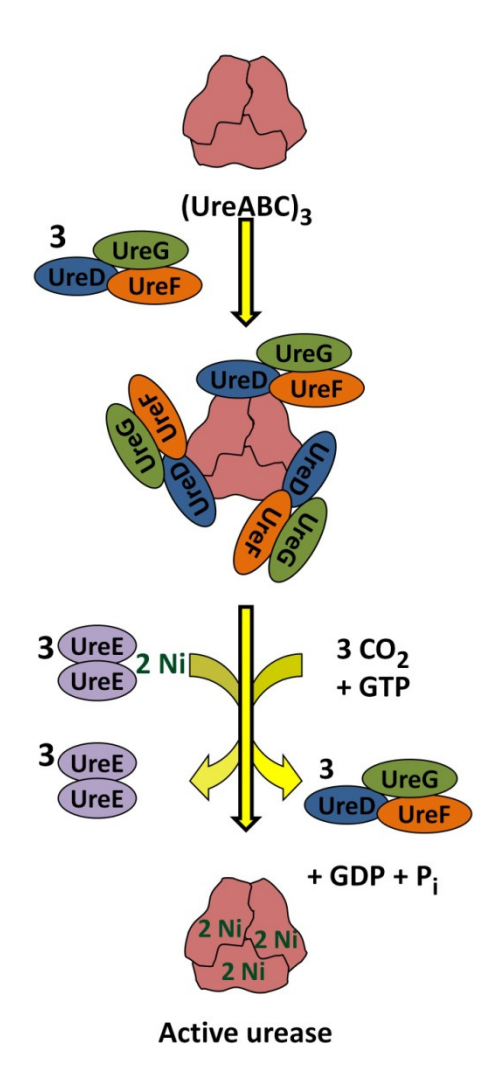


Figure 3.1: Simplified scheme of the urease activation process. Urease is synthesized as an apoprotein, lacking Ni ions and with its active site Lys free of carbamylation. Accessory proteins UreD, UreF, and UreG bind to the apoprotein and, through a process not completely understood, the Lys is carbamylated by CO₂, the metallochaperone UreE delivers Ni, GTP is hydrolyzed, and the auxiliary proteins depart leaving active urease.

The (UreABC—UreD)₃ complex has UreD bound at the vertices of the triangular apoprotein according to small-angle X-ray scattering (SAXS) (12) and chemical cross-linking (13) approaches. When *ureD* is expressed alone the resulting protein is insoluble, but a fusion of the maltose binding protein (MBP) with UreD is soluble and functional (14). Surprisingly, the fusion protein does not bind to (UreABC)₃ in vitro, but it forms a complex with the urease apoprotein

when co-produced *in vivo*. Also of interest, MBP-UreD binds divalent metal ions (~2.5 Ni per protomer, K_d ~50 μ M; ~4 Zn per protomer, K_d ~5 μ M). The structure of UreH (a UreD homologue) from *H. pylori* was recently reported as part of a (UreH—UreF)₂ complex (15). UreH exhibits a novel fold consisting of 17 β -strands and 2 α -helices. The working hypothesis for urease activation suggests that UreD enhances the activation efficiency of urease apoprotein while also acting as a scaffold for the binding of the other auxiliary proteins (2, 4).

(UreABC—UreD—UreF)₃ represents the apoprotein with heterodimers of UreD—UreF binding at its vertices, according to SAXS analysis (12). Chemical cross-linking studies indicate a conformational change takes place in the urease apoprotein within this complex and show a link between UreB and UreF (13). Yeast 2-hybrid experiments carried out using the H. pylori and Proteus mirabilis proteins also support an interaction between UreF and UreD/H (16, 17). Although K. aerogenes UreF is insoluble when produced alone, the fusion proteins with UreF linked to MBP (18) or to UreE (creating UreE-F) (19) are soluble. The gene encoding the fusion protein complements a ureF deletion mutant and binds in vitro to UreABC—UreD or MBP-UreD (14, 19). Truncation variants indicate that the C-terminal 15 residues of UreF are essential for forming the activation complex, and the N-terminal 24 residues are needed for urease activation, but not for binding to the activation complex (19). The crystal structure was solved for truncated H. pylori UreF lacking its C-terminal 21 residues and with its first 24 residues disordered (20). The H. pylori (UreH-UreF)₂ structure contains the last 21 residues that the structure of UreF alone was missing, but the UreF N-terminus also was unstructured in this complex (15). The dimeric UreF protein exhibits an all-alpha-helical fold with highly conserved

residues mapping to one face. Notably, the dimer interface would need to be disrupted to form (UreABC—UreD—UreF)₃. A modeling study suggested a role of UreF as a GTPase activating protein (GAP) for UreG, a small GTPase (21).

UreABC—UreD—UreF—UreG is formed by UreG binding to the above complex or, as likely to occur in the cell, by UreD—UreF—UreG binding to the urease apoprotein. The UreABC—UreD—UreF—UreG complex was shown to have increased urease activation potential when incubated with Mg₂GTP in addition to Ni and bicarbonate (10). A related complex is produced by utilizing the Strep II-tagged version of UreG (UreG_{Str}) to purify UreABC—UreD— UreF—UreG_{Str} (22). UreG itself is soluble and has been characterized from several organisms. In K. aerogenes this protein is a monomer that binds one Ni or one Zn with Kd values of about 5 μΜ (22). UreGs from other microorganisms have slightly different properties. H. pylori UreG dimerizes when Zn is bound, but remains monomeric when Ni is present or in the absence of metal ion (23). UreG from Bacillus pasteurii and Mycobacterium tuberculosis is dimeric with the subunits joined by a disulfide bridge (24, 25). All UreGs contain GTPase-specific motifs including a P-loop, which is necessary for GTP binding, but low or undetectable GTPase activity is found for the isolated proteins, consistent with nucleotide hydrolysis being coupled to urease activation in the larger complex.

UreE is proposed to be the metallochaperone responsible for delivering Ni to the activation complex to allow for maturation of the active site (26). A complex containing all of the urease proteins has been detected (12, 22). Furthermore, Ni or Zn promotes binding

between UreE and UreG (22), also noted with the H. pylori proteins (27).

This chapter examines the effects of UreF variants on urease activity, the interactions of UreF with other urease proteins, and the function of UreF in urease activation. Variant forms of UreF were created on the basis of the *H. pylori* UreF structure and sequence alignments. The competence of each variant protein was assessed for *in vivo* activation of urease. Pull-down analysis of UreE-F constructs was carried out to test the effects of the mutations on *in vivo* and *in vitro* interactions with other urease components. Finally, the properties of UreABC—UreD—UreF—UreG_{Str} and a key UreF variant complex were characterized, the proposed role of UreF as a GAP was assessed, and an alternative hypothesis that UreF functions as a checkpoint for proper metallocenter synthesis was examined.

EXPERIMENTAL PROCEDURES

Plasmids, oligonucleotides, and site-directed mutagenesis. A description of the plasmids used in this study is provided in Table 3.1, and oligonucleotides used here are identified in Table 3.2. Plasmids pKK17 (encoding the complete ureDABCEFG gene cluster) (26), pKKEF (with the UreE-F fusion protein encoded within the complete urease gene cluster), and pET-EF (encoding a translational fusion of UreE and UreF) (19) were mutated by using overlapping oligonucleotides containing the desired mutations and PfuTurbo Hotstart PCR mastermix (Promega). The products were digested using *Dpn*1 and transformed into chemically competent E. coli DH5α cells (Invitrogen). The mutations were confirmed by sequencing (Davis Sequencing, CA), the pET-EF based plasmids were transformed into C41(DE3) competent cells (28), and all other plasmids were transformed into BL21 (DE3) competent cells. In order to examine further the K165A mutation of UreF, plasmid pKK17-K165A was digested with AatII and AvrII and the desired fragment was ligated into similarly digested pKKG (expressing the Strep II-tagged version of UreG along with the other urease genes) (22) to create pKKG-UreF-K165A. The same restriction enzymes were used to replace a fragment of pEC005 (containing ureFG cloned into pACT3) (14) with the DNA encoding the K165A mutation, producing pEC005-UreF-K165A. A DNA fragment encoding UreG T21A was inserted into both pKKG and pEC005 by using AatII and RsrII, forming pKKG-T21A and pEC005-UreG-T21A. Plasmids pKAUD2, pIBA3+UreG, and pEC002, used for production of (UreABC-UreD)3, UreG_{Str}, and MBP-UreD— UreF—UreG, were described previously (7, 14, 22).

Table 3.1: Plasmid properties

Plasmid	Description	Reference
pKK17	Wild-type <i>K. aerogenes</i> urease cluster	(26)
r	(ureDABCEFG) inserted into pKK223-3	(- /
pKK17-P19A, -G21A, -Y23A, -	Single site mutations of pKK17 for studying the	This study
S26A, -E30A, -D60A, -E94A, -	effects of the encoded UreF variants on urease	•
K165A, -F169A, -Q171A, -	activity	
H214A, -E215A, -R220A, -		
L221A, -F222A, -S224A		
pKKEF	Same as pKK17, but with a translational fusion of UreE and UreF	This study
pKKEF-P19A, -G21A, -Y23A, -	Single site mutations of pKKEF for in vivo pull-down	This study
S26A, -E30A, -D60A, -E94A, -	studies using the encoded proteins	
K165A, -F169A, -Q171A, -		
H214A, -E215A, -R220A, -		
L221A, -F222A, -S224A		()
pET-EF	Translationally fused <i>ureEF</i> genes inserted into	(19)
"ET EE DAOA COAA VOOA	pET21 for production of the UreE-F fusion protein	The same and sales
pET-EF-P19A, -G21A, -Y23A, -	Single site mutations of pET-EF for production of	This study
\$26A, -E30A, -D60A, -E94A, -	UreE-F variants for <i>in vitro</i> pull-down studies	
K165A, -F169A, -Q171A, - H214A, -E215A, -R220A, -		
L221A, -F222A, -S224A		
pKKG	Same as pKK17, but with a translational fusion of	(22)
F -	UreG and a Strep II tag	()
pKKG-UreF-K165A	Single site mutation of pKKG encoding the K165A	This study
	UreF variant	
pKKG-T21A	Single site mutation of pKKG encoding the T21A	This study
	variant of Strep II tagged UreG	
pEC005	ureFG fragment cloned into pACT3 for production	(14)
	of UreF and UreG	
pEC005-UreF-K165A	Single site mutation of pEC005 that encodes the	This study
»FC00F UraC T21A	K165A variant of UreF along with UreG Single site mutation of pEC005 that encodes the	This study
pEC005-UreG-T21A	T21A variant of UreG along with UreF	This study
pKAUD2	-	(7)
•	Plasmid for production of (UreABC—UreD) ₃	
pIBA3+UreG	pASK-IBA3plus-derived plasmid for production of	(22)
nEC003	UreG with a <i>Strep II</i> tag fused to its C-terminus <i>ureD</i> cloned into pMal-c2x for production of UreD	(11)
pEC002	fused at its C-terminus to MBP. Used along with	(14)
	pEC005 for production of MBP-UreD—UreF—UreG.	
	precession production of Wibi ofeb ofer ofed.	

Table 3.2: Oligonucloetides used in this study

Purpose	Sequence Sequence
UreF P19A	5' C AGC AGC AAC CTG <i>GCG</i> GTA GGG GGT TAC 3'
variant	5' GTA ACC CCC TAC <u>CGC</u> CAG GTT GCT GCT G 3'
UreF G21A	5' C AAC CTG CCG GTA <i>GCG</i> GGT TAC AGC TGG 3
variant	5' CCA GCT GTA ACC <i>CGC</i> TAC CGG CAG GTT G 3'
UreF Y23A	5' CCG GTA GGG GGT <i>GCG</i> AGC TGG TCC CAG 3'
variant	5' CTG GGA CCA GCT <u>CGC</u> ACC CCC TAC CGG 3'
UreF S26A	5' G GGT TAC AGC TGG <i>GCG</i> CAG GGG CTG GAG TG 3'
variant	5' CA CTC CAG CCC CTG <i>CGC</i> CCA GCT GTA ACC C 3'
UreF E30A	5' G TCC CAG GGG CTG <i>GCA</i> TGG GCT GTG GAA G 3'
variant	5' C TTC CAC AGC CCA <i>TGC</i> CAG CCC CTG GGA C 3'
UreF D60A	5' C TTT TTT ACC GTT <i>GCC</i> CTG CCG CTG TTC 3'
variant	5' GAA CAG CGG CAG <i>GGC</i> AAC GGT AAA AAA G 3'
UreF E94A	5' GG GAA ACT CGT <i>GCC</i> CTG CGG GAG GAA G 3'
variant	5' C TTC CTC CCG CAG <i>GGC</i> ACG AGT TTC CC 3'
UreF K165A	5' G ATG GCC GGC GTC <u>GCG</u> CTG GTC CCC TTC 3'
variant	5' GAA GGG GAC CAG <u>CGC</u> GAC GCC GGC CAT C 3'
UreF F169A	5' C AAG CTG GTC CCC <u>GCC</u> GGC CAG CAG GC 3'
variant	5' GC CTG CTG GCC <i>GGC</i> GGG GAC CAG CTT G 3'
UreF Q171A	5' CTG GTC CCC TTC GGC <u>GCG</u> CAG GCC GCC CAG CAG 3'
variant	5' CTG CTG GGC GGC CTG <u>CGC</u> GCC GAA GGG GAC CAG 3'
UreF H214A	5' C GCC TCT GCC CGG <i>GCG</i> GAA ACC CAA TAC TC 3'
variant	5' GA GTA TTG GGT TTC <u>CGC</u> CCG GGC AGA GGC G 3'
UreF E215A	5' C ATC GCC TCT GCC CGG CAT <u>GCG</u> ACC CAA TAC TCT CGA TTA TTC 3'
variant	5' GAA TAA TCG AGA GTA TTG GGT <u>CGC</u> ATG CCG GGC AGA GGC GAT G 3'
UreF R220A	5' CAT GAA ACC CAA TAC TCT <u>GCG</u> TTA TTC CGT TCC TAG AGC 3'
variant	5' GCT CTA GGA ACG GAA TAA <u>CGC</u> AGA GTA TTG GGT TTC ATG 3'
UreF L221A	5' GAA ACC CAA TAC TCT CGA <i>GCG</i> TTC CGT TCC TAG AGC TTG 3'
variant	5' CAA GCT CTA GGA ACG GAA <u>CGC</u> TCG AGA GTA TTG GGT TTC 3'
UreF F222A	5' C CAA TAC TCT CGA TTA <i>GCG</i> CGT TCC TAG AGC TTG CG 3'
variant	5' CG CAA GCT CTA GGA ACG <i>CGC</i> TAA TCG AGA GTA TTG G 3'
UreF S224A	5' CT CGA TTA TTC CGT <u>GCG</u> TAG AGC TTG CGG CCG 3'
variant	5' CGG CCG CAA GCT CTA <u>CGC</u> ACG GAA TAA TCG AG 3'

Protein purification. E. coli C41(DE3) cells producing UreE-F or its variations were grown overnight in 10 mL lysogeny broth (LB) supplemented with 300 μ g mL⁻¹ ampicillin. The cultures were used to inoculate 1 L of Terrific Broth (TB, Fisher BioReagents) supplemented with 300 μ g

mL⁻¹ ampicillin, grown to optical densities at 600 nm (OD₆₀₀) of 0.4 to 0.6, induced with 0.5 mM isopropyl β -D-1-thiogalactopyranoside (IPTG), and grown overnight at 37 °C. Cells were harvested by centrifugation, resuspended (1 g mL⁻¹) in buffer A (20 mM Tris, pH 7.8, containing 500 mM NaCl and 60 mM imidazole), supplemented with 1 mM phenylmethylsulfonyl fluoride, and sonicated (Branson 450 sonifier, five repetitions of 2 min each at 3 W output power and 50% duty cycle). Disrupted cells were centrifuged at 100,000 x g at 4 °C for one h and the cell-free supernatants were loaded onto a 5 mL Ni-nitrilotriacetic acid (NTA) column equilibrated with buffer A. The column was washed with buffer A until the A₂₈₀ reached baseline, and bound proteins were eluted by using buffer B (20 mM Tris, pH 7.8, containing 500 mM NaCl and 1 M imidazole). Fractions containing UreE-F or its variations were combined and dialyzed overnight into 20 mM Tris, pH 7.8, containing 100 mM NaCl, 1 mM EDTA and 1 mM dithiothreitol (DTT). The proteins were further purified by gel filtration chromatography using a Superdex-75 column (65 cm × 2.0 cm diameter; GE Healthcare) equilibrated in the same buffer.

E. coli cells producing UreABC—UreD—UreF—UreG $_{Str}$ or its variants were grown overnight in 10 mL LB supplemented with 300 μg mL $^{-1}$ ampicillin. The cultures were used to inoculate 1 L of LB containing 300 μg mL $^{-1}$ ampicillin, grown to an OD $_{600}$ of 0.4 to 0.6, induced with 0.1 mM IPTG, and grown overnight at 37 °C. Cells were harvested by centrifugation, resuspended in buffer W (100 mM Tris pH 8.0, 150 mM NaCl, 1 mM EDTA), and sonicated (same protocol as above). Disrupted cells were centrifuged at 100,000 x g at 4 °C for one h and the cell-free supernatant was loaded onto a *Strep*-tactin column. The column was washed with

buffer W until the A₂₈₀ was at baseline, and bound proteins were eluted with the same buffer containing 2.5 mM desthiobiotin. Fractions containing the protein of interest were concentrated and loaded onto a Superdex-200 column equilibrated with 25 mM 4-(2-hydroxyethyl)-1-piperazineethanesulfonic acid (HEPES) buffer, pH 7.4, containing 150 mM NaCl and 1 mM tris(2-carboxyethyl)phosphine (TCEP). Before use in further assays, the protein was dialyzed into buffer with no TCEP.

(UreABC—UreD)₃ and UreG_{Str} were produced using pKAUD2 and pIBA3+UreG, respectively, and purified as previously described (7, 22). MBP-UreD—UreF—UreG was obtained from cells coexpressing pEC005 and pEC002 (14) and isolated as reported earlier (29).

Sodium dodecyl sulfate (SDS)-polyacrylamide gel electrophoresis (PAGE). SDS-PAGE was performed by using standard buffers (30), 12% acrylamide running gels, and 4% stacking gels, except in the case of UreABC—UreD—UreF—UreG $_{Str}$ analysis, when 15% running gels were used.

Pull-down assays using cell-free extracts. Cells containing pKKEF and its variants were grown in 50 mL TB supplemented with ampicillin (300 μg mL $^{-1}$) to an OD₆₀₀ of 0.4 to 0.6, induced with 0.5 mM IPTG, and allowed to grow overnight at 37 °C. Cells were harvested, resuspended in 2 mL buffer A, sonicated, and microcentrifuged (14,000 rpm). Cell-free extracts were added to 200 μ L of Ni-NTA resin, washed with 5 mL buffer A, and then eluted with 250 μ L buffer B. Eluted fractions were examined for the presence of other urease related proteins by using 15% SDS-PAGE.

In vitro pull-down assays. Two distinct types of in vitro pull-down studies were carried

out. (i) UreE-F and its variants were tested for their abilities to bind to purified (UreABC— UreD)₃. The apoprotein complex (12 μM nascent active site, dialyzed into buffer containing 20 mM Tris, pH 7.8, and 100 mM NaCl) was combined with UreE-F and its variants (12 μM protomer concentration in the same buffer) and incubated at room temperature for 20 min. The protein mixtures were applied to 0.5 mL Ni-NTA columns, washed with 5 mL of 20 mM Tris, pH 7.8, containing 100 mM NaCl, and eluted with the same buffer containing 1 M imidazole. (ii) For examining interactions of UreF with UreG, samples of UreE-F or its site-directed variants were combined with purified UreG_{Str} (12 μM of each protomer) in 20 mM Tris, pH 7.8, buffer and incubated for one h at 42 °C. The proteins were applied to 0.5 mL Strep-Tactin columns, washed with 5 mL of 20 mM Tris buffer and eluted with 2 mM desthiobiotin in the same buffer. Each in vitro pull-down assay was analyzed by 12% SDS-PAGE and gel scanning (Alpha Imager 2200), with the intensities of the bands divided by the molecular mass of each protein (MBP-UreD, 72.9 kDa; UreC, 60.3 kDa; UreE-F, 42.8 kDa; UreD, 29.8 kDa; UreF, 25.2 kDa; UreG_{Str}, 23.2 kDa; UreG, 21.9 kDa; UreB, 11.7 kDa; and UreA, 11.1 kDa; though UreA and UreB typically were not included in the calculations due to the aberrant dye-binding behavior of these small subunits) to assess the ratios of interactions.

Urease activity and protein assays. Urease activities were measured by quantifying the rate of ammonia release from urea by formation of indophenol, which was monitored at 625 nm (31). One unit of urease activity is defined as the amount of enzyme required to hydrolyze 1 μ mole of urea min⁻¹ at 37 °C. The standard assay buffer contained 50 mM HEPES, pH 7.8, and 50 mM urea. Protein concentrations were determined by a commercially available protein

assay (Bio-Rad).

Urease activation assays. UreABC—UreD—UreF—UreG $_{Str}$ and its variants were activated for one h at 37 °C in a standard solution containing 100 mM HEPES buffer, pH 8.3, containing 150 mM NaCl, 100 μM NaHCO $_3$, 100 μM NiCl $_2$, and the indicated amounts of GTP (provided as its Li salt with two equivalents of Mg), unless otherwise noted. Experiments to examine the effects of Zn in the activation solution used the concentrations indicated in the figures. After activation, urease activity was measured by using the standard assay, except that the buffer additionally contained 0.5 mM EDTA to prevent Ni-dependent inhibition. Time course experiments were analyzed by using Sigma Plot (Systat Software, Inc.) and the following equation, where Y is the measured urease activity in U/mg, A_{max} is the maximal urease activity generated, t is the time in minutes, and $t_{1/2}$ is the time needed to reach half of the maximal activity.

$$Y = A_{\text{max}}t/(t_{1/2} + t)$$
 (1)

Statistically significant differences in urease activation were determined by a p value < 0.05 when using the Student's t-test.

GTPase activity assays. GTPase activity was measured by monitoring the amount of released phosphate using malachite green (32). Samples of UreABC—UreD—UreF—UreG $_{Str}$ or variants (10 μ M nascent active site) were incubated in standard activation solution with varying amounts of Mg $_2$ GTP. After 1 and 2 h, 100 μ L aliquots were boiled for 5 min and centrifuged to pellet the precipitated protein; 90 μ L of each supernatant was boiled and centrifuged again to

remove more protein; and 80 μ L of each supernatant was added to 20 μ L of malachite green dye in a 96-well plate, mixed, and the absorbance monitored at 620 nm. The readings were compared to a standard curve prepared with known amounts of phosphate. Assays without protein were performed at each GTP concentration to control for GTP hydrolysis over time or at the higher temperatures.

RESULTS

Targets for site directed mutagenesis. K. aerogenes UreF residues were targeted for mutagenesis by using a previously published alignment (an abbreviated alignment is depicted in Figure 3.2) of multiple UreF sequences (20) and the two available H. pylori UreF structures (15, 20). Many conserved residues lie close to the N- or C-termini, with the last 10 residues in the sequence showing high identity. Although residues 1-24 are unstructured in both H. pylori UreF crystal structures (15, 20), this has no consequence for K. aerogenes UreF which is shorter and lacks this N-terminal region. Mapping the highly conserved UreF residues onto the H. pylori crystal structure revealed a clustering on one face of the UreF dimer. (Of interest, the UreF residues at the interface between H. pylori UreF and UreH were poorly conserved and there is little overall sequence similarity between K. aerogenes UreD and H. pylori UreH). Based on the alignment and the structure, 16 K. aerogenes residues were chosen for mutagenesis to Ala (Figure 3.2 and 3.3). These included highly conserved residues near the N-terminus (P19, G21, Y23, S26, and E30), several residues at the C-terminus (H214, E215, R220, L221, F222, and S224), a few conserved potential hydrogen-bond forming residues in the middle (D60, E94 and Q171), one hydrophobic residue (F169), and the only lysine (K165) in the protein. A Lys or an Arg is present at this position in all known UreF sequences, and this positively-charged site is the best candidate for participating in an "Arg-finger"-like manner (33-35) to stimulate GTP hydrolysis in accord with the proposed GAP activity of UreF (21).

K. aerogenes ------MSTAEQRLRLMQLASSNL \mathbf{PVGG} 22 H. pylori MDKGKSVKSTEKSVGMPPKTPKTDNNAHVDNEFLILQVNDAVF**P**I**G**S 47 20 P. mirabilis ------MMLAD--LRLYQLVSPSL \mathbf{P} V \mathbf{G} A B. pasteurii ---MKWGFLMNNQREGSKNHSNIEATNTNPWLLHLIQIHDTAFPTGS K. aerogenes YSWSQGLEWAVEAGWVLDVAAFERWQRRQMTEGFFTVDLPLFARLYR 69 H. pylori YTHSFGLETYIQQKKVTNKESALEYLKANLSSQFLYTEMLSLKLTYE 94 P. mirabilis FTYSOGLEWAIEKGWVCSAETLSDWLSAOMTGTLATLELPILROLOT 67 B. pasteurii FAHSFGMETYIQESDISNEDDLKAFCDMYLRQNLASTDAIIAQEAYR 91 K. aerogenes ACEQGDIAAAQRWTAYLLACRETRELREEERNRGAAFARLLSDWQP- 115 H. pylori SALQQDLKKILGVEEVIMLSTSPMELRLANQKLGNRFIKTLQAMNEL 141 P. mirabilis SLAKGDSDTVKYWCDFMVASRETK**E**LRQEERQRGIAFARLLPQLGI- 113 B. pasteurii LAKENDLOGLIRLENICHAIKLSPETRKGSMMMGROFLOTVOPLNNS 138 K. aerogenes ----DCPPPWRSLCQQSQLAGMAWLGVRWRIALPEMALSLGYSWIE 157 H. pylori DMG-EFFNAYAQKTKDPTHATSYGVFAASLGIELKKALRHYLYAQTS 187 P. mirabilis ----ELDDTLQQRVKQTQLMAFALAAVHWHIDSEKLCCAYVWGWLE 155 B. pasteurii ELFTIWCEKLKNKEIKSHYPVVYGIYTAMLGVDLRTSLETFLYSSIT 185 K. aerogenes SAVMAGVKLVPFGQQAAQQLILRLCDHYAAEMPRALAAPDGDIGSAT 204 H. pylori NMVINCV**K**SVP**L**S**Q**NDGQKILLSLQSPFNQLIEKTLELDESHLCTAS 234 P. mirabilis NTVMSGVKLVPLGQSAGQKMLFALAEQIPAIVELSAHWPQEDIGSFT 202 B. pasteurii SLVONGVRAIPLGONSGVOTIFSLLPVIOETTSRVMTLDLEHLDNNS 232 * * *** * K. aerogenes PLAAIASAR**HE**TOYS**RLF**R**S** 224 H. pylori VONDIKAMOHESLYSRLYMS 254 P. mirabilis PAQVIASSR**HE**TQYT**RLF**R**S** 222 B. pasteurii IGLEIASMK**HE**FLHS**RLF**IS 252

Figure 3.2: Alignment of UreF sequences from selected microorganisms. *Helicobacter pylori, Proteus mirabilis,* and *Bacillus pasteurii* sequences are aligned with *K. aerogenes*. Residues changed to alanine in the *K. aerogenes* protein are highlighted in bold and indicated by an asterisk.

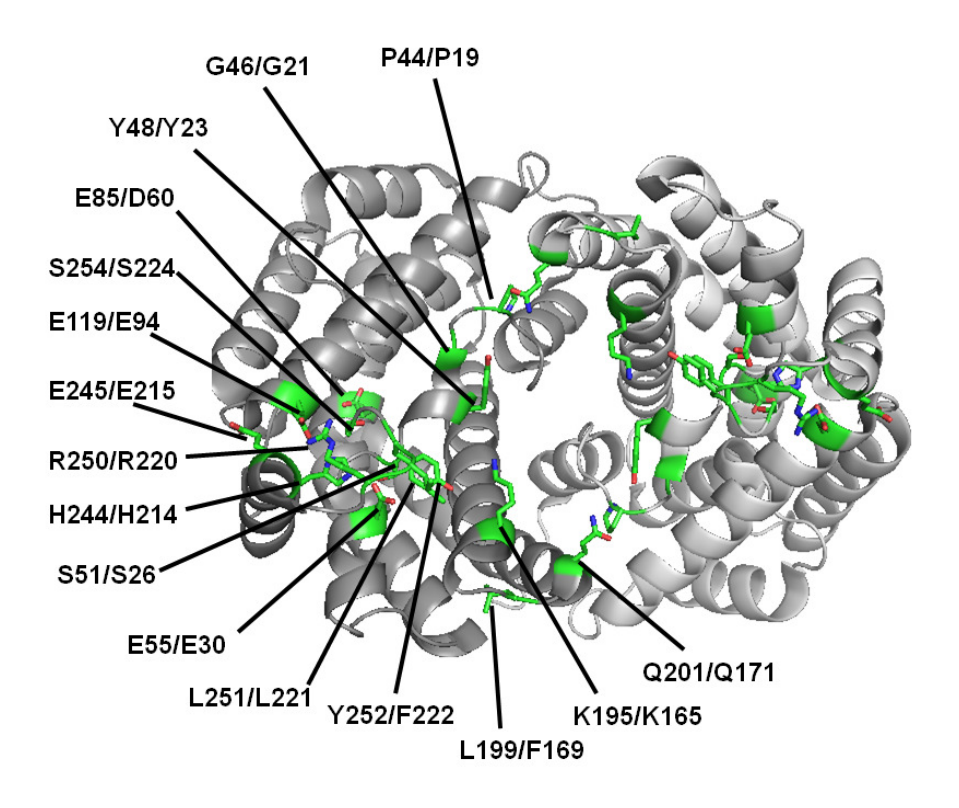


Figure 3.3: Mutagenesis of *K. aerogenes* UreF. The structure depicted is that of *H. pylori* UreF, from the (UreH—UreF)₂ complex (PDB code 3SF5), with the protomers colored in two shates of gray and the residues changed to alanine in the *K. aerogenes* protein shown in green and identified with the *H. pylori* residue number/ *K. aerogenes* residue number.

Mutants in ureF have variable effects on in vivo urease activity. E. coli cells expressing the complete urease operon, but encoding the selected variants of UreF, were shown by SDS-PAGE to produce levels of urease proteins that were essentially identical to those found with the wild-type accessory protein (data not shown). Cell-free extracts of these cultures were examined for urease activities and the results were shown to fall into three general categories (Table 3.3 and Figure 3.4). The mutant cells containing P19A, Y23A, E30A, E94A, H214A, R220A, L221A, F222A, and S224A forms of UreF all had less than 10% of the wild-type activity. These results highlight the critical *in vivo* role of the C-terminal region in urease activation, since altering any one of these highly conserved residues significantly decreased the urease activity. The mutant cells containing G21A, S26A, D60A, K165A, Q171A, and E215A UreF variants

retained between 10 and 70% of the wild-type activity, indicating that they play important but not vital roles individually in the urease activation process. Finally, the mutant containing the F169A form of UreF exhibited wild-type activity, demonstrating the non-essentiality of this residue. The F169A variant of UreF was not characterized further.

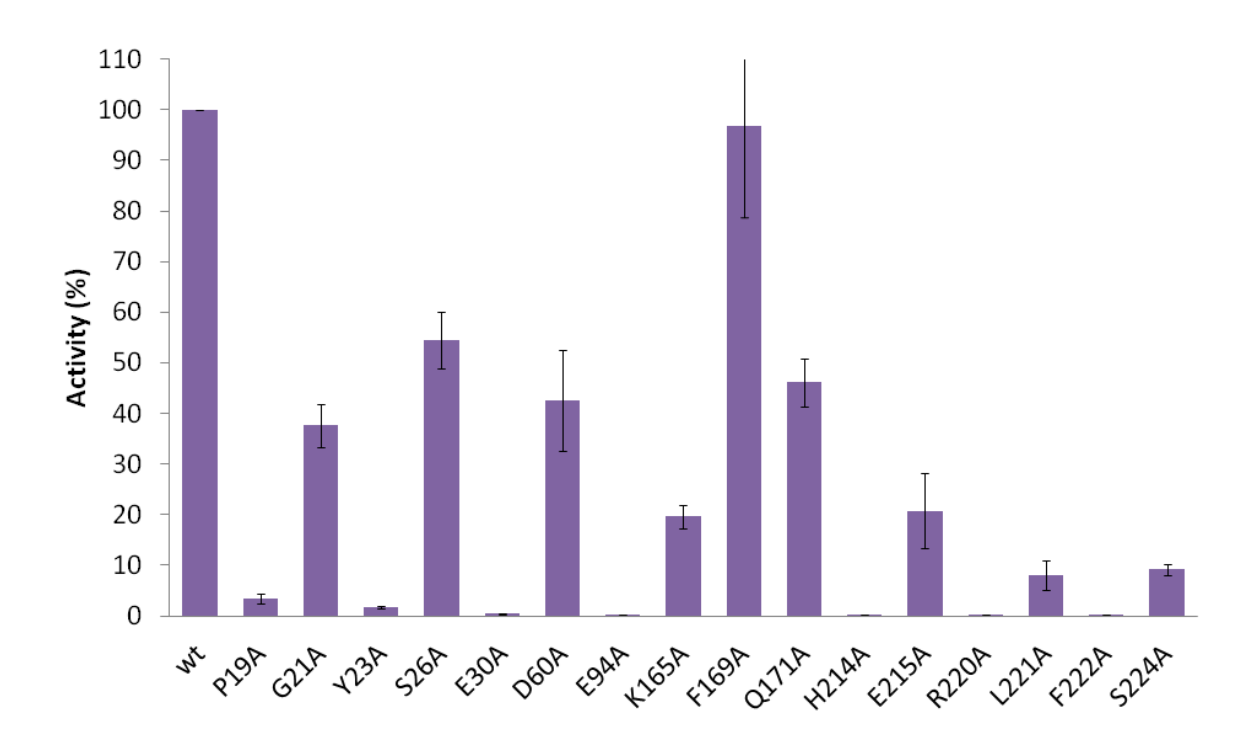


Figure 3.4: Effect of UreF variants on urease activity in cell-free extracts. Percent activity values shown are relative to that of cell-free extracts of cells containing the wild-type urease gene cluster. Measured urease specific activities are provided in Table 3.3

Table 3.3: Effect of UreF variants on urease activity in cell-free extracts

Variant of <i>K.</i>	Corresponding residue	Urease activity	Urease activity
aerogenes UreF	in <i>H. pylori</i> UreF	[µmol min ⁻¹ (mg	(% of wild-type)
		protein) ⁻¹]	
Wild-type		130 ± 4	100
P19A	P44	4.4 ± 1.2	3.5 ± 1.0
G21A	G46	47.4 ± 5.3	37.6 ± 4.2
Y23A	Y48	2.2 ± 0.4	1.8 + 0.3
S26A	S51	68.5 ± 7.3	54.4 ± 5.6
E30A	E55	0.5 ± 0.1	0.4 ± 0.1
D60A	E85	54 ± 13	43 ± 10
E94A	E119	0.3 ± 0.04	0.24 ± 0.03
K165A	K195	24.8 ± 2.9	19.7 ± 2.3
F169A	L199	122 ± 23	97 ± 18
Q171A	Q201	58.1 ± 5.9	46.1 ± 4.7
H214A	H244	0.14 ± 0.04	1.1 ± 0.03
E215A	E245	26.2 ± 9.5	20.8 ± 7.5
R220A	R250	0.24 ± 0.02	0.19 ± 0.02
L221A	L251	10.0 ± 3.6	7.9 ± 2.9
F222A	Y252	0.17 ± 0.01	0.13 ± 0.01
S224A	S254	11.5 ± 1.5	9.1 ± 1.2

UreF variants primarily affect binding of UreG in cell-free extracts. Using constructs that produce variant forms of UreE-F in the context of the other urease proteins, the fusion proteins were purified, along with accompanying proteins, from cell-free extracts by use of Ni-NTA resin. These samples were analyzed by SDS-PAGE (Figure 3.5) and compared to the control sample where "pull-down" analysis of UreE-F resulted in substantial levels of co-purified UreABC, UreD, and, at lesser levels, UreG. Approximately equal levels of UreE-F were produced in all mutant cells according to the results from pull-down analysis as monitored by denaturing gel electrophoresis. The UreE-F protein containing the D60A substitution was not soluble and so the corresponding pull-down sample could not be analyzed. All other UreE-F pull-down samples, regardless of the changes within UreF, contained UreABC and UreD. This result provides confirmation of the proper folding of UreE-F variants. Similarly, UreG remained bound

to UreE-F versions containing S26A, Q171A, and E215A forms of UreF; notably, each of these UreF variants resulted in cell-free extracts retaining at least 20% of wild-type activity. Surprisingly, the UreE-F mutant samples corresponding to G21A and K165A UreF bound less UreG than control samples despite the relatively high levels of urease activity in cell-free extracts of these UreF variants (38 and 20% of wild-type UreF, respectively). The weaker interaction with UreG observed in these pull-down studies apparently could be overcome within the cellular milieu to allow substantial production of active enzyme, especially for the conservative G21A substitution. In contrast, UreG was greatly diminished or absent in pulldown samples from the P19A, Y23A, E30A, E94A, H214A, R220A, L221A, F222A, and S224A UreE-F variants; these results coincide with those for cell-free extracts of the corresponding UreF variants that exhibited <10% of wild type urease activity. Mapping these residues onto the UreF dimer, from the (UreH—UreF)₂ crystal structure (15), identified a clear binding pocket for UreG (yellow and magenta portions of Figure 3.6). These results highlight the importance of both the amino- and carboxyl-terminal residues of UreF for binding UreG.

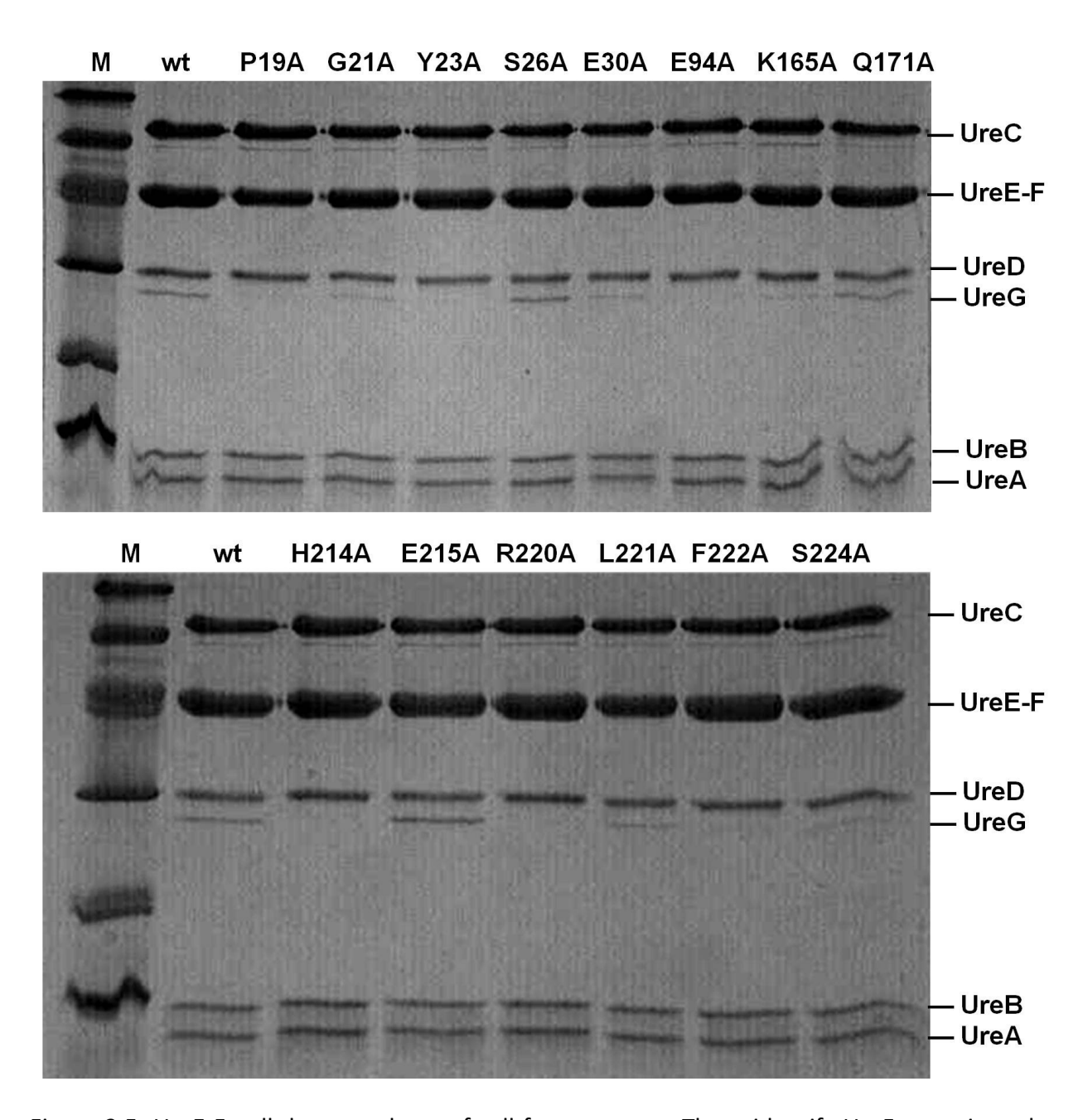


Figure 3.5: UreE-F pull-down analyses of cell-free extracts. These identify UreF mutations that lead to reduction or absence of UreG binding. Extracts of cells containing pKKEF, bearing the complete *ure* cluster with *ureE* and *ureF* fused, and its *ureF* variants were added to Ni-NTA resin, washed, and eluted with 1 M imidazole. Eluted fractions were analyzed by SDS-PAGE using a 15% acrylamide gel. The lane labeled M denotes the marker proteins (97.4, 66, 45, 31, 21.5, and 14.4 kDa).

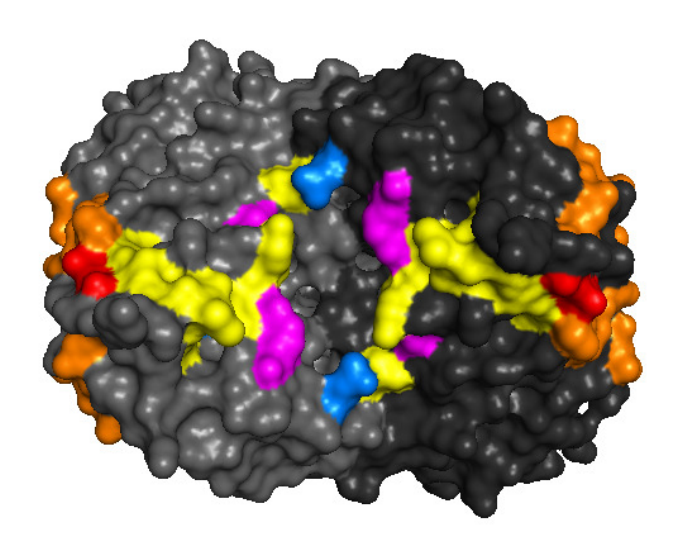


Figure 3.6: UreF mutations affecting UreG binding. The two protomers of *H. pylori* UreF are shown in different shades of grey in space fill mode (PDB code 3SF5). Residues are colored to indicate the corresponding side chains of *K. aerogenes* UreF where mutation to Ala had no effect on UreG binding (blue), mutations resulting in low levels of UreG binding and <10% urease activity (yellow), mutations causing reduced UreG binding but retention of >10% urease activity (magenta), and mutation leading to only 21% activity but retention of UreG binding (red). Residues that interact with UreH in *H. pylori* are colored orange or red.

ureF variants affect in vitro binding to (UreABC—UreD)3 and UreG_{Str}. Prior studies had shown that (UreABC—UreD)3 could bind, at low stoichiometry, to UreE-F according to pull-down studies using a Ni-NTA column (19). That work reported the purified UreE-F as being predominantly monomeric according to gel filtration chromatography; however, re-evaluation of the native size by the same approach (in similar buffer conditions, but containing 100 mM NaCl rather than 200 mM NaCl) revealed the isolated protein to be primarily dimeric (~73 kDa), with a small amount of larger molecular weight aggregates. Each of the variant UreE-F proteins exhibited similar profiles, consistent with their presence as dimeric structures (and providing evidence for proper folding), except for D60A UreE-F that was insoluble and therefore not studied. Each purified UreE-F variant was combined with isolated (UreABC—UreD)3, the

mixtures were chromatographed on a Ni-NTA resin, and the extents of interaction between the proteins were analyzed by SDS-PAGE (an example using E30A UreE-F mixed with (UreABC— UreD)₃ is illustrated in Figure 3.7A) and quantified by gel scanning (Table 3.4). The original version of UreE-F bound (UreABC-UreD)3 such that 0.32 UreC protomer was associated per UreE-F protomer, consistent with each (UreE-F)₂ dimer binding 0.21 (UreABC—UreD)₃ molecules under these conditions. The small amount of complex obtained in this in vitro study (using equivalent concentrations of UreE-F and UreABC—UreD incubated at room temperature for 20 min) is less than that observed for UreE-F pull-down studies from cell-free extracts (Figure 3.5), consistent with cellular factors acting to enhance productive interaction. All the UreE-F variants except for the L221A variant bound less (UreABC—UreD)₃ than the fusion protein containing wild-type UreF; nevertheless, some interaction was retained in all cases. The P19A, G21A, and Y23A variants all bound about 70% of the amount of (UreABC-UreD)₃ compared to the original UreE-F, while the other UreE-F variants bound less than 50% of that bound by the control protein. These results demonstrate that none of the sites of substitution are essential for stabilizing the interaction between K. aerogenes UreF and (UreABC—UreD)3, a result that is nicely compatible with the *H. pylori* (UreH—UreF)₂ structure (15).

Table 3.4: Binding of UreABC—UreD by control and variant UreE-F samples $^{\it a}$

UreE-F variant	Ratio of UreABC—UreD/UreE-F
Wild-type	0.32
P19A	0.21
G21A	0.22
Y23A	0.22
S26A	0.15
E30A	0.13
E94A	0.05
K165A	0.14
Q171A	0.13
H214A	0.05
E215A	0.13
R220A	0.11
L221A	0.34
F222A	0.15
S224A	0.08

^a Determined by *in vitro* pull-down studies with Ni-NTA and gel scanning comparison of bands for UreC and UreE-F.

An analogous series of studies was carried out by using Strep-tactin resin and $UreG_{Str}$ to examine the interactions of this protein with UreE-F and its variants. A representative gel depicting the interaction of $UreG_{Str}$ with the E30A variant of UreE-F is shown in Figure 3.7B and the measured ratios of protein binding for all variants are provided in Table 3.5. The Strep-tactin chromatography approach avoided the use of Ni, needed for the Ni-NTA resin, due to the known interaction between UreG and UreE in the presence of this metal ion (22). Interaction between $UreG_{Str}$ and UreE-F was maximized by incubating the mixture at 42 °C without NaCl prior to chromatography, resulting in 0.63 UreE-F protomer bound per $UreG_{Str}$. A much weaker interaction between these proteins was noted at 37 °C (data not shown) and is consistent with UreD facilitating the UreE-F/UreG interaction in the pull-down studies from cell-free extracts,

shown in Figure 3.5. This *in vitro* interaction assay with its artificial conditions provided trends that substantially confirmed the results from the UreE-F pull-down assays using cell-free extracts. UreG $_{Str}$ bound at least 75% of the S26A, Q171A, H214A, E215A, R220A, and S224A variant UreE-F proteins compared to control UreE-F. Similarly, 65-70% of control levels were found for P19A, Y23A, and F222A UreE-F, indicating only minor roles for those residues in stabilizing the binding between UreF and UreG. In contrast, the G21A, E30A, E94A, K165A, and L221A UreE-F variants exhibited substantially weaker binding (< 50% compared to control UreE-F) to UreG $_{Str}$. I conclude the residues associated with the latter positions are located at the UreF:UreG interface under these conditions, which represent only a subset of the interface residues when (UreABC—UreD) $_3$ is present as shown in Figure 3.5.

Table 3.5: Binding of control and variant UreE-F by UreG_{Str} ^a

UreE-F variant	Ratio of UreE-F/UreG _{Str}
Wild-type	0.63
P19A	0.42
G21A	0.30
Y23A	0.43
S26A	0.54
E30A	0.18
E94A	0.28
K165A	0.26
Q171A	0.55
H214A	0.50
E215A	0.49
R220A	0.55
L221A	0.25
F222A	0.42
S224A	0.52

^a Determined by *in vitro* pull-down studies using *Strep*-tactin resin and gel scanning

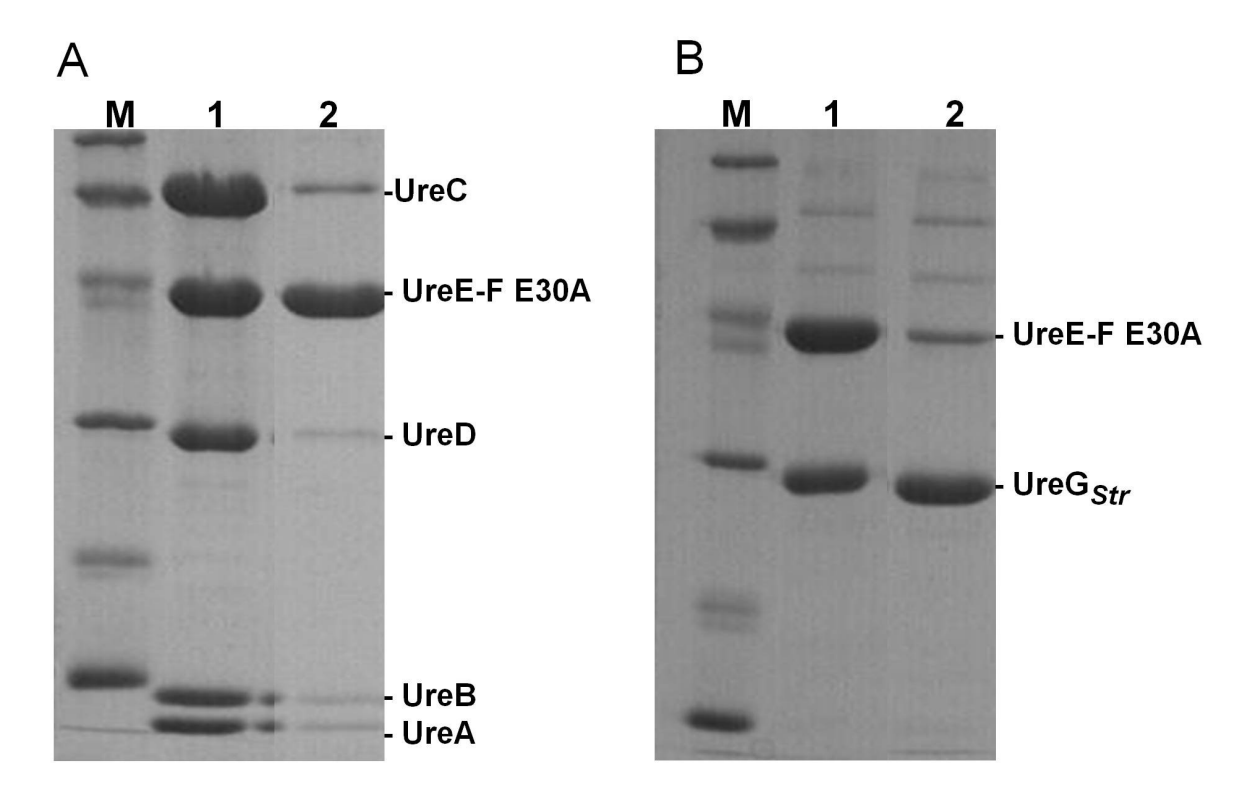


Figure 3.7: *In vitro* pull-down assay examples. A. Pull-down assay for UreE-F mixed with (UreABC—UreD)₃. In this example, E30A UreE-F was mixed with (UreABC—UreD)₃ (lane 1) then bound to Ni-NTA resin and eluted, along with any associated proteins, by addition of imidazole (lane 2). B. Pull-down assay for UreG $_{Str}$ mixed with UreE-F. In this example, UreG $_{Str}$ was mixed with E30A UreE-F (lane 1) then bound to *Strep*-tactin resin and eluted, along with any associated proteins, by addition of desthiobiotin (lane 2). For each panel, the lane labeled M denotes the marker proteins (97.4, 66, 45, 31, 21.5, and 14.4 kDa).

Examination of UreF as a GTPase activating protein. In order to test the hypothesis that UreF acts as a GAP for UreG, several protein complexes containing UreF and UreG were tested for their GTPase activity by using a malachite green assay to detect product phosphate. First, UreE-F was incubated with UreG $_{Str}$ to examine whether the isolated proteins could stimulate GTPase activity (N.B., purified K. aerogenes UreG is essentially inactive (36)). Unfortunately, control assays using UreE-F alone revealed the presence of trace levels of contaminating GTPase in the protein preparation that was not eliminated by Ni-NTA or gel filtration chromatography, so this effort was halted since only UreG of the accessory proteins should

have GTPase activity. The urease-free MBP-UreD—UreF—UreG complex (*14, 29*) also was investigated as a platform for testing the GAP hypothesis. This heterotrimeric complex appeared to possess GTPase activity; however, the complex containing the P-loop (T21A) variant of UreG, used as a negative control, also exhibited this activity. The assay result again indicated trace contamination by a GTPase so work on that complex was abandoned. As an alternate approach, studies were carried out with the previously described UreABC—UreD—UreF—UreG_{Str} species (*22*) after performing an additional step of purification involving gel filtration chromatography.

UreABC—UreD—UreF—UreG $_{Str}$ and the complex containing the K165A UreF variant were purified (Figure 3.8A) for testing whether the highly conserved, positively-charged residue at position 165 functions like the Arg finger of a GAP (33-35). Consistent with the weakened binding of UreG in the K165A UreE-F pull-down studies utilizing cell-free extracts (Figure 3.5), the complex prepared with the UreF variant possessed less UreG $_{Str}$ when examined after size exclusion chromatography. The complex also was prepared (gel not shown) using the T21A variant of UreG $_{Str}$ as a negative control that would be incapable of hydrolyzing GTP (10). Whereas the wild-type complex exhibited an initial increase in urease activity with increasing levels of GTP in the activation mixture, followed by a decrease in activation at greater GTP concentrations, the complex containing the T21A P-loop substitution in UreG resulted in decreasing extents of urease activation (possibly due to sequestration of Ni) with increasing GTP (Figure 3.8B). Significantly, the activities generated with these two complexes in the absence of GTP were similar. By contrast, the complex containing K165A UreF exhibited a

decrease in activation competence with added GTP, but the overall level of urease activation was significantly greater than for the wild-type complex. Analogous activity patterns were obtained for samples subjected to activation for 2 h (data not shown); i.e., the complex formed with K165A UreF demonstrated greater activation competence in a GTP-independent manner compared to the wild-type complex (with or without GTP).

The extent of GTP hydrolysis for each urease activation sample was assessed after 1 h by using the malachite green assay (Figure 3.8C). The complex containing T21A UreG released little phosphate, with no further increase after 2 h of incubation, indicating the absence of contaminating GTPase. The wild-type complex gave rise to an approximately linear increase in phosphate concentration with increasing amounts of GTP. At small GTP concentrations, the amount of phosphate formed was roughly proportional to the amount of active urease formed, but at concentrations greater than 75 µM GTP the amount of phosphate formed continued to increase while the activity diminished, consistent with an uncoupling of these processes. The complex containing K165A UreF possessed greater GTPase activity than the complex containing wild-type UreF at most GTP concentrations, demonstrating that K165 does not facilitate GAP activity. The comparatively large amount of phosphate produced by the variant complex also indicates that GTPase activity was significantly uncoupled from urease activation.

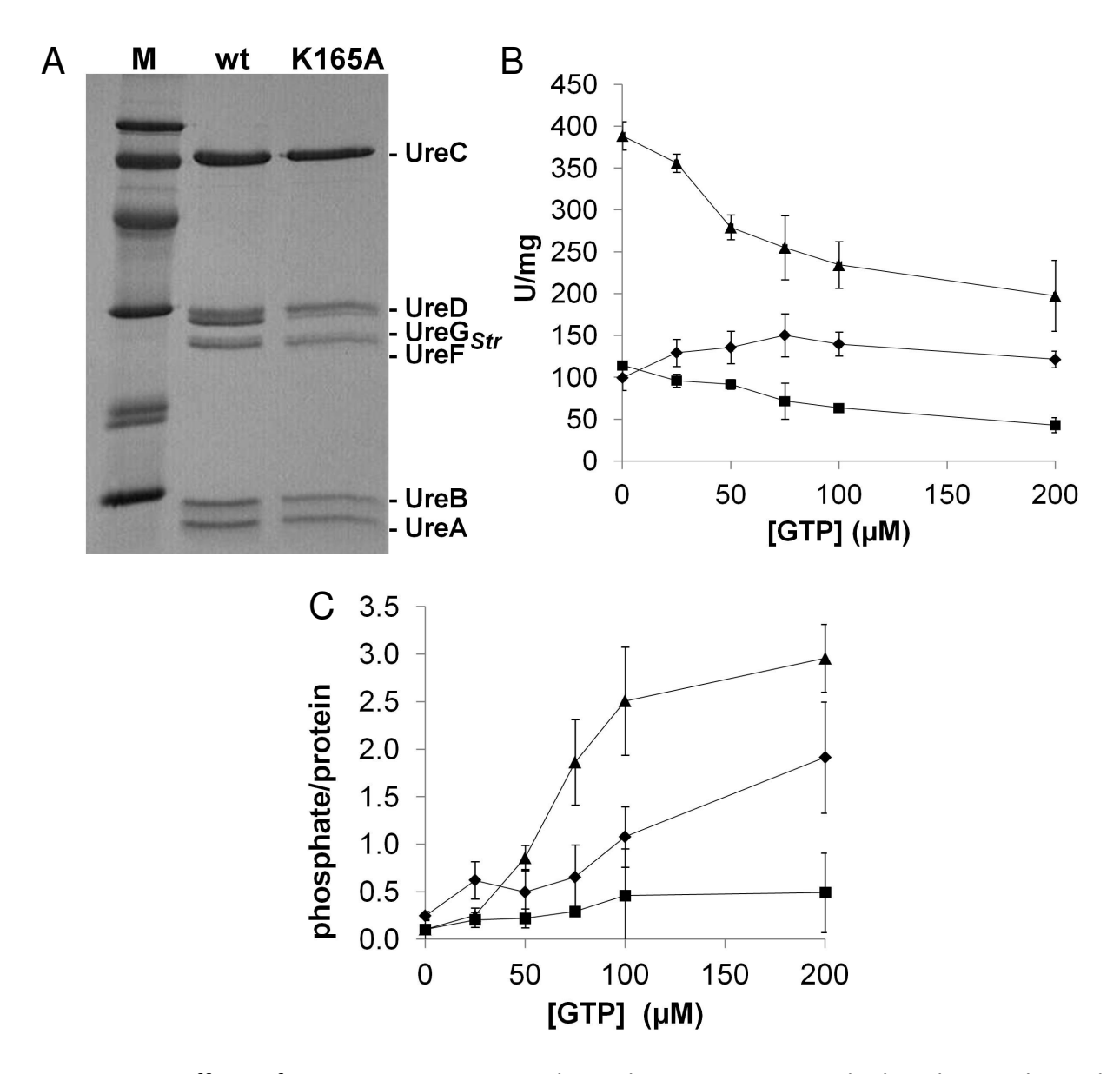


Figure 3.8: Effect of K165A UreF on GTP-dependent activation and phosphate release by UreABC—UreD—UreF—UreG $_{Str}$. (A) SDS-PAGE analysis of purified UreABC—UreD—UreF—UreG $_{Str}$ and UreABC—UreD—UreF(K165A)—UreG $_{Str}$ after purification by affinity resin and gel filtration chromatography. M denotes the marker proteins (97.4, 66, 45, 31, 21.5, and 14.4 kDa). (B) Urease activation assays for versions of UreABC—UreD—UreF—UreG $_{Str}$. Proteins (10 μ M) were incubated for one h at 37 °C in standard activation solution with the indicated concentrations of Mg $_{2}$ GTP. Aliquots were removed and assayed for urease activity. (C) Phosphate released by UreABC—UreD—UreF—UreG $_{Str}$ during activation as in (B). Symbols used in (B) and (C): UreABC—UreD—UreF—UreG $_{Str}$ with wild-type UreF (\spadesuit), K165A UreF (\spadesuit), or T21A UreG $_{Str}$ (\blacksquare).

UreF functions to increase the fidelity of urease activation. The experiments described above demonstrate that a defective UreF enhances the GTPase activity of UreABC—UreD—UreF—UreG $_{Str}$ and cast doubt on the hypothesis that this protein serves as a GAP. Because the GTPase activity of the complex containing K165A UreF appears to be less coupled to urease activation than that with wild-type protein, we hypothesize that UreF plays a non-GAP role; specifically, we propose that UreF is a gatekeeper that increases the fidelity of the activation process. Related to this notion, activation of the isolated urease apoprotein is known to generate activity in only ~15% of the nascent active sites even though the protein is fully metallated and carbamylation takes place (37, 38); thus, complete activation must somehow overcome the formation of the improperly formed metallocenters. Two experiments were carried out to explore the hypothesis that UreF enhances the fidelity of urease activation.

A time course activation experiment was performed in Ni-limiting conditions (i.e. 50 μ M Ni versus 100 μ M Ni, as used above) for the UreABC—UreD—UreF—UreG_{Str} complex and the same complex containing K165A UreF, using activation assays with and without 75 μ M Mg₂GTP (Figure 3.9). The resulting data were fitted to equation 1 to calculate maximal activities and the times needed to reach half-maximal activities. These fits ignored the possible slight diminishments in activation capacities for samples after incubation at 37 °C for 5 h. The complex containing K165A UreF activated quickly ($t_{1/2}$ 37 \pm 12 min) and reached a maximal activity of 225 \pm 16 U/mg. The presence of GTP led to slower activation ($t_{1/2}$ 77 \pm 18 min) and a smaller final activity level (177 \pm 14 U/mg), possibly due in part to chelation of Ni by GTP. In

contrast, the wild-type complex was slow to activate whether GTP was absent or present ($t_{1/2}$ 83 ± 12 min and 80 ± 20 min, respectively), it formed little activity without GTP (118 ± 6 U/mg), and with GTP it reached approximately the same maximum activity (228 ± 19 U/mg) as observed for the complex containing K165A UreF in the absence of nucleotide. These results are compatible with the hypothesis that UreF enhances the efficiency of the process by improving the coupling to GTP hydrolysis, decreasing the rate of activation, and assuring the maximal amount of properly formed metallocenter.

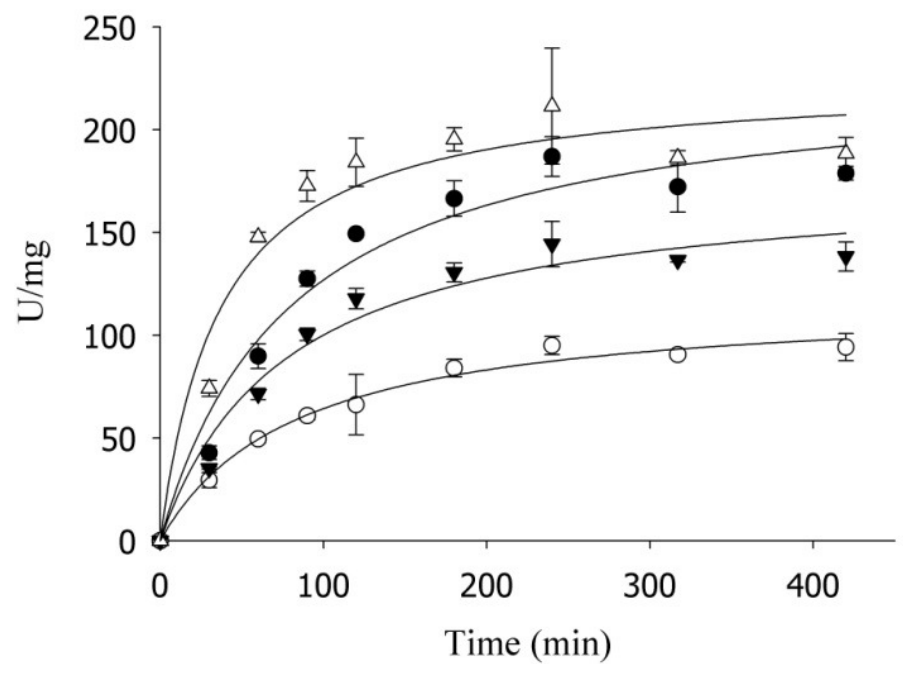


Figure 3.9: Comparison of activation time course for UreABC—UreD—UreF—UreG $_{Str}$ complex and UreABC—UreD—UreF(K165A)—UreG $_{Str}$. Proteins (0.5 μ M) were incubated in standard activation buffer except for only containing 50 μ M Ni. The wild—type and K165A complexes were incubated in the absence (o and Δ , respectively) or the presence (\bullet and $, \blacksquare$ respectively) of 75 μ M Mg $_2$ GTP. Fits using equation 1 are shown for each data set.

As a more direct approach to evaluate this potential gatekeeper role of UreF, we assessed the effect of added Zn ions on the activation of UreABC—UreD—UreF—Ure G_{Str}

containing wild-type and K165A accessory protein. Zn is known to compete effectively with Ni and hinder production of urease activity during activation of (UreABC)3, (UreABC-UreD)3, and (UreABC-UreD-UreF)₃ (7, 8, 38), but its effects on UreABC—UreD—UreF—UreG had never been examined. As illustrated in Figure 3.10, the presence of Zn in the activation mixture decreases the level of urease activity generated for both complexes studied whether or not GTP is present. The complexes were activated at three concentrations of Zn (0, 2.5, and 5.0 µM) and activities were measured at 1, 2, and 4 h to ensure maximal activation for analysis. After 2 h, both the wild-type and the K165A variant complexes had reached full activity according to the control assays without Zn, so that time point was analyzed. Whereas the activity of complex containing wild-type UreF activated with GTP (solid black bar) was equivalent to the K165A UreF-containing complex (with or without GTP) in the absence of Zn (hatched and gray bars, respectively), the wild-type complex with GTP generated significantly more activity (p < 0.05) than the other mixtures in the presence of low concentrations of Zn. These results indicate that wild-type UreF allows the GTPase activity of UreG to partially protect against improper metallocenter assembly. UreF thus plays an important role in coupling the GTPase activity to urease activation, insuring proper di-Ni cluster formation.

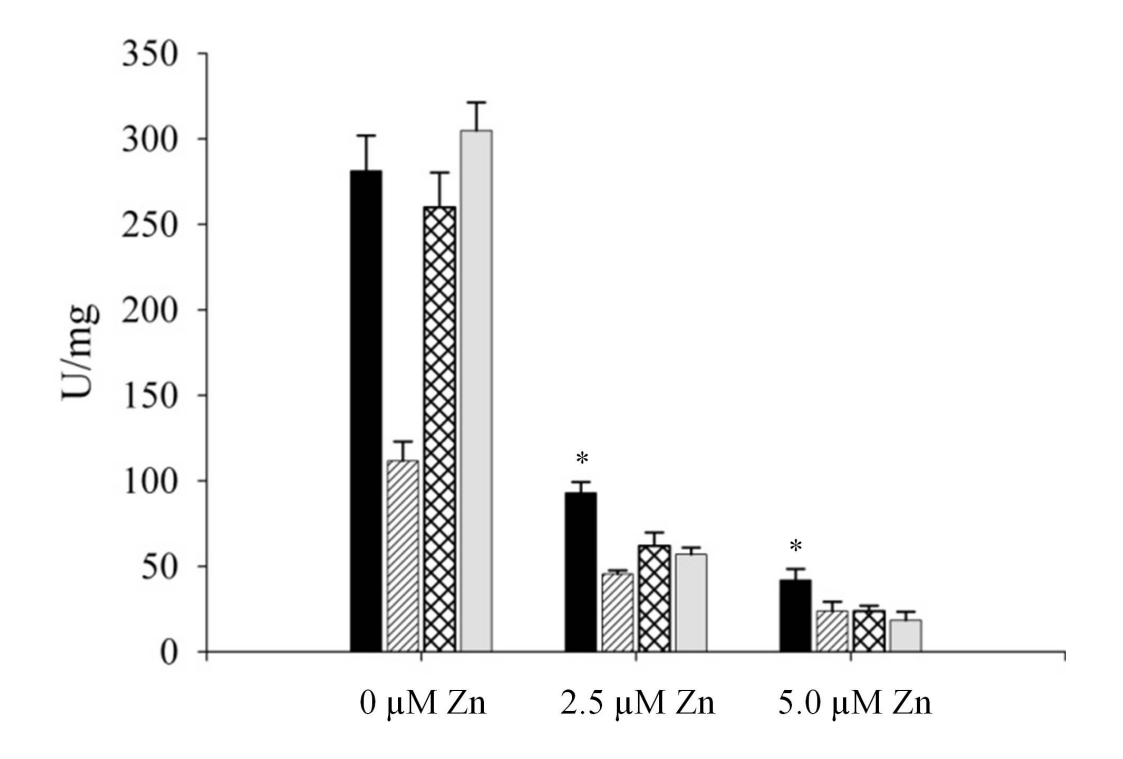


Figure 3.10: Zn inhibition of UreABC—UreD—UreF—UreG $_{Str}$ (0.5 μ M) activation under standard conditions for complexes containing wild-type and K165A UreF. Protein complexes (0.5 μ M) were incubated for two h at 37 °C in standard activation solution with the indicated concentrations of ZnSO $_4$. The wild-type and K165A complexes were incubated in the presence (black and hatched, respectively) or absence (diagonal and grey, respectively) of 75 μ M Mg $_2$ GTP. The asterisks indicate statistically significant differences (p < 0.05) of the sample indicated versus the samples subjected to the same conditions.

DISCUSSION

This study has significantly enhanced our understanding of the UreF urease accessory protein by clarifying its interactions with UreG and its role in urease activation. Prior efforts had shown that free K. aerogenes UreF is insoluble (8) whereas a truncated version of the H. pylori protein is soluble and was structurally defined (20). In addition, soluble forms of UreF are known to be found in various complexes, including (UreH—UreF)2 from H. pylori (15) and the following K. aerogenes species: MBP-UreD-UreF-UreG (14), (UreABC-UreD-UreF)3 (8), and UreABC—UreD—UreF—UreG (9). The (UreH—UreF)₂ structure defined how UreF interacts with the UreD homologue and mutational studies in the same work provided evidence that Y48 and R250 in the H. pylori UreF protein (corresponding to Y23 and R220 in K. aerogenes UreF) are critical for binding UreG (15); however, other specific residues involved in UreG binding were not defined. There is no crystal structure available for any UreG sample, perhaps because the isolated protein cannot be crystallized due to its intrinsic disorder according to NMR, circular dichroism, and fluorescence spectroscopic analyses (39, 40), so modeling of UreF/UreG interaction (15) can provide only a crude notion of the potential interface surfaces. The present investigations extend knowledge of residues critical to this interface and provide new experimental insights into the role of UreF in urease activation.

The current study targeted sixteen highly conserved UreF residues for mutagenesis as a means to identify their importance in urease activation and UreG binding. Urease assays of cell-free extracts from cultures containing the complete urease gene cluster showed that nine of the mutants exhibited less than 10% of the wild type activity, including those producing the

Y23A and R220A UreF variants (comparable to the two H. pylori UreF variants mentioned above), confirming their importance in urease activation. UreE-F pull-down assays using cellfree extracts showed that substitutions affecting each of these nine residues had reduced levels of UreG binding, with six leading to the absence of associated UreG. The G21A and K165A variants had somewhat greater urease activity (38 and 20 U/mg, respectively), but also had reduced amounts of UreG. These important residues map to a 1300 Å² surface on UreF (Figure 3.6), and are close to the binding surface for UreD, consistent with how the three proteins are known to work together for urease activation. None of the site-directed mutations greatly affected the interaction between UreF and UreABC-UreD, as expected on the basis of the (UreH—UreF)2 crystal structure which showed that only one of the highly conserved residues we chose to mutate (E215) is located at the UreD binding surface. It is intriguing that the UreG binding site on UreF has so many highly conserved residues, whereas the UreD and urease binding sites on this protein are not highly conserved. Possibly related to this finding, UreG is the most highly conserved urease accessory protein whereas alignments of UreD or UreF proteins each exhibit significantly less similarity.

We attempted to directly test the proposed role of UreF as a GAP (21) by comparing the activation properties of UreABC—UreD—UreF—UreG_{Str} complexes containing wild-type and K165A UreF. K165 is the only Lys in *K. aerogenes* UreF and this position is always occupied by a Lys or Arg residue in homologues; thus, this positively-charged residue could reasonably correspond to the typical Arg finger motif that is found in GAP proteins (33-35). The Arg finger of GAPs plays a dual role in generating the nucleophilic water molecule needed for hydrolysis

and stabilizing the transition state (34). Urease assays using cell-free extracts showed that K165 of UreF plays a non-essential role in urease activation, with 20% of the wild-type urease activity retained when using a culture that synthesizes K165A UreF along with the other urease proteins. In vitro assays using wild-type and variant UreABC—UreD—UreF—UreG_{Str} complexes unexpectedly demonstrate that the species containing K165A UreF results in enhanced levels of urease activity. I don't have a simple explanation for why the in vivo and in vitro results differ in this manner; however, I note that the urease activation conditions are quite distinct for those two processes. For the purified complex, activation of the K165A UreF-containing version is inhibited, not enhanced, by GTP. More significantly, the variant complex exhibits greater GTPase activity than the wild-type complex; thus ruling out the possibility that K165 serves in the Arg finger role of a GAP. Although K165 does not function as an Arg finger, it remains possible that R220, another highly conserved and positively-charged residue (in this case near the critically important C-terminus), could serve in this manner. Our UreE-F pull-down assays using cell-free extracts reveal the lack of UreG binding to the complex containing the R220A variant of UreE-F, so it was not possible to test the effect of mutating this residue in UreABC— UreD—UreF—UreG_{Str} as was accomplished with the K165A UreF variant. If R220 could act as an Arg finger, one would need to postulate that K165 modulates its effect so that the K165A variant leads to greater GTPase activity. There are examples of GAP-GTPase interactions that do not involve an Arg finger, for example the Rap-RapGAP complex (41, 42). Nevertheless, the above studies greatly reduce the possibility that UreF acts as a GAP, thus encouraging us to consider and test other hypotheses for its function.

The finding that UreABC—UreD—UreF—UreG_{Str} activation is less coupled to GTPase activity when using K165A UreF and the demonstration of increased urease activity resulting from the substituted version of UreF led us to consider a gatekeeper role for this protein; i.e., UreF would help to ensure proper metallocenter assembly during urease activation. The complexes with the two forms of UreF have the same final activation competence, but that containing wild-type protein requires GTP while that with K165A UreF is inhibited by the nucleotide. The time course assays reveal a more rapid activation of the K165A UreFcontaining complex (lacking GTP) than noted in the complex with wild-type UreF (with or without GTP), consistent with wild-type UreF hindering the rate of activation while insuring greater fidelity of metallocenter biosynthesis. In contrast, the K165A variant allowed the process to occur more quickly but possibly with less control. UreG's GTPase activity appears to play a role in controlling the rate of activation, and when this activity is uncoupled from activation (i.e., when using K165A UreF) urease activity is generated much faster. It is likely more important that the timing is tightly regulated in the cell compared to the idealized environment of the test tube, since the K165A variant only has 20% of the wild type activity in vivo. The GTPase activity could play a role in gating the timing of the Ni transfer to the active site in order to prevent the metal from binding incorrectly (as in the 85% of the urease apoprotein that becomes carbamylated and binds Ni, yet remains inactive when subjected to activation conditions as mentioned earlier). This hypothesis is supported by the demonstration that the complex formed with wild-type UreF (coupled to GTPase activity) is more resistant to inhibition by Zn during activation than is the case for the variant complex. We propose that UreF induces a conformational change in, or stabilizes the structure of, UreG that allows for the

latter protein's hydrolytic capacity while ensuring a tight coupling between GTP hydrolysis and proper metal assembly. Replacing K165 with Ala leads to greater uncoupling of the activation and hydrolysis steps, thus yielding enhanced rates of activation under favorable conditions, but allowing incorrect metal assembly when Zn is present, and possibly having additional negative consequences *in vivo*. This model is compatible with the finding that GTPase activity is not essential *in vitro* for partial activation, as has long been known for (UreABC)₃, (UreABC—UreD)₃, and (UreABC—UreD—UreF)₃ (8, 9, 38), but the full set of accessory proteins allows for greater final levels of activation to occur with UreF increasing the fidelity of the process. Thus, when all urease accessory proteins, including UreE, are present, urease can be activated fully (11).

The suggestion that GTPase activity can be used as a checkpoint has been reported for other proteins in the same family as UreG. For example, the GTPase activity of HypB, a protein that functions in hydrogenase maturation in *E. coli*, is thought to gate Ni transfer into hydrogenase with the participation of the Ni-binding protein SlyD (*43*). Similarly, MeaB, another member of the small GTPase family, serves a gating function for incorporating coenzyme B₁₂ into methylmalonyl-CoA mutase (*44*). We propose that UreF works to improve the coupling of UreG's GTPase activity to Ni insertion into urease.

In conclusion, we have confirmed that mutations affecting a series of highly conserved UreF residues have dramatic effects on *in vivo* urease activity. Using these same UreF variants in UreE-F pull-down assays with cell extracts or by carrying out interaction studies with purified UreF and UreG components, we have identified several UreF residues that make up the binding

surface for UreG. We have also evaluated a proposed role of UreF as a GAP and obtained no evidence to support this hypothesis since a variant UreF gave rise to increased GTPase activity. Finally, we provide evidence that UreF is needed for coupling GTPase activity to ensure proper metallocenter assembly, where the gating function of UreF increases the fidelity of activation—especially when competing Zn is present.

REFERENCES

REFERENCES

- 1. Mobley, H. L. T., Island, M. D., and Hausinger, R. P. (1995) Molecular biology of microbial ureases *Microbiol. Rev. 59*, 451-480.
- 2. Carter, E. L., Flugga, N., Boer, J. L., Mulrooney, S. M., and Hausinger, R. P. (2009) Interplay of metal ions and urease, *Metallomics* 1, 207-221.
- 3. Witte, C.-P. (2011) Urea metabolism in plants, *Plant Science 180*, 431-438.
- 4. Zambelli, B., Musiani, F., Benini, S., and Ciurli, S. (2011) Chemistry of Ni²⁺ in urease: sensing, trafficking, and catalysis, *Accounts of Chemical Research 44*, 520-530.
- 5. Jabri, E., Carr, M. B., Hausinger, R. P., and Karplus, P. A. (1995) The crystal structure of urease from *Klebsiella aerogenes*, *Science 268*, 998-1004.
- 6. Lee, M. H., Mulrooney, S. B., and Hausinger, R. P. (1990) Purification, characterization, and *in vivo* reconstitution of *Klebsiella aerogenes* urease apoenzyme, *J. Bacteriol.* 172, 4427-4431.
- 7. Park, I. S., Carr, M. B., and Hausinger, R. P. (1994) *In vitro* activation of urease apoprotein and role of UreD as a chaperone required for nickel metallocenter assembly, *Proc. Natl. Acad. Sci. U.S.A.* 91, 3233-3237.
- 8. Moncrief, M. B. C., and Hausinger, R. P. (1996) Purification and activation properties of UreD-UreF-urease apoprotein complexes, *J. Bacteriol.* 178, 5417-5421.
- 9. Park, I. S., and Hausinger, R. P. (1995) Evidence for the presence of urease apoprotein complexes containing UreD, UreF and UreG in cells that are competent for *in vivo* enzyme activation, *J. Bacteriol.* 177, 1947-1951.
- 10. Soriano, A., and Hausinger, R. P. (1999) GTP-dependent activation of urease apoprotein in complex with the UreD, UreF, and UreG accessory proteins, *Proc. Natl. Acad. Sci. U.S.A. 96*, 11140-11144.
- 11. Soriano, A., Colpas, G. J., and Hausinger, R. P. (2000) UreE stimulation of GTP-dependent urease activation in the UreD-UreF-UreG-urease apoprotein complex, *Biochemistry 39*, 12435-12440.
- 12. Quiroz-Valenzuela, S., Sukuru, S. C. K., Hausinger, R. P., Kuhn, L. A., and Heller, W. T. (2008) The structure of urease activation complexes examined by flexibility analysis, mutagenesis, and small-angle X-ray scattering, *Arch. Biochem. Biophys* 480, 51-57.
- 13. Chang, Z. Z., Kuchar, J., and Hausinger, R. P. (2004) Chemical cross-linking and mass spectrometric identification of sites of interaction for UreD, UreF, and urease, *J. Biol. Chem.* 279, 15305-15313.

- 14. Carter, E. L., and Hausinger, R. P. (2010) Characterization of *Klebsiella aerogenes* urease accessory protein UreD in fusion with the maltose binding protein, *J. Bacteriol.* 192, 2294-2304.
- 15. Fong, Y. H., Wong, H. C., Chuck, C. P., Chen, Y. W., Sun, H., and Wong, K.-B. (2011) Assembly of preactivation complex for urease maturation in *Helicobacter pylori*, *J. Biol. Chem.* 286, 43241-43249.
- 16. Heimer, S. R., and Mobley, H. L. T. (2001) Interaction of *Proteus mirabilis* urease apoenzyme and accessory proteins identified with yeast two-hybrid technology, *J. Bacteriol.* 183, 1423-1433.
- 17. Rain, J. C., Selig, L., De Reuse, H., Battaglia, V., Reverdy, C., Simon, S., Lenzen, G., Petel, F., Wojcik, J., Schachter, V., Chemama, Y., Labigne, A. S., and Legrain, P. (2001) The protein-protein interaction map of *Helicobacter pylori, Nature 409*, 211-215.
- 18. Kim, K. Y., Yang, C. H., and Lee, M. H. (1999) Expression of the recombinant *Klebsiella aerogenes* UreF protein as a MalE fusion, *Arch. Pharm. Res.* 22, 274-278.
- 19. Kim, J. K., Mulrooney, S. B., and Hausinger, R. P. (2006) The UreEF fusion protein provides a soluble and functional form of the UreF urease accessory protein, *J. Bacteriol.* 188, 8413-8420.
- 20. Lam, R., Romanov, V., Johns, K., Battaile, K. P., Wu-Brown, J., Guthrie, J. L., Hausinger, R. P., Pai, E. F., and Chirgadze, N. Y. (2010) Crystal structure of a truncated urease accessory protein UreF from *Helicobacter pylori*, *Proteins 78*, 2839-2848.
- 21. Salomone-Stagni, M., Zambelli, B., Musiani, F, and Ciurli, S. (2007) A model-based proposal for the role of UreF as a GTPase-activating protein in the urease active site biosynthesis, *Proteins 68*, 749-761.
- 22. Boer, J. L., Quiroz-Valenzuela, S., Anderson, K. L., and Hausinger, R. P. (2010) Mutagenesis of *Klebsiella aerogenes* UreG to probe nickel binding and interactions with other urease-related proteins, *Biochemistry 49*, 5859-5869.
- 23. Zambelli, B., Turano, P., Musiani, F., Neyroz, P., and Ciurli, S. (2009) Zn²⁺-linked dimerization of UreG from *Helicobacter pylori*, a chaperone involved in nickel trafficking and urease activation, *Proteins 74*, 222-239.
- 24. Zambelli, B., Stola, M., Musiani, F., De Vriendt, K., Samyn, B., Devreese, B., Van Beeumen, J., Turano, P., Dikiy, A., Bryant, D. A., and Ciurli, S. (2005) UreG, a chaperone in the urease assembly process, is an intrinsically unstructured GTPase that specifically binds Zn²⁺, *J. Biol. Chem. 280*, 4684-4695.
- 25. Zambelli, B., Musiani, F., Savini, M., Tucker, P., and Ciurli, S. (2007) Biochemical studies

- on *Mycobacterium tuberculosis* UreG and comparative modeling reveal structural and functional conservation among the bacterial UreG family, *Biochemistry 46*, 3171-3182.
- 26. Colpas, G. J., Brayman, T. G., Ming, L. J., and Hausinger, R. P. (1999) Identification of metal-binding residues in the *Klebsiella aerogenes* urease nickel metallochaperone, UreE, *Biochemistry 38*, 4078-4088.
- 27. Bellucci, M., Zambelli, B., Musiani, F., Turano, P., and Ciurli, S. (2009) *Helicobacter pylori*UreE, a urease accessory protein: specific Ni²⁺- and Zn²⁺-binding properties and interaction with its cognate UreG, *Biochem. J. 422*, 91-100.
- 28. Miroux, B., and Walker, J. E. (1996) Over-production of proteins in *Escherichia coli*: Mutant hosts that allow synthesis of some membrane proteins and globular proteins at high levels, *J. Mol. Biol. 260*, 289-298.
- 29. Carter, E. L., Boer, J. L., Farrugia, M. A., Flugga, N., Towns, C. L., and Hausinger, R. P. (2011) The function of UreB in *Klebsiella aerogenes* urease, *Biochemistry 50*, 9296-9308.
- 30. Laemmli, U. K. (1970) Cleavage of structural proteins during assembly of head of bacteriophage-T4, *Nature 227*, 680.
- 31. Weatherburn, M. W. (1967) Phenol-hypochlorite reaction for determination of ammonia, *Anal. Chem. 39*, 971-974.
- 32. Baykov, A. A., Evtushenko, O. A., and Avaeva, S. M. (1988) A malachite green procedure for orthophosphate determination and its use in alkaline phosphatase-based enzyme immunoassay, *Anal. Biochem.* 171, 266-270.
- 33. Ahmadian, M. R., Stege, P., Scheffzek, K., and Wittinghofer, A. (1997) Confirmation of the arginine-finger hypothesis for the GAP-stimulated GTP-hydrolysis reaction of Ras, *Nature Struct. Biol. 4*, 686-689.
- 34. Resat, H., Straatsma, T. P., Dixon, D. A., and Miller, J. H. (2001) The arginine finger of RasGAP helps Gln-61 align the nucleophilic water in GAP-stimulated hydrolysis of GTP, *Proc Natl Acad Sci 98*, 6033-6038.
- 35. Scheffzek, K., and Ahmadian, M. R. (2005) GTPase activating proteins: structural and functional insights 18 years after discovery, *Cell. Mol. Life Sci. 62*, 3014-3038.
- 36. Moncrief, M. B. C., and Hausinger, R. P. (1997) Characterization of UreG, identification of a UreD-UreF-UreG complex, and evidence suggesting that a nucleotide-binding site in UreG is required for in vivo metallocenter assembly of *Klebsiella aerogenes* urease, *J. Bacteriol.* 179, 4081-4086.
- 37. Park, I. S., and Hausinger, R. P. (1995) Requirement of carbon-dioxide for *in vitro* assembly of the urease nickel metallocenter, *Science 267*, 1156-1158.

- 38. Park, I. S., and Hausinger, R. P. (1996) Metal ion interactions with urease and UreDurease apoproteins, *Biochemistry* 35, 5345-5352.
- 39. Neyroz, P., Zambelli, B., and Ciurli, S. (2006) Intrinsically disordered structure of *Bacillus* pasteurii UreG as revealed by steady-state and time-resolved fluorescence spectroscopy, *Biochemistry 45*, 8918-8930.
- 40. Zambelli, B., Cremades, N., Neyroz, P., Turano, P., Uversky, V. N., and Ciurli, S. (2012) Insights in the (un)structural organization of *Bacillus pasteurii* UreG, an intrinsically disordered GTPase enzyme, *Mol. Biosyst. 8*, 220-228.
- 41. Chakrabarti, P. P., Suveyzdis, Y., Wittinghofer, A., and Gerwert, K. (2004) Fourier transform infared spectroscopy on the Rap-RapGAP reaction, GTPase activation without an arginine finger, *J. Biol. Chem. 279*, 46226-26233.
- 42. Scrima, A., Thomas, C., Deaconescu, D., and Wittinghofer, A. (2008) The Rap-RapGAP complex: GTP hydrolysis without catalytic glutamine and arginine residues, *EMBO J. 27*, 1145-1153.
- 43. Kaluarachchi, H., Zhang, J. W., and Zamble, D. B. (2011) *Escherichia coli* SlyD, more than a Ni(II) reservoir, *Biochemistry 50*, 10761-10763.
- 44. Padovani, D., and Banerjee, R. (2009) A G-protein editor gates coenzyme B-12 loading and is corrupted in methylmalonic aciduria, *Proc. Natl. Acad. Sci. U.S.A. 106*, 21567-21572.



Additional Studies, Conclusions, and Remaining Questions

Portions of this chapter were adapted from Carter, E. L., Boer, J. L., Farrugia, M. A., Flugga, N., Towns, C., and Hausinger, R. P. (2011) The function of UreB in *Klebsiella aerogenes* urease activation, *Biochemistry*, *50*, 9296-9308.

ADDITIONAL STUDIES

The following sections describe experiments that were not incorporated into chapters 2 or 3. In addition to this text, I summarize all constructs I've generated in a succinct table provided as an appendix.

Metal analysis of (UreABC*)₃ and (UreAC)₃

One of the questions surrounding urease activation is how Ni gets into the active site, which is buried in the UreC subunit. Previous studies have indicated that UreB may undergo a conformational change during the activation process allowing for greater access to the active site (Figure 4.1). For example, chemical cross-linking studies demonstrated that Lys 382 in UreC crosslinked to Lys 76 in UreB when UreD and UreF were present, whereas the crystal structure of urease shows those two residues are distant from each other (1). Furthermore, SAXS analyses showed that the UreD and UreF accessory proteins bind near UreB (2). In order to investigate the role of UreB, UreB alone and the apoprotein complex (UreAC)3 were purified and characterized. Part of this characterization included metal analysis of urease with and without UreB present to see how much Ni was bound. Metal analysis was carried out on activated (i.e., with added Ni and bicarbonate) (UreAC)3, (UreABC*)3 (formed by mixing purified (UreAC)₃ with a 5-fold excess of UreB and incubating at room temperature for 30 min before activation), and the complex formed by activating (UreAC)₃ followed by addition of UreB.

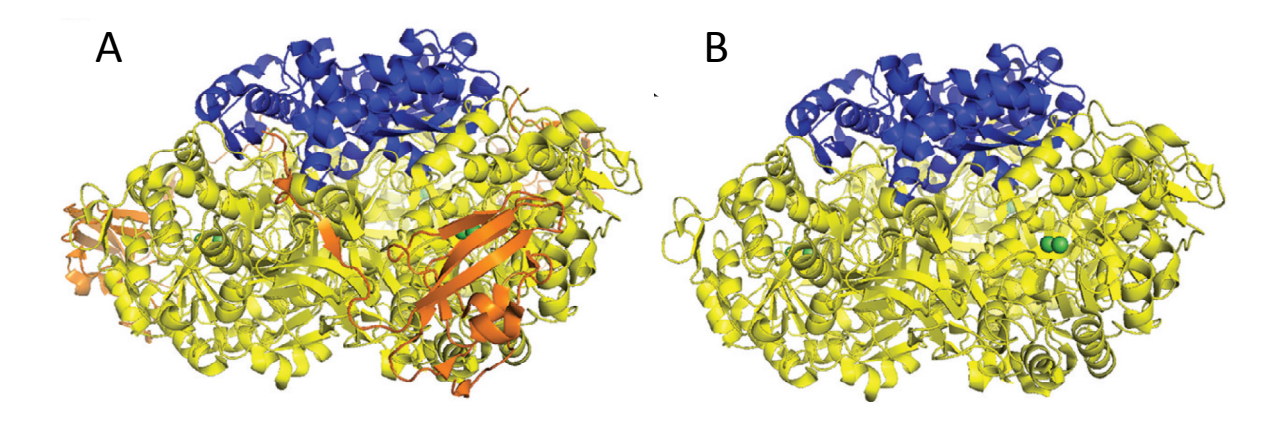


Figure 4.1: UreB of *K. aerogenes* urease blocks access to the active site. A. Urease structure with UreA in blue, UreB in orange, UreC in yellow, and Ni atoms in green. B. Same as A with UreB removed

To assess the nickel content of activated (UreABC*)₃, I mixed 120 μL of (UreAC)₃ (370 μ M heterodimer in HT buffer (50 mM HEPES (pH 7.8) and 1 mM TCEP)) with 120 μ L of UreB (1450 µM in HT buffer) and incubated the mixture for 30 min at ambient temperature. The mixture was diluted to 10 µM UreC protomer with 4.2 mL of standard activation buffer (100 mM HEPES (pH 8.3), 150 mM NaCl, 100 mM NaHCO₃, and 100 μM NiCl₂) and incubated at 37 °C for 60 min. The sample was concentrated with a 10,000 MWCO Amicon centrifugal filter device (prewashed with deionized water) to 300 μL and either immediately chromatographed on a 1 cm × 43 cm Sephacryl S300 HR column (GE Healthcare) equilibrated in 100 mM HEPES (pH 8.3) or treated with 10 mM EDTA for 5 min at ambient temperature and chromatographed in the same buffer with 1 mM EDTA. Fractions of interest were verified for protein content with SDS-PAGE, allowed to equilibrate for at least 16 h at 4 °C, concentrated by use of 10,000 MWCO Amicon centrifugal filter devices, and analyzed in parallel with protein-free buffer for metal content by inductively coupled plasma-atomic emission spectroscopy (ICP-AES) (Chemical Analysis Laboratory, University of Georgia, Athens, GA). For studies focusing on the nickel content of (UreAC)₃ after activation, a similar methodology was employed as described above except that (UreAC)₃ (120 μ L, 370 μ M in HT buffer) was directly diluted to a final UreC protomer concentration of 10 μ M in activation buffer, followed by the same incubation, concentration, and gel filtration steps with and without EDTA. Lastly, 4.3 mL of (UreAC)₃ (UreC protomer final concentration of 10 μ M) was subjected to standard activation conditions at 37 °C for 60 min, mixed with 120 μ L of UreB (1450 μ M in HT buffer), incubated at ambient temperature for 30 min, and analyzed for nickel content after concentration, with or without EDTA treatment, and gel filtration chromatography as described above.

To examine the effect of inclusion of UreB on Ni²⁺ incorporation into urease apoprotein, samples that had been subjected to the standard activation conditions were analyzed for metal content by ICP-AES (Table 4.1). For comparison, 0.53 equiv of Ni per heterotrimer was associated with authentic (UreABC)₃ apoprotein that was activated by use of standard conditions and treated with EDTA (3), whereas 1.74 or 1.83 equiv of Ni was incorporated into the sample that was not treated with chelator (3, 4). When using (UreABC*)₃, obtained by mixing UreB with (UreAC)₃ before activation, the metal content of the EDTA-treated sample was 1.00 Ni per heterodimer, whereas samples not treated with chelator possessed 2.56 equiv of metal. In contrast, (UreAC)₃ subjected to activation conditions bound only 0.10 equiv of nickel if treated with chelator but still bound 2.57 equiv in the absence of EDTA. Finally, (UreAC)₃ that was activated and then mixed with UreB contained 0.18 equiv of nickel with

EDTA treatment and 2.78 equiv of metal without the chelator.

Table 4.1: Metal content of urease apoprotein samples subjected to activation conditions

Complex	Ni content ^b + EDTA	Ni content - EDTA
(UreABC*) ₃	1.00 ± 0.04	2.56 ± 0.27
(UreAC) ₃	0.10 ± 0.03	2.57 ± 0.36
(UreAC) ₃ then add UreB	0.18 ± 0.04	2.78 ± 0.17

^a Activation conditions involved incubating the protein for 1 h at 37 °C in 100 mM HEPES (pH 8.3), 150 mM NaCl, 100 mM NaHCO₃, and 100 μ M NiCl₂. ^b Ni content per UreC subunit.

These results indicate that UreB plays a vital role in protecting the Ni in the active site from chelation, as well as insuring it is incorporated correctly. Only when UreB is present before activation is the Ni content still high after EDTA is added (1 equivalent of Ni per UreC compared to 0.1 and 0.18 equivalents when UreB is not present or added after activation). Adding UreB to activated (UreAC)₃ is not sufficient; UreB cannot trap a pre-formed metallocenter but must be present during the activation process.

Crystallization Attempts

In order to understand the urease activation process in greater detail, I made several attempts to crystallize selected proteins. The structure of UreF was unknown when I began my thesis research and there is still no structure for UreG, so both of these accessory proteins were targets for crystallization. In addition, the urease variant containing G11P UreB was known to be a low activity mutant (where G11 is in a flexible region of UreB proposed to be important for the conformational change needed for activation) (2), and this protein was studied to further examine the potential implications of UreB movement in urease activation. All microbatch crystallization efforts were carried out using an Oryx4 robot from Douglas Instruments overseen by Professor Michael Garavito.

UreE-F. Purified UreE-F (5) (9 mg/mL in 20 mM Tris, pH 7.8, 300 mM NaCl, 1 mM EDTA, and 10% glycerol) was used for microbatch screening using two commercially available sets of 96 conditions each (Hampton Research). One condition (0.1 M HEPES, pH 7.5, 4.3 M NaCl) produced needle-shaped crystals after 2 weeks at 20 °C. Twenty-four sitting drop conditions were set up by varying the condition that produced crystals by varying the pH by 1 unit in each direction and reducing the concentration of NaCl in 0.2 M increments to 2.0 M in order to get a different crystal form, but those attempts were not successful.

UreG. Purified UreG (6) (10 mg/mL) in 100 mM Tris, pH 8.0, 150 mM NaCl and 1 mM EDTA was used for microbatch crystal screening under the same initial screens as UreF, but no crystals were found after one month under these conditions.

(UreAB(G11P)C)₃. Purified enzyme (2) (18 mg/mL) in 20 mM Tris, pH 7.0, 1 mM EDTA, and 1 mM DTT was used for microbatch crystal screening using the same microbatch screens, which included the condition that was used to crystallize urease (7). One condition (0.2 M sodium acetate trihydrate, 0.1 M Tris-HCl, pH 8.5, 30% w/v PEG 4000) resulted in small crystals after one week at 20 °C. Sitting drop experiments were set up by varying the concentrations of the sodium acetate trihydrate, Tris-HCl, and PEG 4000; however, the crystals in the original condition were not reproducible.

XAS studies on UreG

UreG binds one Ni or one Zn ion per monomer (Chapter 2), but mutagenesis efforts to determine the ligands that bind the metal were largely unsuccessful. As another method to learn about the ligands for the metal binding site in UreG, I provided samples to Professor Michael Maroney at University of Massachusetts for XAS (X-ray absorption spectroscopy)

analysis. XAS is a method that can determine the number and types of atoms that ligate the metal as well as their distance from the metal.

UreG and UreG_{Str} were purified as described in chapter 2. Proteins were dialyzed into buffer containing 50 mM HEPES (pH 7.4) and 200 mM NaCl overnight. 1 mL samples of 100 μM UreG_{Str} or UreG were dialyzed overnight into 250 mL of the same buffer that also contained 200 μM NiCl₂ or ZnCl₂. The next morning the samples were concentrated to 0.5 mL and, in the same step involving a G-25 column (GE Healthcare), excess metal was removed and 25% glycerol was added. The eluate was concentrated to 70 µL by using 0.5 mL Amicon 10,000 MWCO ultracentrifugal filters. A portion (20 μL) of the concentrated protein was used to assess protein and metal concentrations and 50 µL was flash-frozen by using liquid nitrogen and stored at -80 °C until they could be shipped. Samples were analyzed for protein concentration by using a Nanodrop spectrophotometer (the extinction coefficients of each protein are 22,430 cm $^{-1}$ M $^{-1}$ for UreG_{Str} and 16,740 cm $^{-1}$ M $^{-1}$ for UreG) and for metal content by using PAR (8). The Zn samples had a significant amount of precipitation and were not concentrated enough to send for XAS analysis. Table 4.2 describes the samples sent. XAS data have been collected for the samples, but analysis is still in progress.

Table 4.2: Samples sent for XAS analysis

Sample	Protein Concentration	Ni concentration
UreG	1560 μΜ	770 μΜ
UreG _{Str}	885 μΜ	600 μΜ

In vitro pull-down assays with UreE-F and MBP-UreD

In addition to the studies described in Chapter 3 that involved mixing UreE-F and its

variants with (UreABC—UreD)₃ or UreG_{Str} and pulling out the complexes that bind NTA or Strep-tactin resin, respectively, to determine protein:protein interactions, I also carried out amylose resin pull-down studies with MBP-UreD. These studies were done at 37 °C (where the interaction between UreD and UreF was weak) and at 42 °C (where a ratio of 1.8:1 MBP-UreD:UreE-F was seen) (9). Unfortunately, as described below, these studies were difficult to interpret and did not add to our knowledge of the UreD—UreF interface.

Interactions between UreF and UreD were analyzed by using purified MBP-UreD and UreE-F. The UreE-F fusion protein and its variants (10 μ M) were incubated with 2 μ M MBP-UreD at 37 °C (a temperature that leads to a lesser amount of interaction) or 42 °C (a temperature that was previously shown to promote maximal interaction) for one h, added to amylose resin at 1/5 the volume of the assay, rocked for one h at room temperature, washed with five fold the assay volume, and eluted in buffer containing 10 mM amylose (9). Assays were analyzed by 12% SDS-PAGE and gel scanning (Alpha Imager 2200), with the intensities of the bands divided by the relative molecular mass of each protein (MBP-UreD, 72.9 kDa; UreEF, 42.8 kDa) to assess the ratios of interactions.

The interactions between MBP-UreD and wild-type or variant UreE-F proteins were analyzed at two temperatures. Samples incubated at 37 °C yielded a 0.4:1 ratio of MBP-UreD to UreE-F using the wild-type fusion protein, and, surprisingly, the ratio increased in half of the experiments when using mutant protein samples. Samples incubated at 42 °C yielded a 1.8:1 MBP-UreD to UreE-F ratio using the wild-type protein, and the ratio increased for all but three of the mutants proteins (E94A was similar to wild type, whereas K165A and Q171A were slightly lower) (Table 4.3). The large binding ratios were attributed to MBP-UreD aggregation; thus, no

further conclusions could be discerned from the data. The crystal structure of (UreH—UreF)₂ revealed that E215 was the only residue changed to alanine that was involved in the UreD-UreF interface, further confirming concerns about aggregation in MBP-UreD.

Table 4.3: Binding of control and mutant UreE-F to MBP-UreD a

UreE-F	Ratio of UreE-F/MBP-UreD at	Ratio of UreE-F/MBP-UreD at
	-	-
mutation	37 °C	42 °C
wt	0.41	1.81
P19A	0.58	2.39
G21A	0.94	2.41
Y23A	0.65	2.64
S26A	0.51	2.66
E30A	0.18	2.49
E94A	0.99	1.89
K165A	1.22	1.24
Q171A	1.00	1.39
H214A	0.25	2.09
E215A	0.25	2.21
R220A	0.31	2.91
L221A	0.36	2.98
F222A	0.42	3.12
S224A	0.29	2.94

^a Determined by *in vitro* pull-down studies using amylose resin and gel scanning

Characterization of MBP-UreD—UreF—UreG

GTPase activity and contamination. In order to investigate the hypothesis UreF acts as a GAP for the GTPase UreG (see chapter 3), MBP-UreD—UreF—UreG and MBP-UreD—UreF—UreG(T21A) (as a control that cannot hydrolyze GTP) were purified and their GTPase activities were characterized. Experiments detailed below showed this complex had a contaminating GTPase that was not removed by the purification steps, so a His-tagged version of MBP-UreD—UreF—UreG (with the His-tag located at the amino terminus of MBP) along with the T21A UreG and K165A UreF variant complexes were tested. This complex also had GTPase contamination,

so another method for testing the hypothesis had to be found. This section details the purification and testing of the two complexes.

MBP-UreD—UreF—UreG was purified as described previously from E. coli BL21 (DE3) cells containing plasmids pEC002 (encodes MBP-UreD) and pEC005 (encodes UreF and UreG) (9). His-MBP-UreD—UreF—UreG was purified from E. coli BL21 (DE3) cells containing pCDF-MBP-UreD (created by Nicholas Flugga, a construct that adds a His-tag to the N-terminus of MBP) and pEC005. Cells containing pCDF-MBP-UreD and pEC005 were grown at 37 °C in 1 L of LB containing 100 μ g mL⁻¹ of spectinomycin and 45 μ g mL⁻¹ of chloramphenical to an O.D.₆₀₀ of 0.4 to 0.6, and induced with 0.5 mM IPTG overnight at 22 °C. Cells were harvested by centrifugation, resuspended in buffer A (20 mM Tris, pH 7.8, containing 200 mM NaCl and 20 mM imidazole), sonicated, and centrifuged at $100,000 \times g$ for 1 h. Cell-free extracts were loaded onto a 5 mL Ni-NTA column, washed until the A₂₈₀ reached baseline, and eluted with buffer B (20 mM Tris, pH 7.8, containing 200 mM NaCl and 1 M imidazole). Protein was pooled and dialyzed into TEB (20 mM Tris pH 7.8, 1 mM EDTA, and 1 mM β-mercaptoethanol) with 25 mM NaCl. Protein was then loaded onto a 20 mL amylose column, washed with TEB plus 25 mM NaCl, and eluted with buffer containing 10 mM maltose. Fractions containing the protein complex were pooled and loaded onto a Superdex-200 column (65 cm \times 2.0 cm diameter; GE Healthcare) equilibrated in TEB plus 100 mM NaCl. Fractions eluting off this column were tested for GTPase activity.

Complexes containing the K165A variant of UreF were made by digesting plasmid pKK17-K165A with AatII and AvrII and ligating into a similarly digested pEC005 (9), forming

plasmid pEC005-UreF-K165A. Complexes containing T21A UreG were formed by digesting plasmid pKAU17T21A (10) with AatII and RsrII and ligating into similarly digested pEC005 (9), forming plasmid pEC005-UreG-T21A. These plasmids were double transformed with either pEC002 (for forming MBP-UreD—UreF—UreG variant complexes) (9) or pCDF-MBP-UreD (for forming His- MBP-UreD—UreF—UreG variant complexes).

To determine how much phosphate was produced during GTPase assays, a malachite green reagent was utilized (11). A 100 μ L fraction was added to 900 μ L of buffer (100 mM Hepes, pH 7.8, and 25 mM NaCl) containing 500 μ M Mg₂GTP and incubated at 37 °C for the indicated amount of time, then 100 μ L was removed and added to 700 μ L of buffer, with 200 μ L of malachite green dye subsequently added. The samples were vortexed, transferred to 1 mL cuvettes, and the absorbances at 620 nm were read after 5 min. Samples were compared to a standard curve with known concentrations of phosphate.

For MBP-UreD—UreF—UreG-containing fractions from the Superdex-200 column, malachite green assays were used to monitor phosphate release from Mg₂GTP. Figures 4.2 and 4.3 show SDS-PAGE gels of the fractions tested for the wild-type and T21A UreG-containing complexes, respectively. Tables 4.4 and 4.5 show the changes in phosphate concentration from 20 to 40 min in the GTPase assays incubated at 37 °C and the protein concentrations of the fractions as determined by Bradford assay for the same complexes.

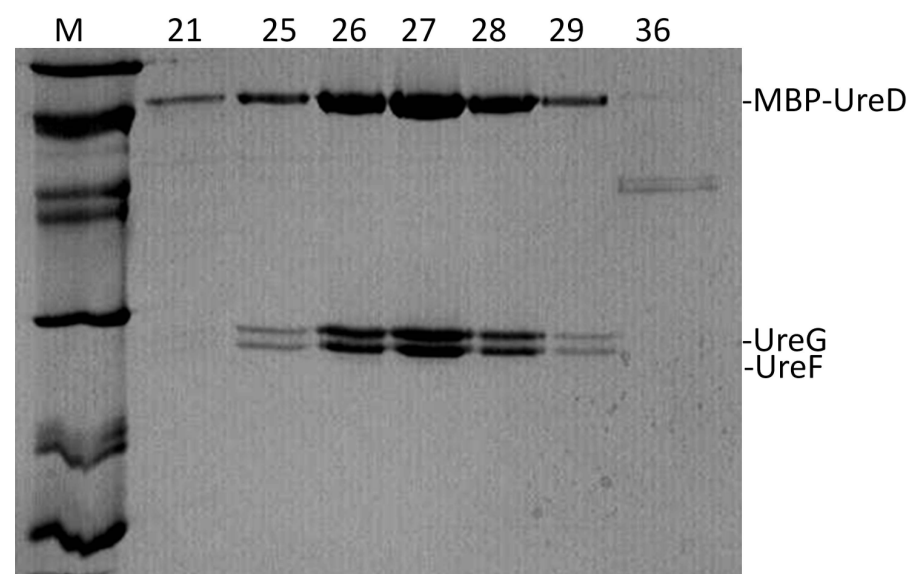


Figure 4.2: Fractions of MBP-UreD—UreF—UreG tested for GTPase activity. SDS-PAGE analysis of MBP-UreD—UreF—UreG fractions eluted from a Superdex-200 column.

Table 4.4: GTPase activities of MBP-UreD—UreF—UreG samples. Fractions assessed for GTPase activity can be visualized in Figure 4.2. Protein concentrations were determined by Bradford assays. Incubations contained 100 μ L of sample and were incubated at 37°C for up to 40 min. Malachite green assays were performed after 20 and 40 min and the differences in phosphate concentrations (Δ PO₄) between the pairs of analyses were recorded. If the difference was calculated to be negative, the Δ PO₄ concentration was rounded up to zero.

	Δ [PO ₄]	[Protein]	$[PO_4]/(mg ml^{-1})$
Fraction	(20 to 40 min) (μM)	(mg mL ⁻¹)	
blank	0	0	0
21	24	0.06	400.00
25	0.55	0.08	6.88
26	0	0.31	0.00
27	8.07	0.45	17.93
28	4.14	0.27	15.33
29	1.09	0.04	27.25

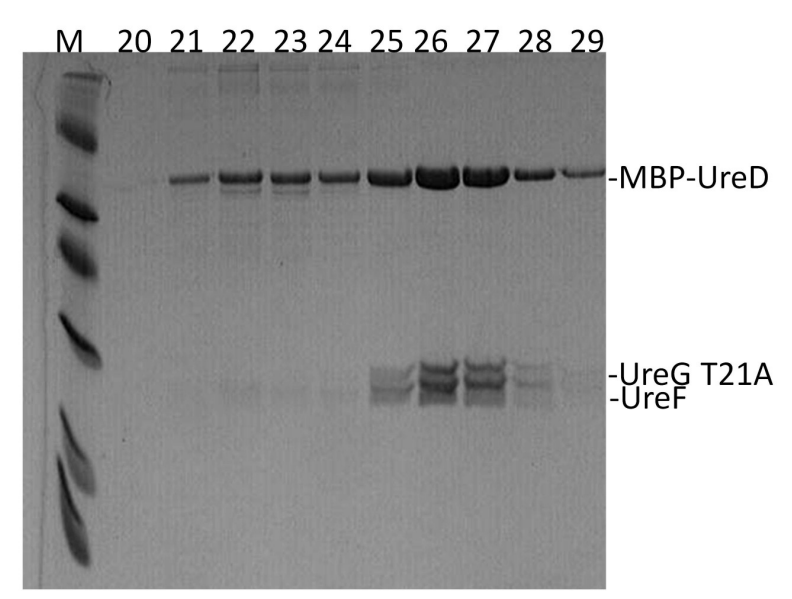


Figure 4.3: Fractions of MBP-UreD—UreF—UreG(T21A) tested for GTPase activity. SDS-PAGE analysis of MBP-UreD—UreF—UreG(T21A) fractions eluted from a Superdex-200 column.

Table 4.5: GTPase activities of MBP-UreD—UreF—UreG(T21A) samples. Fractions assessed for GTPase activity can be visualized in Figure 4.3. Protein concentrations were determined by Bradford assays. Assays contained 100 μ L of sample and were incubated at 37 °C for up to 40 min. Malachite green assays were carried out after 20 and 40 min and the differences in phosphate concentrations between pairs of samples were calculated. If the difference was negative, the Δ PO₄ concentration was rounded up to zero.

Fraction	Δ[PO ₄]	[Protein]	[PO ₄]/(mg ml ⁻¹)
	(20 to 40 min) (μM)	$(mg mL^{-1})$	
Blank	0	0	0
20	5.33	0.02	266.50
21	11.58	0.10	115.80
22	8.75	0.15	58.33
23	0	0.13	0.00
24	0	0.12	0.00
25	5.85	0.21	27.86
26	9.34	0.45	20.76
27	5.22	0.34	15.35
28	4.76	0.16	29.75
29	0	0.06	0.00

As seen in Figures 4.2 and 4.3 and Tables 4.4 and 4.5, the maximal GTPase activity did not coincide with the fractions containing the most MBP-UreD—UreF—UreG complex and the sample containing the T21A UreG mutation (that should be incapable of hydrolyzing GTP) had

significant activity. These results confirm the presence of a contaminating GTPase in these samples. In order to overcome this concern, His-MBP-UreD—UreF—UreG as well as that complex containing the K165A UreF or the T21A UreG mutations were purified and tested for GTPase activity in a similar way as the non His-tagged complex, except that the phosphate concentration was measured after 1 h incubation with 300 µM Mg2GTP (Figure 4.4 and Table 4.6). Unfortunately, the samples had the same type of GTPase contamination that did not correlate with the major protein peaks and was similar in the control complex containing T21A UreG. Additionally, UreG tended to dissociate from the T21A and K165A complexes during the final step of purification, adding to the difficulty of accurately measuring GTPase activity. These studies highlight the difficulty of measuring very small amounts of GTPase activities in samples that contain contaminating amounts of highly active GTPases.

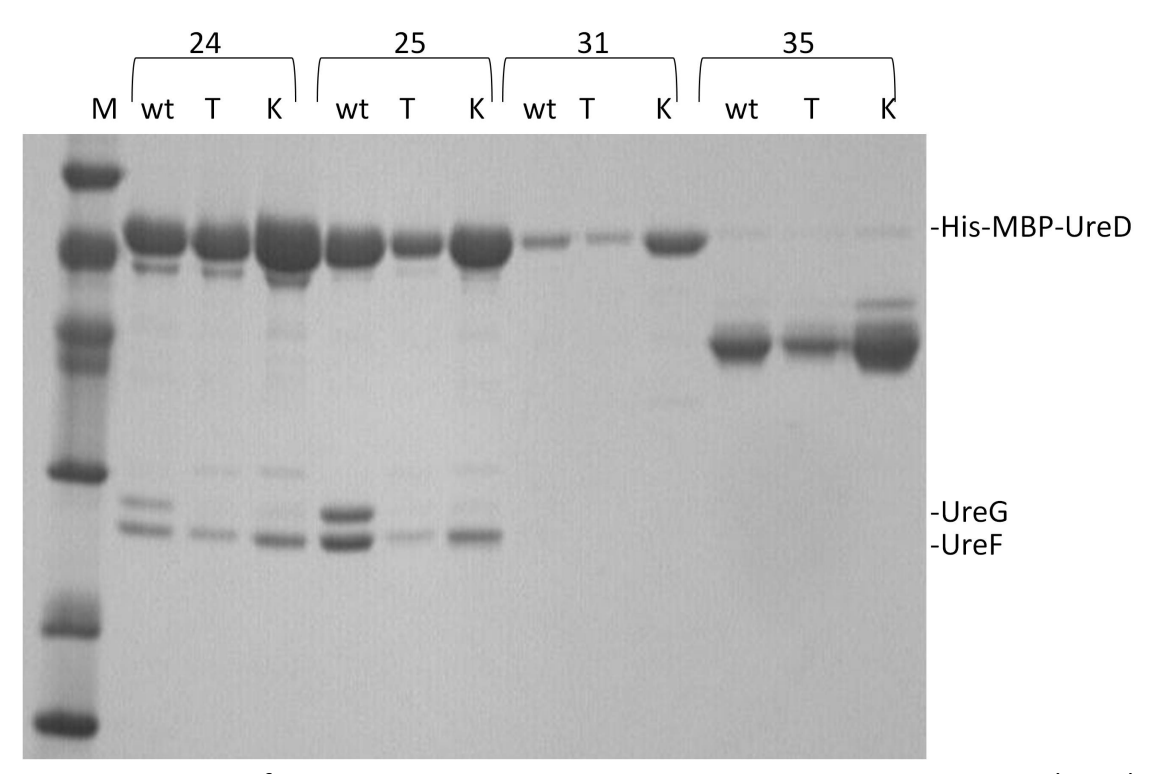


Figure 4.4: Fractions of His-MBP-UreD—UreF—UreG, His-MBP-UreD—UreF—UreG(T21A), and His-MBP-UreD—UreF(K165A)—UreG that were tested for GTPase activity. SDS-PAGE analysis of

(Figure 4.4 con't) fractions eluted from a Superdex-200 column, with lanes labeled with fraction number above the brackets and protein below (wt is the wild-type complex, T is the form containing T21A UreG, and K is the species containing K165A UreF.)

Table 4.6: GTPase activity of His-MBP-UreD—UreF—UreG and variants. Phosphate contents after incubating selected fractions from Superdex-200 containing His-MBP-UreD—UreF—UreG for 1 h at 37 $^{\circ}$ C with 300 μ M GTP.

Fraction # - protein content	[PO ₄] after 1 h	[protein]	[PO ₄]/(mg ml ⁻¹)
	(μM)	(mg mL ⁻¹)	
Blank	12.05	0	0
20 – wt	158.70	0.62	255.97
20 - T21A	93.90	0.53	177.17
20 - K165A	141.27	0.72	196.21
24 – wt	22.99	0.36	63.86
24 - T21A	16.87	0.30	56.23
24 - K165A	30.13	0.69	43.67
25 - wt	21.97	0.49	44.84
25 - T21A	19.47	0.17	114.53
25 - K165A	42.09	0.45	93.53
31 – wt	12.98	0.03	432.67
31 - T21A	12.70	0.15	84.67
31 - K165A	12.89	0.15	85.93
35 – wt	13.44	0.13	103.38
35 - T21A	12.05	0.06	255.97
35 - K165A	14.18	0.24	177.17

causes the dissociation of Components within the MBP-UreD—UreF—UreG complex, pull-down assays using amylose resin were carried out in the presence and absence of 400 μ M GTP. MBP-UreD—UreF—UreG (2 μ M) was incubated in buffer containing 100 mM Hepes, pH 7.8, and 25 mM NaCl, with or without 400 μ M GTP for 1 h at 37 °C. Those samples were added to 150 μ L of amylose resin which had been equilibrated in the same buffer, rocked at room temperature for 1 h, washed with five fold the assay volume, and eluted in 10 mM maltose. Figure 4.5 shows the results of these two assays. GTP had no effect on the amounts of UreF and UreG bound to

the MBP-UreD, indicating that incubation with GTP does not cause the accessory proteins to dissociate from each other in this time frame.

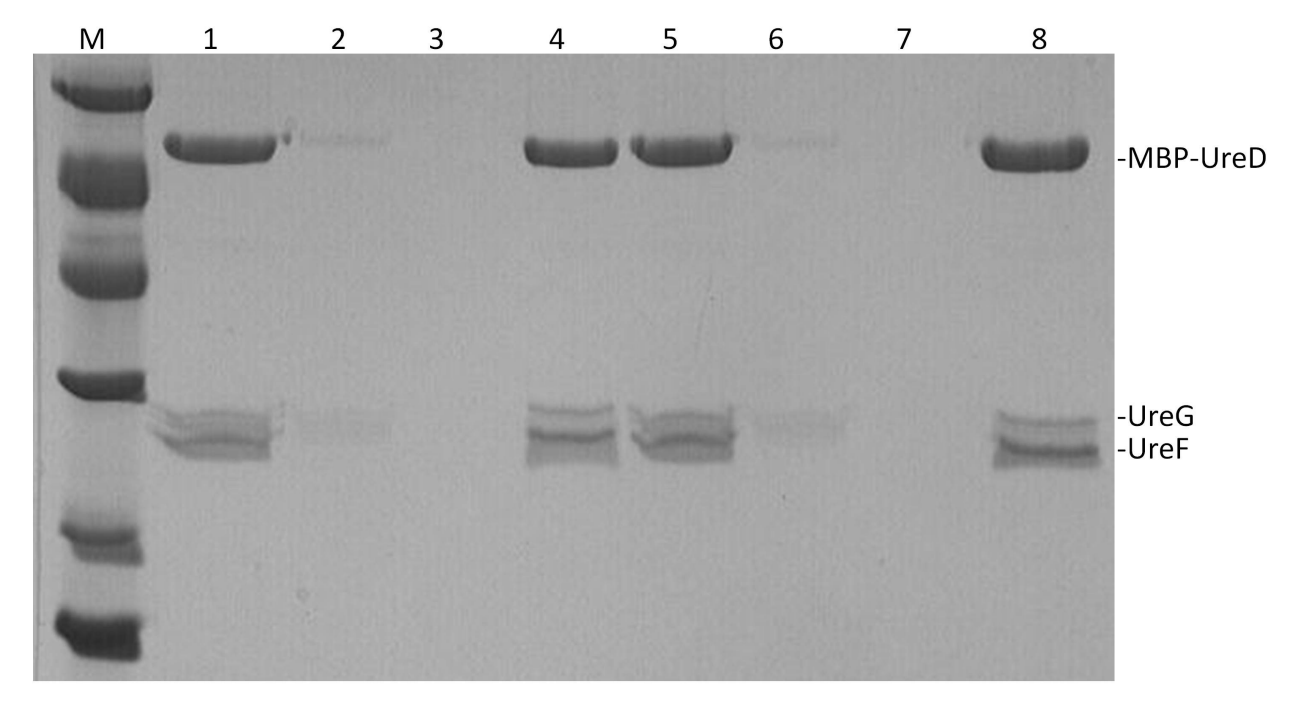


Figure 4.5: Effect of adding GTP to MBP-UreD—UreF—UreG. Lanes: 1-4, no GTP added to starting material, first wash, final wash, and elution; lanes 5-8 are the same as 1-4 except for the assay with GTP.

Characterization of UreABC—UreD—UreF—UreG_{Str}

Superdex-200 profile. As a final purification step, UreABC—UreD—UreF—UreG_{Str} was concentrated and chromatographed on a Superdex-200 column equilibrated in 100 mM Hepes, pH 7.8, 150 mM NaCl, and 1 mM β -mercaptoethanol. Three peaks and a shoulder were evident in the chromatogram. The largest molecular weight peak and the shoulder correspond to the full complex, the middle peak to (UreABC)₃, and the third to UreG_{Str} (Figure 4.6).

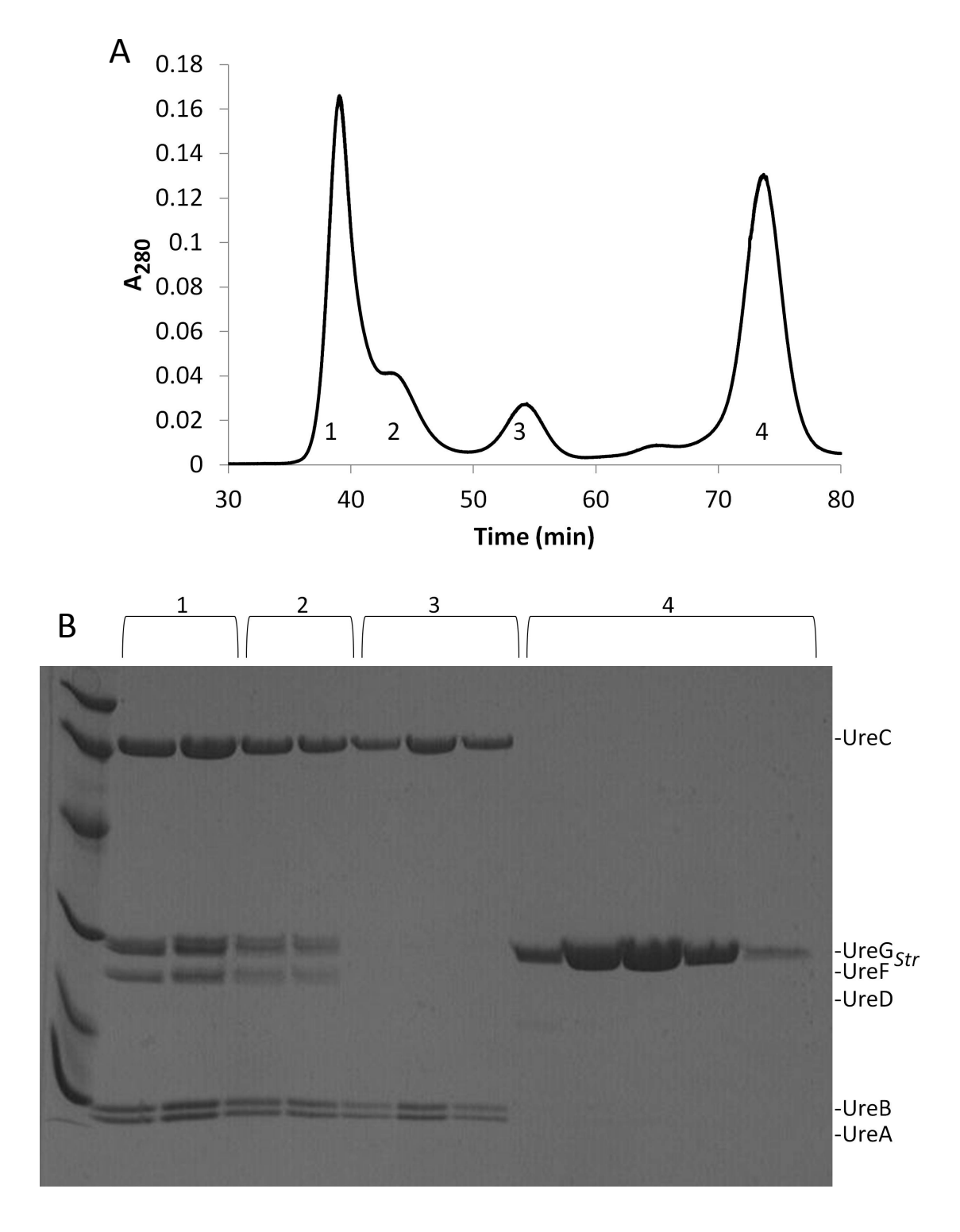


Figure 4.6: Gel filtration profile of UreABC—UreD—UreF—UreG $_{Str}$. A. Chromatograph produced using concentrated UreABC—UreD—UreF—UreG $_{Str}$. B. SDS-PAGE of fractions from the labeled peaks on the chromatograph. Peaks 1 and 2 correspond to the complex, peak 3 to (UreABC) $_3$, and peak 4 to UreG $_{Str}$.

Native gel for $UreABC-UreD-UreF-UreG_{Str}$. To compare the quaternary structure of UreABC-UreD-UreF-UreG_{Str} with that of the non-tagged complex (10), I used a Blue native gel (3-12% gradient; Invitrogen). The buffers recommended by Invitrogen were utilized and the gel was run at 150 V for 90 min. The gel (Figure 4.7) showed that the Strep-tagged complex's smallest molecular weight form migrated at the same size as the non-tagged complex, but some of the larger molecular weight bands were not present in the tagged complex. The Strep-tag may interfere with larger complex formation, or cause the complex to be in a slightly different conformation that does not allow for the same oligomeric states. This change in quaternary structure does not affect the ability of the tagged complex to activate, however.

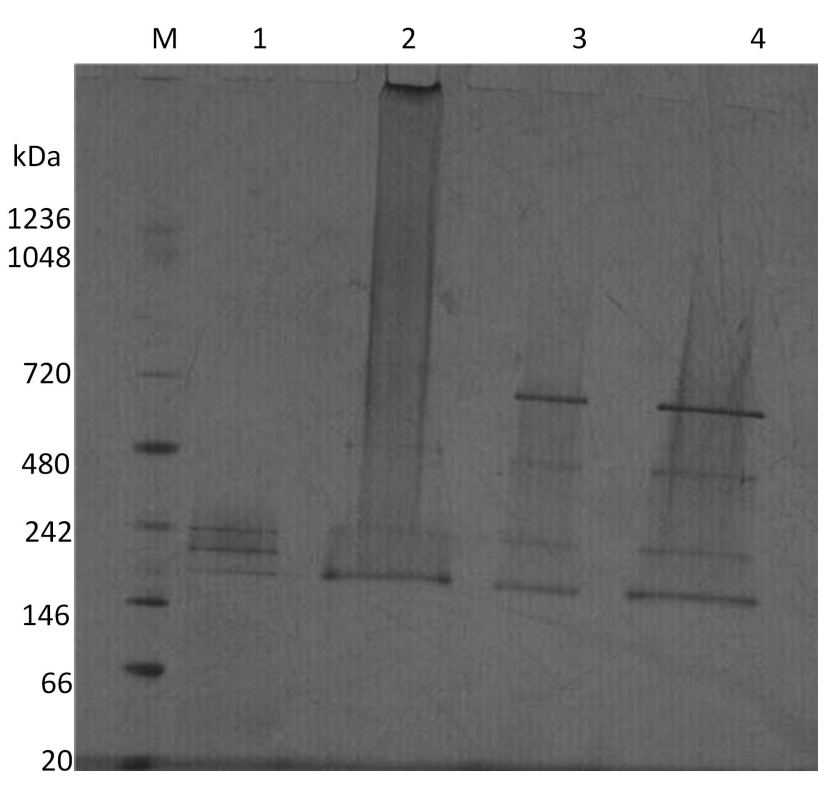


Figure 4.7: Native gel of UreABC—UreD—UreF—UreG $_{Str}$ and UreABC—UreD—UreF—UreG. Lane 1: Purified UreABC—UreD—UreF—UreG $_{Str}$. Lane 2: Same as lane 1, but protein was concentrated three fold. Lane 3: UreABC—UreD—UreF—UreG. Lane 4: Same as 3, but protein was concentrated two fold.

Stability of UreABC—UreD—UreF—UreG_{Str}. To quantify how much phosphate precipitates with the UreABC—UreD—UreF—UreG_{Str} protein as a control for experiments in Chapter 3, the complex (10 μM) was mixed with 100 μM PO₄ and boiled for 3 min. Unlike the samples that had been activated with Ni, bicarbonate, and various concentrations of GTP, this sample did not precipitate. This complex was boiled for 7 additional min, and still no precipitation was noted. This surprising finding was examined further by comparing samples that had been activated for 1 h with buffer (100 mM Hepes, pH 8.3, 150 mM NaCl), 100 µM Ni and 100 µM bicarbonate (with and without 200 µM GTP) to a sample that sat at 37 °C for 1 h in buffer without Ni, bicarbonate, or GTP. All samples were boiled for 5 min, centrifuged, and the supernatant solutions were electrophoresed (Figure 4.8). The non-activated complex retained all proteins in the supernatant fraction after boiling, whereas similar treatment of the activated complex apparently lead to UreD and UreF precipitation, as well as insolubility of most of the UreC. This experiment demonstrates the surprising thermal stability of the UreABC—UreD— UreF—UreG_{Str} pre-activation complex, although the reason for this behavior is unknown.

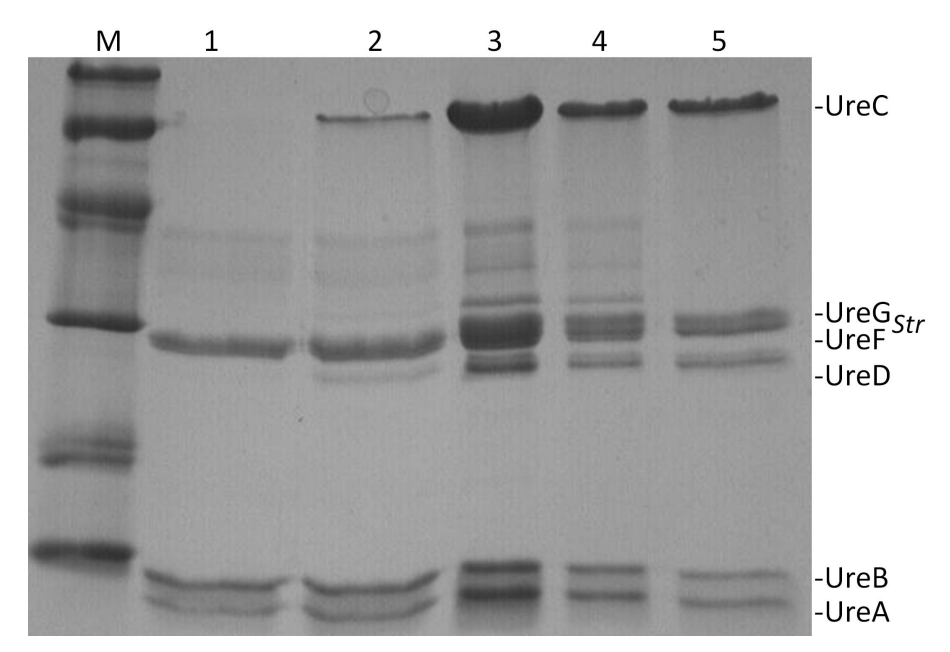


Figure 4.8: Thermal stability of UreABC—UreD—UreF—UreG $_{Str}$. Proteins were activated at 37 °C for 1 h under varying conditions, boiled for 5 min, centrifuged, and the supernatants were analyzed by SDS-PAGE. Lane 1: Complex activated with 100 μ M NiCl $_2$ and 100 μ M NaHCO $_3$. Lane 2: Complex activated with 100 μ M NiCl $_2$, 100 μ M NaHCO $_3$, and 200 μ M Mg $_2$ GTP. Lane 3: Complex activated in only buffer. Lane 4: Complex activated in only buffer, with a smaller amount of protein loaded onto gel. Lane 5: Non-activated control.

CONCLUSIONS AND REMAINING QUESTIONS

This thesis has succeeded in answering some of the prior questions about urease activation, but in answering these points other questions have arisen. In chapter 2, I characterized a *Strep*-tagged version of UreG, as well as 12 variant proteins in an attempt to identify the metal-binding residues. Using UreG_{Str} I showed that the protein binds one Ni or one Zn at the same site with a similar K_d (~3 μ M) based on competition assays with ⁶³Ni. Out of all the mutations tested, C72A was the only one that had an effect on metal binding, as shown by equilibrium dialysis and UV-visible spectroscopy. Other efforts are underway (XAS analysis) to identify the other residues involved in chelating the metal, but the question remains open. I also demonstrated that UreG and UreE interact in the presence of metal, which led to the hypothesis that UreE transfers Ni to UreG, which passes it on to UreD and finally into the active site. This hypothesis needs to be tested in more depth in order to fully understand the role metal binding in UreG plays in the overall activation process.

In chapter 3, I described 16 alanine mutations of highly conserved residues in UreF. Of great significance, I identified several residues that play a role in the binding between UreF and UreG. Since we do not know the structure of UreG, one open question (difficult to answer without the UreG crystal structure, although potentially accessible to cross-linking analysis) is which residues on UreG interact with counterparts on UreF? In chapter 2 I showed Asp80 plays a role in the interaction of UreG with the UreABC—UreD—UreF complex, but there is certainly more than one residue involved in that interaction. It is challenging to choose other residues in UreG for mutagenesis when specifically looking for that interaction since so many residues are

highly conserved. A broader question is why the binding site for UreG on UreF is so highly conserved, yet the interface between UreF and UreD is not, as shown in the crystal structure.

In chapter 3 I also described how UreF acts as a "gate" and, using residue K165, allows for GTP hydrolysis to be connected to urease activation, slowing down the activation process and leading to protection against incorrect assembly with Zn. This discovery substantially answers the question of what role GTPase activity plays in urease activation, but it also opens up several more questions. Is the metal binding site in UreG important for this gating? Since UreG binds Ni and Zn with approximately equal affinity when purified alone, can it distinguish between the two metals when it is in complex with UreD and UreF? Is UreF directly involved in determining the correct metal? Is Zn the only metal for which there is protection, or do other transition metals such as Fe, Cu, and Co have the same effect? I demonstrated K165 is not the GAP residue in UreF, but that does not completely rule out a GAP role for UreF. In particular, R220 is a highly conserved positively-charged residue that could also play that role, a possibility that is difficult to test because UreG does not bind to the UreABC—UreD—UreF(R220A) complex.

In conclusion, my studies have greatly furthered our knowledge about UreG and UreF and their roles in urease activation. There is now a clearer picture of the interaction between UreG and UreE, and between UreG and UreF. UreG's metal binding properties have been partially characterized. The role of GTPase activity in urease activation has been solved, at least in part; it is a "gate" guarding against incorrect metal incorporation in conjunction with UreF. UreF's role in connecting the GTPase to the activation process has been elucidated to a large extent. Thus, my studies have provided important insights for understanding the overall urease

activation process, and this new understanding may be relevant to metallocenter activation in other enzymes.

REFERENCES

REFERENCES

- 1. Chang, Z. Z., Kuchar, J., and Hausinger, R. P. (2004) Chemical cross-linking and mass spectrometric identification of sites of interaction for UreD, UreF, and urease, *J. Biol. Chem.* 279, 15305-15313.
- 2. Quiroz-Valenzuela, S., Sukuru, S. C. K., Hausinger, R. P., Kuhn, L. A., and Heller, W. T. (2008) The structure of urease activation complexes examined by flexibility analysis, mutagenesis, and small-angle X-ray scattering, *Arch. Biochem. Biophys* 480, 51-57.
- 3. Yamaguchi, K., Cosper, N. J., Stalhandske, C., Scott, R. A., Pearson, M. A., Karplus, P. A., and Hausinger, R. P. (1999) Characterization of metal-substituted Klebsiella aerogenes urease, *J.Biol. Inorg. Chem.* 4, 468-477.
- 4. Park, I. S., and Hausinger, R. P. (1996) Metal ion interactions with urease and UreDurease apoproteins, *Biochemistry 35*, 5345-5352.
- 5. Kim, J. K., Mulrooney, S. B., and Hausinger, R. P. (2006) The UreEF fusion protein provides a soluble and functional form of the UreF urease accessory protein, *J. Bacteriol.* 188, 8413-8420.
- 6. Moncrief, M. B. C., and Hausinger, R. P. (1997) Characterization of UreG, identification of a UreD-UreF-UreG complex, and evidence suggesting that a nucleotide-binding site in UreG is required for in vivo metallocenter assembly of *Klebsiella aerogenes* urease, *J. Bacteriol.* 179, 4081-4086.
- 7. Jabri, E., Carr, M. B., Hausinger, R. P., and Karplus, P. A. (1995) The crystal structure of urease from *Klebsiella aerogenes*, *Science 268*, 998-1004.
- 8. Hunt, J. B., Sue H. Neece, and Ann Ginsburg. (1985) The use of 4-(2-pyridylazo) resorcinol in studies of zinc release from *Escherichia coli* aspartate transcarbamoylase, *Anal. Biochem.* 146, 150-157.
- 9. Carter, E. L., and Hausinger, R. P. (2010) Characterization of *Klebsiella aerogenes* urease accessory protein UreD in fusion with the maltose binding protein, *J. Bacteriol.* 192, 2294-2304.
- 10. Soriano, A., and Hausinger, R. P. (1999) GTP-dependent activation of urease apoprotein in complex with the UreD, UreF, and UreG accessory proteins, *Proc. Natl. Acad. Sci. U.S.A. 96*, 11140-11144.
- 11. Baykov, A. A., Evtushenko, O. A., and Avaeva, S. M. (1988) A malachite green procedure for orthophosphate determination and its use in alkaline phosphatase-based enzyme immunoassay, *Anal. Biochem.* 171, 266-270.

Appendix A

Table A.1: Plasmids used in this work.

Plasmid	Description	Reference
pASK-IBA3plus	Plasmid for creating fusion proteins with a <i>Strep</i> -tag II (WSHPQFEK) at the C-terminus	IBA
pASK-IBA5plus	Plasmid for creating fusion proteins with a <i>Strep</i> -tag II at the N-terminus	IBA
pEC007	Modified pACT3 to encode UreE	(1)
pKK17	K. aerogenes ureDABCEFG gene cluster inserted into pKK223-3	(2)
pKAUG-1	Modified pKAUD2 containing only K. aerogenes ureG.	(3)
pIBA5+G	Modified pASK-IBA5plus to encode UreG _{Str}	This work
pIBA3+GK20A, pIBA3+GE25A, pIBA3+GC28A, pIBA3+GD33A, pIBA3+GD49A, pIBA3+GE68A, pIBA3+GC72A, pIBA3+GH74A, pIBA3+GD80A, pIBA3+GS111A, pIBA3+GS115A, pIBA3+GD120A pIBA3+GD127A	Modified pIBA3+G to encode the K20A, E25A, C28A, D33A, D49A, E68A, C72A, H74A, D80A, S111A, S115A, D120A and D127A variants of UreG _{Str}	This work
рККС	Modified pKK17 encoding UreG _{Str}	This work
pKKGK20A, pKKGE25A, pKKGC28A, pKKGD33A, pKKGD49A, pKKGE68A, pKKGC72A, pKKGH74A, pKKGD80A, pKKGS111A, pKKGS115A, pKKGD127A	Modified pKKG encoding the K20A, E25A, C28A, D33A, D49A, E68A, C72A, H74A, H74C, H74N, D80A, S111A, S115A, and D127A variants of UreG _{Str}	This work

Table A.1 (con't) pKK17-P19A, -G21A, -Y23A, - S26A, -E30A, -D60A, -E94A, - K165A, -F169A, -Q171A, - H214A, -E215A, -R220A, - L221A, -F222A, -S224A	Single site variants of pKK17 for studying the effects of these UreF variants on urease activity	This work
pKKEF	Same as pKK17, but with a translational fusion of UreE and UreF	(4)
pKKEF-P19A, -G21A, -Y23A, - S26A, -E30A, -D60A, -E94A, - K165A, -F169A, -Q171A, - H214A, -E215A, -R220A, - L221A, -F222A, -S224A	Single site variants of pKKEF for <i>in</i> vivo pull-down studies	This work
pET-EF	Translationally fused <i>ureEF</i> genes inserted into pET21	(4)
pET-EF-P19A, -G21A, -Y23A, - S26A, -E30A, -D60A, -E94A, - K165A, -F169A, -Q171A, - H214A, -E215A, -R220A, - L221A, -F222A, -S224A	Single site mutants of pET-EF for production of UreE-F variants for <i>in vitro</i> pull-down studies	This work
pKKG-UreF-K165A	Single site mutant of pKKG encoding the K165A UreF variant	This work
pKKG-T21A	Single site mutant of pKKG encoding the T21A variant of <i>Strep II</i> tagged UreG	This work
pKAUD2	Plasmid for production of (UreABC—UreD) ₃	(5)
pEC005	ureFG fragment cloned into pACT3 for production of UreF and UreG	(1)
pEC005-UreF-K165A	Single site mutant of pEC005 that encodes the K165A variant of UreF along with UreG	This work
pEC005-UreG-T21A	Single site mutant of pEC005 that encodes the T21A variant of UreG along with UreF	This work
pEC002	ureD cloned into pMal-c2x for production of UreD fused at its C-terminus to MBP. Used along with pEC005 for production of MBP-UreD—UreF—UreG.	(1)
pCDF-MBP-UreD	malE-ureD cloned into pCDF-1b to produce MBP-UreD with an N-terminal His ₆ tag	(6)
	-	

References

REFERENCES

- 1. Carter, E. L., and Hausinger, R. P. (2010) Characterization of *Klebsiella aerogenes* urease accessory protein UreD in fusion with the maltose binding protein, *J. Bacteriol.* 192, 2294-2304.
- 2. Colpas, G. J., Brayman, T. G., Ming, L. J., and Hausinger, R. P. (1999) Identification of metal-binding residues in the *Klebsiella aerogenes* urease nickel metallochaperone, UreE, *Biochemistry 38*, 4078-4088.
- 3. Park, I. S. (1994) Thesis, in *Microbiology*, Michigan State University, East Lansing, MI.
- 4. Kim, J. K., Mulrooney, S. B., and Hausinger, R. P. (2006) The UreEF fusion protein provides a soluble and functional form of the UreF urease accessory protein, *J. Bacteriol.* 188, 8413-8420.
- 5. Park, I. S., Carr, M. B., and Hausinger, R. P. (1994) *In vitro* activation of urease apoprotein and role of UreD as a chaperone required for nickel metallocenter assembly, *Proc. Natl. Acad. Sci. U.S.A.* 91, 3233-3237.
- 6. Carter, E. L., Boer, J. L., Farrugia, M. A., Flugga, N., Towns, C. L., and Hausinger, R. P. (2011) The function of UreB in *Klebsiella aerogenes* urease, *Biochemistry 50*, 9296-9308.